Solvation Properties of Ionic Liquid Mixtures

Sachini Kadaoluwa Pathirannahalage

THESE

en vue de l'obtention du grade de Docteur, délivré par

l'ECOLE NORMALE SUPERIEURE DE LYON

en cotutelle avec

RMIT University

Ecole Doctorale N° 206
Ecole Doctorale de chimie (Chimie, Procédés, Environnement)

Discipline : Chimie

Soutenue publiquement le 21/09/2023, par :

Sachini KADAOLUWA PATHIRANNAHALAGE

Solvation Properties of Ionic Liquid Mixtures

Propriétés de résolution des mélanges liquides ioniques

Devant le jury composé de :

LE, Tu	Professeure	RMIT University	Examinatrice
CHRISTOFFERSON, Andrew	Professeur	RMIT University	Examinateur
CROFT, Anna	Professeure	Loughborough University	Rapporteure
PADUA, Agilio	Professeur des universités	ENS de Lyon	Examinateur
RODRIGUEZ, Hector	Professeur	Universidade de Santiago de Compostela	Rapporteur
GREAVES, Tamar	Professeur	RMIT University	Co-tutrice de thèse
COSTA GOMES, Margarida	Directrice de recherche	ENS de Lyon	Directrice de thèse

Solvation Properties of Ionic Liquid Mixtures

A thesis submitted in fulfilment of the requirements for the degree of Doctor of Philosophy

Sachini Piumika Kadaoluwa Pathirannahalage

BSc (Physics) (Dean's Scholar, Honours), RMIT University

School of Science

College of Science, Technology, Engineering and Maths

RMIT University

19th January 2023

Declaration

I certify that except where due acknowledgement has been made, this research is that of the author alone; the content of this research submission is the result of work which has been carried out since the official commencement date of the approved research program; any editorial work, paid or unpaid, carried out by a third party is acknowledged; and, ethics procedures and guidelines have been followed.

In addition, I certify that this submission contains no material previously submitted for award of any qualification at any other university or institution, unless approved for a joint-award with another institution, and acknowledge that no part of this work will, in the future, be used in a submission in my name, for any other qualification in any university or other tertiary institution without the prior approval of the University, and where applicable, any partner institution responsible for the joint-award of this degree.

I acknowledge that copyright of any published works contained within this thesis resides with the copyright holder(s) of those works.

I give permission for the digital version of my research submission to be made available on the web, via the University's digital research repository, unless permission has been granted by the University to restrict access for a period of time.

I acknowledge the support I have received for my research through the provision of an Australian Government Research Training Program Scholarship.

Sachini P. Kadaoluwa Pathirannahalage

Acknowledgments

First and foremost, I would like to thank my supervisors Tam, Tu, Andrew, and Margarida. Attempting to complete a PhD on time in the middle of a global pandemic would be a ludicrous idea if I wasn't being supported by the best supervisory team. All of you have been completely supportive and understanding during this project and had guided me through some of the most difficult days and months of my life. This PhD served not only as an academic journey, but also a personal one and each of my supervisors served as a great mentor to me during this time. I consider myself very lucky to have your expertise and enthusiasm on my supervisory team. I genuinely do not believe I would have been capable of completing this thesis without you as my supervisors.

I would also like to acknowledge the Physics department at RMIT University and all the individuals who make it such an outstanding learning environment. I have spent over one third of my life at RMIT and countless people here made that time extremely fun and productive. From the PSA parties to the end of year cricket matches, I'll never forget the experiences I was lucky enough to have at RMIT. Special shout out to Katherine, Karen, Yik, Jordan(s), Adam, Liam, Josh and Kyla, for all your love and support. I consider myself extremely lucky to have met life-long friends during my studies and I owe you all at least a pint or two for the support you've given me.

To the molecular assembly group at RMIT, you've been the best colleagues one could have asked for. Stuart, Hayden, Dilek and Sarigama, you're all certainly more than colleagues, we've had some crazy times in and out of the lab. Every single person in our lab has contributed in one way or another to my thesis, either by helping with synchrotron times or by giving me a pep talk when everything seemed bleak. Most importantly, I would like to thank Shveta and Asoka, for all your help with experiments and keeping the lab in one piece during the six odd years I spent in the molecular assembly lab. Both of you were/are the backbone of the lab and our group.

To the ionic liquids research team at ENS de Lyon, who I wish I had the opportunity to spend more time with, thank you for welcoming me with open arms. I had the time of my life meeting every one of you, drinking wine on the Rhône, having game picnics and lunch breaks that were far too long. To

Katya, Laura, Oli, Adriaan, Guillaume and Natalie, thank you for not only being fun colleagues but also awesome friends. And of course, thank you for all your expertise and all the laughs, Agilio. You were the best non-official supervisor I could've asked for.

I would also like to extend my sincerest gratitude to every collaborator who helped in many capacities from large XFEL experiments to computational collaborations ranging from machine learning to molecular dynamics simulations. This thesis would not have been possible without all your expertise on so many different topics and I feel very lucky to have been able to be part of so many successful teams. Special thank you to Andrew Martin and Connie for taking care of me during the foot infection saga in 2019 during the XFEL experiment.

Parts of this work was completed at the SAXS/WAXS beamline at the Australian synchrotron. Thank you to all the beamline scientists who made weeklong beamtimes fun and productive. Blindly following any opportunities which led me to more "scientific sleepovers" at the Australian Synchrotron led me to my PhD and I'll forever be grateful to the technical staff who facilitate our ambitious ideas.

Last but certainly not least, I have a whole village to thank for raising me and helping me get this far in my academic career. I feel extremely privileged to have been able to continue my passion for Physics for as long as I have. මගේ අම්මටයි නාත්නටයි හැමදේටම ස්තුතියි. To my sisters Hirushi and Udara, you are my biggest inspiration in life, thank you for being the best support system I never had to ask for. To Ishani and Dilshin, even if you don't understand what I do, I know you'll always have my back during every crisis. This PhD was difficult, but it would've been impossible without each one of you.

I know I will look back at this thesis in another 50 years and reminisce about how ridiculously, insanely fun my PhD was, and I owe it all to every single person I interacted with, had a laugh with and collaborated with. Thank you for being an integral part of some of the best years of my life!

Table of contents

List of Figures

List of Tables

List of Abbreviations and Acronyms

AIL	Aprotic ionic liquids
ANN	Artificial neural network
BRANNLP	Bayesian regularized artificial neural network with Laplacian prior
C12E4	Tetraethylene glycol monododecyl ether
CAC	Critical aggregation concentration
CMC	Critical micelle concentration
COSMO-RS	Conductor-like Screening Model for Real Solvents
CPOM	Cross polarised optical microscopy
CPP	Critical packing parameter
CTAB	Cetyltrimethylammonium bromide
DFT	Density-functional theory
DSC	Differential scanning calorimetry
DTAB	Dimethyldioctadecylammonium bromide
EAN	Ethylammonium nitrate
EtAN	Ethanolammonium nitrate
IL	Ionic liquid
LAMMPS	Large-scale Atomic/Molecular Massively Parallel Simulator
LCP	Liquid crystal phase
LINCS	LINear Constraint Solver
LJ	Lennard-Jones
MD	Molecular dynamics
ML	Machine learning
MLR	Multiple linear regression
MLREM	Multiple linear regression with expectation maximization
MSD	Mean square displacement

NPT	Isothermal–isobaric ensemble
NVT	Canonical ensemble
OPC	Optimal point charge
OPLS	Optimized Potentials for Liquid Simulations
PIL	Protic ionic liquids
PME	Particle-mesh Ewald
PPPM	Particle-particle particle-mesh
QSPR	Quantitative structure property relationship
RDF	Radial distribution function
SANS	Small angle neutron scattering
SAXS	Small angle x-ray scattering
SDS	Sodium dodecyl sulfate
SEE	Standard error of estimation
SEP	Standard error of prediction
SLC	Standard laboratory conditions
SLD	Scattering length density
SOS	Sodium octyl sulfate
SPC	Single point charge
ST	Surface tension
VMD	Visual Molecular Dynamics
WAXS	Wide angle x-ray scattering

Abstract

Ionic liquids (ILs) are salts with low melting points, often resulting in a liquid state at room temperature. ILs are regarded as highly tailorable designer solvents with many potential applications, such as in organic synthesis, energy storage devices and as solvents for biological molecules. However, for many applications the use of ILs is limited due to their cost and viscosity. One approach used to address this is combining ILs with molecular solvents. However, currently there is insufficient knowledge about the interaction of these IL-molecular solvents with solutes and interfaces, particularly regarding which ions or molecular solvent molecules are involved in solvating various solutes. This thesis expands our understanding and provides insight into the tools available to investigate solvent behaviour of ionic liquids at a molecular level using both experiments and computational simulations.

Machine learning was initially used to understand the trends between chemical structure and physicochemical properties of protic ionic liquids (PILs) in the presence of water. Due to the vast sample space in the field of PILs, it is near impossible to characterise these mixtures experimentally. Machine learning, which allows for the input of experimental data from which extrapolations can be made about new ILs, is a novel technique which has sparked great interest within our field. Machine learning models were created using linear regression and neural network methods using literature experimental viscosity and conductivity data to predict 8605 viscosity values and 8580 conductivity values. The viscosity and ionic conductivity of 10 new PILs of these predicted values were verified experimentally as part of this thesis, which demonstrates that high quality machine learning models can be crafted to complement experimental studies in the future. The machine learning study also demonstrated that physical properties of PILs are subject to drastic changes with minute changes to their chemical structure. This motivated the need to develop a deeper understanding of the role of a PIL in mixtures.

Ethylammonium nitrate (EAN) and ethanolammonium nitrate (EtAN), two PILs which are quite structurally similar with a small change in their chemical structures of replacing a hydrogen with a hydroxyl group, were chosen as the PILs for further investigation. While PILs are widely studied in the literature due to the ease with which they can be synthesised and favourable physical properties such as low viscosity, questions remain regarding how their solvent properties alter in the presence of water. The self-assembly of surfactants Cetyltrimethylammonium bromide (cationic), sodium octyl sulfate (anionic) and Tetraethylene glycol monododecyl ether (non-ionic) in PIL-water mixtures were probed to understand the solvation properties of PILs in the presence of water. The methods used to investigate these properties included surface tensiometry and small angle x-ray scattering (SAXS), both of which were used to understand ternary mixtures of PILs with surfactants and water. Surface tensiometry was able to show that the critical micelle concentration was greatly affected by the concentration of the PILs. The presence of PIL in the mixture led to an initial decrease in the CMC but led to an overall increase in the CMC across all surfactants above 5 mol% of the PIL. To confirm the presence of self-assembled structures in the ternary mixtures, SAXS was used. The SAXS experiments proved to be difficult for EAN due to contrast issues but scattering from micelles were observed in EtAN solutions. No scattering was observed for the EAN rich solvent, whereas for similar concentrations of EtAN x-ray scattering could be observed. To solve the conundrum regarding why such similar PILs led to vastly different results, it was decided computational techniques are necessary.

Molecular dynamics (MD) was explored as a complementary computational technique to probe deeper into the experimental data. As a starting point, a systematic review of 31 existing water models was performed to understand which water model force-field would be suitable for mixing with existing IL force-fields. OPC3 water model was deemed to be suitable for the purposes of this thesis to combine with the existing OPLS EAN force-field. These force-fields were combined with existing force-fields for the three surfactants to probe the molecular level interactions between the EAN-water mixtures and the surfactants which self-assemble into micelles. The simulations suggested that ethylammonium ions, which are supposed to be in the bulk solvent, were in fact participating in the micelle formation with

the surfactants. This provided an explanation regarding the contrast issues which led to inconclusive results from SAXS experiments.

The overall objective of this thesis was to gain a fundamental understanding of how PILs behave in mixtures with other solvents and solutes. To achieve this, a wide variety of experimental and computational techniques had to be explored to understand the mixtures from different perspectives, where that be experimentally or at a molecular level using simulations. The work done during this thesis will form a basis for future work in the space of molecular dynamics and machine learning models for PILs and their mixtures.

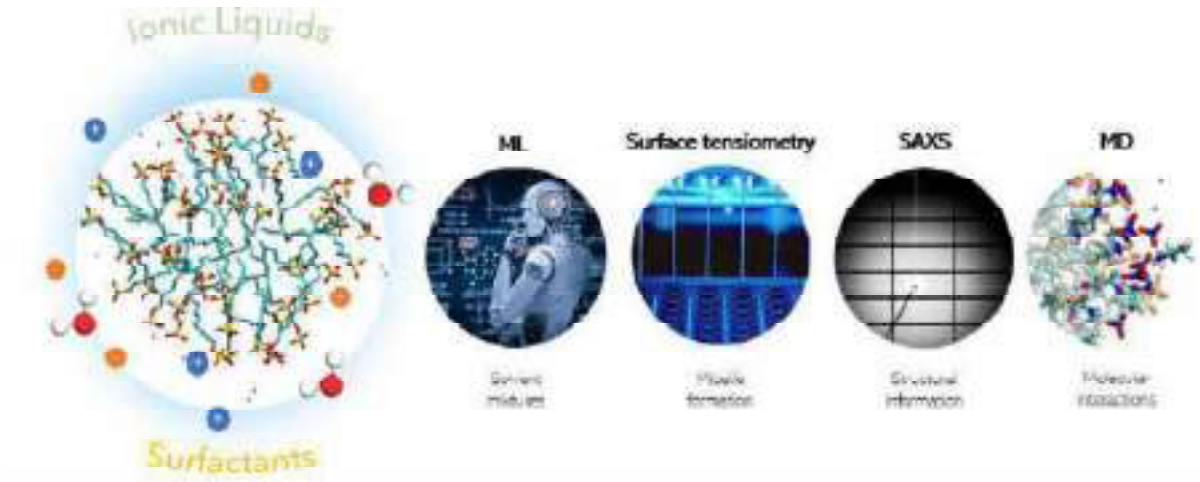

Figure A.1. Illustration of properties of ionic liquid mixtures investigated and the methods used in the thesis.

1 Introduction

Ionic Liquids (ILs) are salts with melting points under 100 °C, mainly due to poorly coordinated ions which cannot pack efficiently and hydrogen bonding. The main advantage in using ILs is their versatility as a solvent. Various features such as polarity, cation alkyl chain length, anion nucleophilicity, hydrophobicity, pH, salt kosmotropicity and ionicity can be altered to tailor for a specific application by changing the structure of the cation and the anion.[1] There are two main categories of ILs; aprotic ionic liquids (AILs) and protic ionic liquids (PILs), where PILs are synthesised through proton transfer from a Brønsted acid to a Brønsted base.[2] PILs are the largest known solvent class capable of promoting self-assembly of surfactants and they will be the focus of this thesis.

In recent years, the field of ionic liquids has shifted from neat ILs to exploring IL-water mixtures for various applications, due to the costs and viscosity issues associated with using neat ILs. However, it is unclear what factors and parameters allow ILs to be successful co-solvents, and what the new solvent properties are. The overall objective of this thesis was to gain understanding into the behaviour of ionic liquids in mixtures with water and various solutes using both experimental and computational tools.

1.1 Protic ionic liquids (PILs)

PILs are a subclass of ionic liquids with an available proton. Unlike AILs which generally require complex synthesis and purification processes, PILs can be synthesised via a straightforward Brønsted acid-base reaction:

$$Brønsted\ acid + brønsted\ base \rightarrow PIL\ cation + PIL\ anion$$

This allows PILs to be created via automated high-throughput processes, which along with generally cheap precursors, makes them cheaper and faster to produce than AILs. PILs are also easier to purify

than AILs. Water can be removed during the synthesis process using vacuum methods due to the low volatility of PILs, and PIL synthesis does not involve any halides. Incremental changes to the cation and anion structure of PILs can lead to vast differences in their bulk physicochemical properties. Therefore, it is difficult to predict and categorise PILs and their property trends. High throughput experimental efforts have been pursued in recent years due to the sheer number of available cation and anion combinations.[3-4] Figure 1.1 depicts a subset of PILs which are widely studied in the literature, with incrementally increasing carbon chains and branching on the cation, paired with nitrate or formate anions.

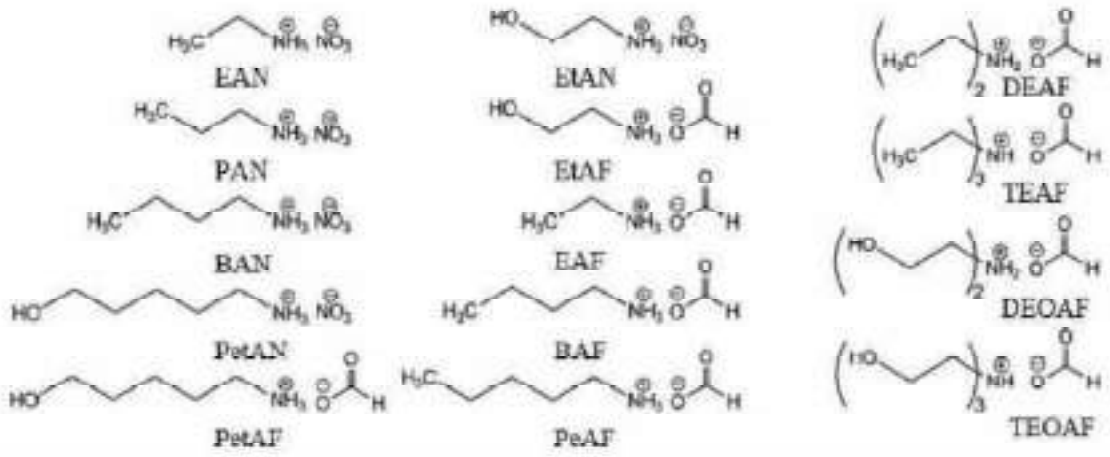

Figure 1.1. Examples of widely used protic ionic liquids. Reproduced from ref [5].

In addition, PILs are the largest known class of solvents demonstrating the ability to support amphiphile self-assembly.[6] PILs which can promote self-assembly allow us to understand interactions between solvents and solutes. In this thesis we aim to use self-assembly as a process to give us insights into the solvation properties of PILs.

The available protons in PILs lead to a hydrogen bonded network akin to water.[7] The hydrogen bonded network allows PILs to have high cohesive energy density. Like water, PILs are highly polar hydrogen-bonded solvents, which exhibit behaviour associated with the hydrophobic effect. This effect, as it

applies to PILs can be generalised as the solvophobic effect. This hypothesis was first suggested by Evans et al. in 1981[8]. Figure 1.2 depicts how the hydrogen network in EAN was illustrated by Evans and how it compares to the H-network in water.

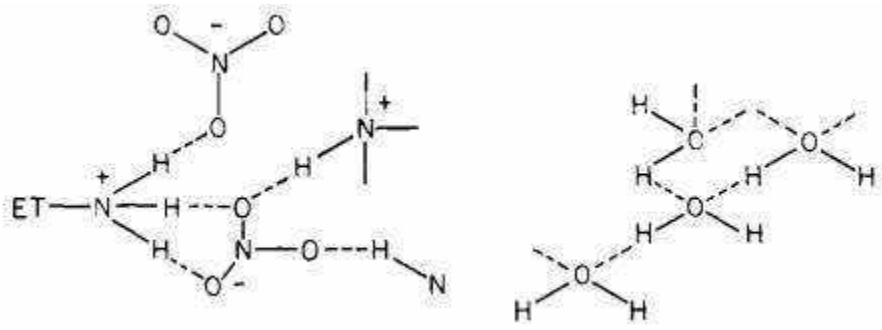

Figure 1.2. Hydrogen bond networks in ethylammonium nitrate and water. Reproduced from [8].

1.1.1 Physicochemical properties of PILs

To gain insight into the intermolecular interactions of ionic liquids, the physicochemical solvent properties of PILs can be characterised experimentally. Thermal properties such as melting point, a defining feature of ILs, can be characterised using differential scanning calorimetry (DSC). The melting point of ILs tend to be defined as under 100 °C, mostly defined to separate ILs from molten salts. The ILs are, in theory, not supposed to have boiling points, due to their non-volatile nature. However, the proton transfer between the precursor acid and base reaction can sometimes be reversible. If so, then upon heating, the molecular species can evaporate, with typically the amine being more volatile than the acid, which leads to the proton transfer reaction going backwards, creating more molecular species and less ions. Due to this instability, some PILs have a boiling point as is expected for molecular solvents.

The density and viscosity of ILs tend to be higher than water and other molecular solvents. One key issue in using ILs for industry applications is their high viscosity at room temperature, which increases as the length of carbon chains in ILs increase. A low melting point, viscosity, and vapour pressure, as

well as high thermal stability and ionic conductivity are often considered desirable properties of PILs in various applications. Mixing PILs with water, which leads to lower viscosity, is considered to be very useful. However, the properties of the resulting mixtures are not well characterised.

It is no simple task to characterise the vast number of ILs which can be synthesised by precursor acids and bases. ILs are also complex to characterise at the nanoscale due to the polar-apolar separation sometimes leading to liquid nanostructure. To gain structural information regarding ILs and their nanostructure, a host of experimental techniques can be used. Scattering techniques such as dynamic light scattering (DLS) and small angle x-ray and neutron scattering (SAXS and SANS) can provide insight into the liquid nanostructure of ILs. While microscopy techniques such as cross-polarised optical microscopy (CPOM) and electron microscopy can be used to visualise and qualitatively understand solutes in ILs, techniques are required to understand the systems quantitatively. The refractive indices of ILs also tend to be higher than that of water, which leads to contrast issues during light scattering techniques as the refractive index of ILs tend to be similar to surfactants and biomolecules.

There has been significant focus in the literature regarding the evaluation of structure-property relationships and physicochemical properties for PILs, as summarised in Table 1.1.[2-3, 9-10] Physical properties such as density, viscosity, surface tension, liquid nanostructure, ability to promote self-assembly, as well as thermal properties melting and boiling points, glass transitions have been reported extensively. Changes in the chemical structure of the PIL proposes significant changes to its solvent properties. Yalcin et al[11] summarised the relationship between chemical structure changes and physicochemical properties for 17 unique PILs as shown in Table 1.1.

Table 1.1. Summary of trends in physicochemical properties with changes to PIL chemical structures, summarising whether they decrease (dec), increase (inc) or no change (NC) as properties of the cation and anion vary. Reproduced from [11] based on the 17 ILs listed below [a].

	Cation				Anion	
	Increasing alkyl chain length	Hydroxyl group	Branching on alkyl chain	Branching on alkyl hydroxyl chain	Inorganic compared to organic	Increasing alkyl chain length
Surface tension	Dec	Inc	Complex (formates)	NC-Dec	Dec	Dec
Density	Dec	Inc	Complex (formates)	Inc	Inc	Dec
Viscosity	Inc	Inc	Dec	Inc	NC (with E cation) Dec (with Et) cation	Inc
Refractive index	Inc	Dec (nitrates)	Dec	Inc	NC (with E cation) Dec (with Et) cation	Dec
Ionic conductivity	Dec	Dec	Inc	Dec	Inc	Dec
Glass transition	Inc	Inc	Dec	Inc	Dec	Inc
Melting point	Inc	Inc (nitrates)	Inc	Inc	Inc	Inc

[a] List of 17 ILs: ethylammonium formate (EAF), ethanolammonium formate (EtAF), diethylammonium formate (DEAF), diethanolammonium formate (DEtAF), triethylammonium formate (TEAF), triethanolammonium formate (TEtAF), butylammonium formate (BAF), pentylammonium formate (PeAF), ethylammonium nitrate (EAN), ethanolammonium nitrate (EtAN), butylammonium nitrate (BAN), pentylammonium nitrate (PeAN), ethylammonium acetate (EAA), ethanolammonium acetate (EtAA), diethanolammonium acetate (DEtAA), triethanolammonium acetate (TEtAA) and pentylammonium acetate (PeAA).

1.1.2 Physicochemical properties of PIL mixtures

The physicochemical properties vary even more as molecular solvents are introduced into PILs as a co-solvent. This is largely because there are many interactions occurring, such as van der Waals, charge, entropic, hydrogen bonding and solvophobic interactions. Depending on the ratio of PIL to molecular solvent, the role of the PIL changes as the amount of molecular solvent present increases. The acid-base equilibria can also shift with the addition of excess water. While there is an inherent assumption that ionic liquids consist simply of the cation and the anion, the presence of water can lead to molecular

speciation, leading to charged pairs and neutral clusters. These effects were observed for AILs and is summarised for molar conductivity in AIL-molecular solvents mixtures by MacFarlane et al. in Figure 1.3.

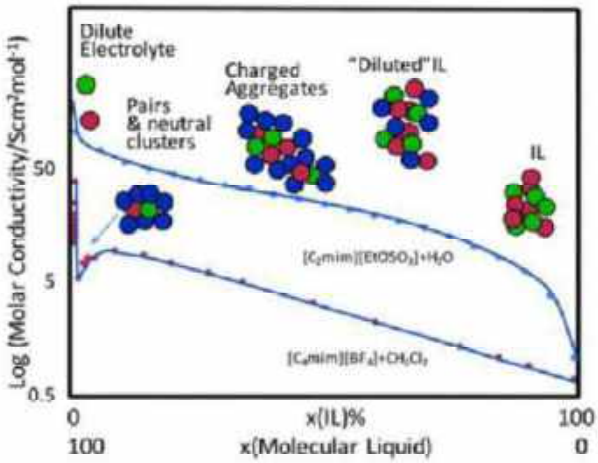

Figure 1.3. Molar conductivity trends in two AILs: water–1-ethyl-3-methylimidazolium ethyl sulfate and dichloromethane–1-butyl-3-methylimidazolium tetrafluoroborate with varying water concentrations. Reproduced from [12].

In mixtures of IL-molecular solvents, at concentrations less than 5 mol% of the IL, the solvent mixture acts as a dilute electrolyte, wherein trends are consistent with trends observed in conventional salts. As the IL concentration increases in these solvent mixtures, physicochemical properties reflect a mixture wherein the two solvents co-exist as co-solvents, both contributing to the overall properties observed. After a specific amount of IL is reached in the mixture, literature suggests that IL overtakes as the primary solvent, wherein IL-IL interactions dominate over interactions between molecular solvent-molecular solvent and molecular solvent-IL properties. ILs dictating the critical micelle concentration (CMC) of an amphiphile during self-assembly in binary mixtures is a prime example of this behaviour.[13] The nanostructure of ILs, segregation of polar and non-polar species, persist for dilutions up to 10 mol% water per IL and it has been shown that water is taken up within polar domains of an IL. This dilution changed the nanostructure by changing the volume fraction of polar and non-polar regions, and in turn changes the CMC.

The concentration ranges and behaviour of these different stages vary for specific ILs and molecular solvents, so it is difficult to make general assumptions regarding the concentration ranges where each solvent dominates as the primary solvent in an IL-molecular solvent mixture. As shown by previous studies, surfactant self-assembly can provide insights regarding the solvent environment in which it occurs. Yalcin et al. has explored the chemical environment of binary PIL-molecular solvent mixtures using dyes as probe molecules. The results indicated that the solvation parameters of the binary mixtures deviated considerably from the ideal solvation behaviour. They suggested preferential solvation was solute-dependent and the results demonstrate using PILs in mixtures with molecular solvents can enhance the solvation capabilities.[14]

1.1.3 Ethylammonium nitrate (EtAN) and ethanolammonium nitrate (EAN)

While AILs have received greater attention in the literature than PILs, the first ionic liquids reported were two prominent protic ionic liquids. EtAN which has a melting point of 52-55 °C was first reported in 1888 by Gabriel and Weiner[2], while EAN with its melting point of 12.5 °C was reported in 1914 by Walden.[15] EAN and EtAN remain a popular choice of PIL due to their low viscosity, melting point and ability to dissolve solutes while being miscible with some molecular solvents, such as water.[14] EAN and EtAN serve as an interesting comparison for PIL structure property relationships due to their very similar molecular structure which leads to widely different bulk solvent properties. The only difference between EAN and EtAN chemically is the presence of a hydroxyl group in EtAN as shown in Figure 1.4.

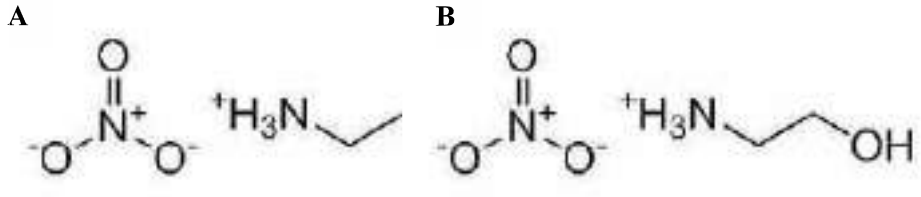

Figure 1.4. The chemical structures of the protic ionic liquids (PILs). A) Ethylammonium nitrate (EAN) and B) ethanolammonium nitrate (EtAN).

This minute difference in chemical structure leads to EtAN having a greater ability to form H-bonds due to the OH group, while in contrast EAN is amphiphilic due to the alkyl chain. While there have been a significant number of literature studies investigating structure property relationships of PILs, investigating how the bulk solvent properties are affected by differences in chemical structure, there are large gaps in our knowledge regarding how interactions with solutes and molecular solvents are affected by these changes in PIL structures. The molecular level interactions due to PIL structural differences and how they affect self-assembly still requires future investigation.

1.2 Novel data analysis techniques for PILs: Machine learning

To thoroughly understand the structure-property relationships of ILs and develop new models for understanding trends and predicting properties, novel data analysis techniques are necessary. There are large datasets for the thermal and physical properties of neat ILs which have been built up over time from research in many different groups.[2, 16-17] In addition, to investigate the vast number of IL possibilities, high throughput experimental methods and computational modelling have been used to screen various ILs solvent properties which can rapidly increase the data available. As the use of ILs combined with a co-solvent is increasing, we need methods to obtain and interrogate this multi-variable data. For all these systems there are likely to be a combination of some dominant trends, along with weaker ones. Consequently, it can be difficult to extract structure-property relationships from IL data, and there is a need for advanced data analysis methods.

Structure-property relationships have been studied, since the natures of the anions and cations, and the interactions between these are usually directly translated to the IL's physical properties. However, quantitative structure property relationship (QSPR) is difficult for ILs and experimentally and/or computationally costly because inter- and intramolecular interactions are not completely understood for all types of ILs. In literature, computational methods such as molecular dynamics[18], Monte-Carlo, ab initio calculations[19], and Conductor-like Screening Model for Real Solvents (COSMO-RS)[20] have been employed. The biggest drawback from these methods is that they are all computationally costly. Similar issues arise with experimental determination of structure-property relationships, with even high throughput methods tending to be laborious for the number of possible ILs.

Machine learning and advancements in artificial intelligence brings forth a new age of QSPR determination. ML models can be devised to understand structure-property relationships of large data spaces, and to predict properties of new structures. This is currently an exciting emerging field in the greater IL community where machine learning models are being devised to interrogate trends in IL data and predict new IL properties.[21] The number of studies using ML in the field of ILs has steadily increased in recent years, as summarised by Figure 1.5.

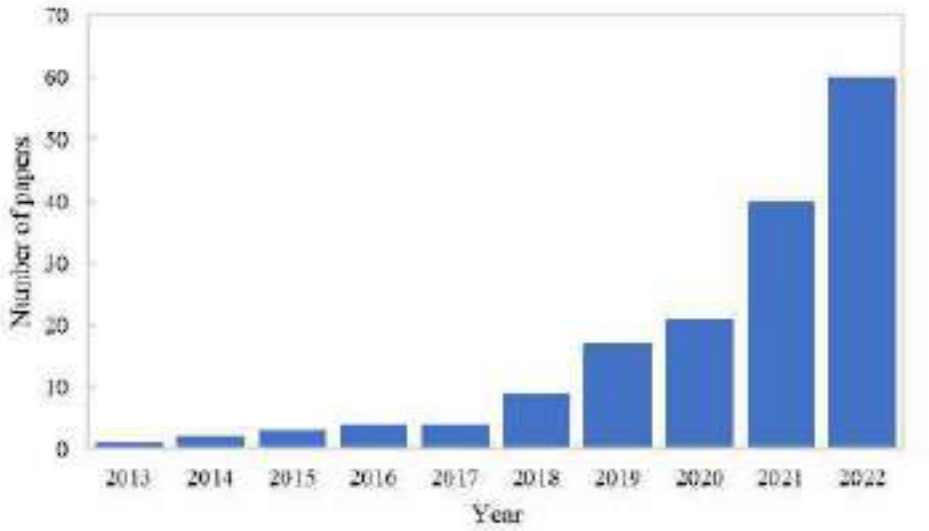

Figure 1.5. Number of search results on webofscience with topics “ionic liquids” and “machine learning” in recent years.

Most existing literature which uses machine learning to investigate ILs focuses on a few physical properties of ILs in the development of their machine learning models and extracts information relevant to these properties from databases. Beckner et al. recently devised an adaptive learning and design strategy using a combination of neural network training, genetic algorithm search and molecular dynamics.[22] They focused on C_p and ρ and used experimental information contained in the ILThermo database as a starting point for training the neural networks. Both Keshavarz et al. and Paduszynski have devised models for predicting ρ,[23-24] while Paterno et al. and Zhao et al. have developed QSPR (quantitative structure-property relationship)[25] models for modelling C_p.[26-27] Ionic liquid toxicity and CO_2 solubility have also been predicted with machine learning models.[28-29] Previously, machine learning has been used to interrogate the IL solvents properties for an experimental dataset in order to understand the relationship between the surface tension and liquid nanostructure and the solvent composition of non-stoichiometric aqueous protic IL solvents.[30] This work suggested that high quality machine learning models can be developed to interrogate IL properties using multiple linear regression (MLR) and artificial neural network (ANN) methods.

There is a noticeable lack of literature when it comes to PILs in the ML literature for IL discovery. This is certainly a topic we need to investigate because unlike aprotic ILs, it is easier to produce PILs in a high throughput manner due to the more straightforward synthesis and purification process.

1.2.1 Machine learning modelling method

The data requirement for machine learning varies greatly based on what information is intended to be gathered from the model. For the models and data sets we will discuss in this thesis, machine learning was performed on datasets with 20 or more values. While it is imperative to have a large enough dataset to perform machine learning models on, it is even more important to have a wide variety of data from trusted sources. This data was then separated into training and test data. A subset of the data was used

for training the model, and this model was then tested on the complete data set. In this study, two types of machine learning algorithms will be explored: multiple linear regression (MLR) and artificial neural networks (ANN). These algorithms were chosen as representative models due to their simplicity and their success in literature for use with IL systems.[9, 31]

MLR can give insights regarding the structure property relationships of an IL data set. It is a statistical regression model, which is simple in nature, and seeks to find linear relationships between variables, while assigning a weighting to each factor. MLR algorithms will be created with input descriptors, as according to the generalised model equation noted in Equation 1.1:

$$Y_i = Int_i + \sum_{n=1}^{a} C_{x,i} X_n \quad (1.1)$$

Where Y_i is the generated output variable, Int_i are the intercepts, C_i are the regression coefficients and X are the selected input descriptors.

ANN are non-linear models which can be generated with the same input variables. Much like the neural networks in our brains, artificial neural networks seek to emulate a simplified version of how neurons in our nervous system operate, establishing connections between different nodes in the system. The one used in this study is a three-layer network with a hidden layer node which will result in a single output node. A schematic of an ANN model is shown in Figure 1.6.

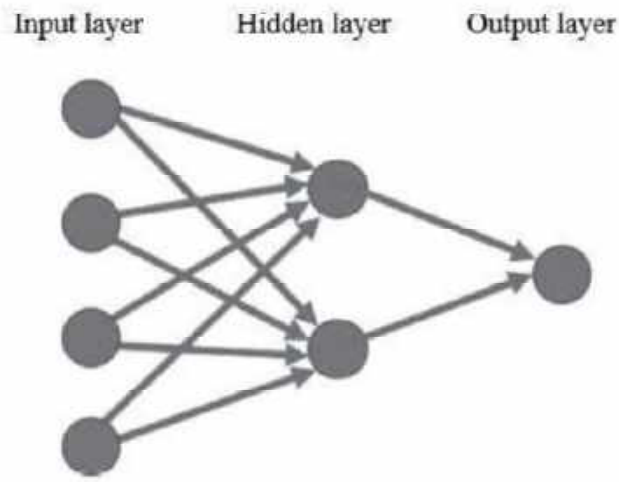

Figure 1.6. Illustration of a simple artificial neural network model. Reproduced from [32].

The different models will be assessed to determine the best model for investigating the dataset for the current study. The MLR will be used to understand the complex physicochemical properties and their relationships with the structure of ILs and ANN will be used for predicting properties of new ILs.

1.2.2 Descriptors

Descriptors are used to describe a material in quantified ways a ML model can understand them. These descriptions can range from composition of starting materials used during the synthesis process to microscopic and macroscopic properties of the material. Molecular descriptors can be categorised into broad categories which include:

- Constitutional: information about atom types
- Topological: descriptions of how atoms are connected and their resulting properties
- Physicochemical: properties such as solubility, charges, dipole moment
- Structural: descriptions of size, shape and surface properties of molecules
- Quantum-chemical: partial charges, polarizability, orbital energies etc calculated using density functional theory (DFT), and ab initio quantum-chemical programs.

These descriptors can be calculated using software such as DRAGON and CODESSA and the choice of descriptors are important to the quality of the model predictions. The calculated descriptors are usually sifted to find the non-zero and non-correlated descriptors before they are used in the model. For example, in the case of ILs, it is important to include key constitutional descriptors about the cations and anions of the ionic liquids, as well as physicochemical and structural information about the bulk liquid properties.

1.2.3 Performance of models

To ensure the accuracy and usefulness of the model, statistical criteria are used to assess them. These variables are approximated by dividing the available data into a training set and a test set. The variables calculated include R^2 (the coefficient of determination), which is the square of the correlation coefficient between the training and test sets. The standard error of estimation (SEE) and standard error of prediction (SEP) can also be calculated to assess the robustness of the models using the root mean square values of the difference between training and test sets of data. The standard error can be calculated using equation 1.2 below:

$$\sigma = \sqrt{\frac{\Sigma(Y_{measured} - Y_{predicted})^2}{Total\_entries}} \qquad (1.2)$$

The SEE and SEP are the preferred assessment of quality of the models because unlike R^2, they are independent of the number of data points in the training set or the number of descriptors. Successful models tend to have R^2 values close to 1 and their SEE and SEP values are similar and small.

1.3 Amphiphile self-assembly

Self-assembly is the spontaneous aggregation of molecules into 3-D nanostructures.[33] Amphiphiles are molecules containing polar hydrophilic and nonpolar hydrophobic constituents which display self-assembly behaviour in selective solvents. Water is by far the most commonly used and well-studied solvent available for amphiphile self-assembly. Model amphiphiles such as polymers and surfactants, are important to gain understanding of solute-solvent interactions. The self-assembly of amphiphiles in solvents can give us insights regarding the solvation properties and the solvent environment of ILs.[13, 34-36]

1.3.1 Surfactants for self-assembly

Amphiphiles are molecules which consist of both hydrophilic and hydrophobic components. In most cases the hydrophobic part is a long hydrocarbon chain while the hydrophilic head of the amphiphile can be non-ionic or ionic. Non-ionic surfactants often consist of a hydrophilic poly(ethylene oxide) chain, connected to a hydrophobic alkyl chain, such as the polyoxyethylene alkyl ethers, C_nE_m. Anionic surfactants are widely used as detergents and soaps for cleaning purposes and have a negatively charged headgroup consisting of sodium, potassium, or ammonium ions. Cationic surfactants consist of positively charged headgroups such as a quaternary ammonium or a halide ion. Cetyltrimethylammonium bromide is one of the most widely used cationic surfactants. Amphiphiles are also referred to as surface active agents, or surfactants, because of their ability to reduce interfacial tension due to their amphiphilicity leading them to migrate to the interface.

The surfactants chosen as model amphiphiles during the current study are shown in Figure 1.7. These consist of the cationic surfactant cetyltrimethylammonium bromide (CTAB), a nonionic amphiphile tetraethylene glycol monododecyl ether ($C_{12}E_4$), as well as sodium octyl sulfate (SOS), an anionic surfactant with a shorter alkyl chain than the commonly used sodium dodecyl sulfate (SDS).

A **B**

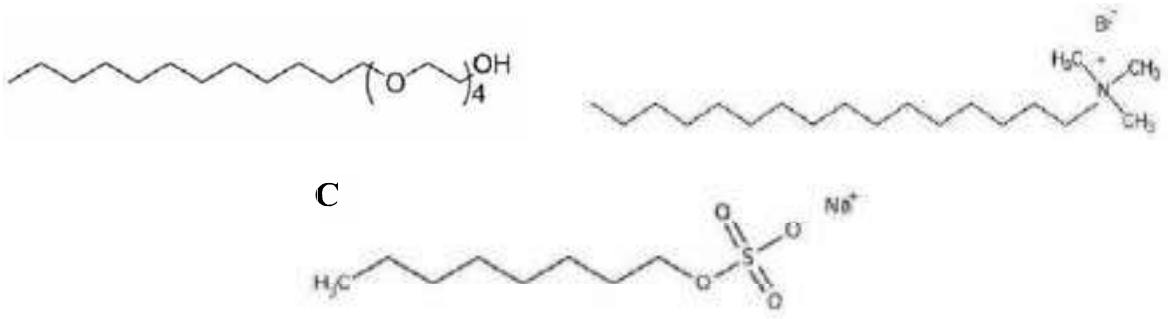

Figure 1.7. The chemical structures of solutes used during study: A) tetraethylene glycol monododecyl ether ($C_{12}E_4$), B) cetyltrimethylammonium bromide (CTAB) and C) sodium octyl sulfate (SOS).

Both CTAB and $C_{12}E_4$ have previously been shown to self-assemble into micelles in PILs, including EAN and EtAN.[37-38] These micelles tend to have up to 2 times higher critical micelle concentrations compared to that in water. The common anionic surfactant of SDS has limited solubility in PILs, therefore SOS, a surfactant with a shorter alkyl chain was selected to improve solubility. SOS has previously shown to form micelles in water and mixed catanionic systems (cationic and anionic mixtures)[39] but there are currently no studies exploring them in ILs. While there are some studies exploring EAN-molecular solvent mixtures and their effect on surfactant self-assembly, there are no comprehensive studies which explore the full range of concentrations.[13, 34, 40] There is also a gap in the literature when it comes to anionic surfactants. A comprehensive literature review of these surfactants and existing studies are described in later sections.

1.3.2 Self-assembly in water

In the case of water, amphiphiles tend to form 3-D structures so that the hydrophobic part of the molecule is secluded from the water by the hydrophilic parts, through the hydrophobic effect. At low concentrations, amphiphiles self-assemble into different shapes such as spheres and cylinders, based on their geometry.[41] These are named micelles. At higher concentrations, the order of the structures being formed increases and, the micelles can form hexagonal, lamellar or cubic phases.[42] Figure 1.8 illustrates some of the 3-D structures which can be formed by amphiphiles during self-assembly.

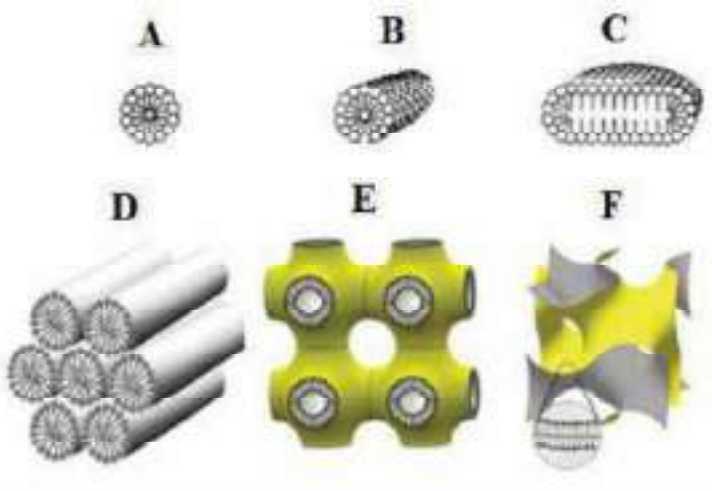

Figure 1.8. Structures of amphiphile self-assembly phases. (A) spherical micelles; (B) cylindrical micelles; (C) bicelles (disks); (D) hexagonal phase; (E) bicontinuous cubic phase Im3m; (F) bicontinuous cubic phase Ia3d. Adapted from [43].

Micelle shapes observed via SAXS can vary based on critical packing parameter (CPP),

$$C_{pp} = \frac{v}{al_c} \tag{1.3}$$

where v= the volume of the hydrocarbon, a= the effective area of the head group, and l_c= the length of the lipid tail(s). Based on the CPP, the shapes can range from spherical micelles, bilayers to inverted micelles (hexagonal phase). Figure 1.9 summarises the range of different shapes available for surfactants to form as CPP varies.

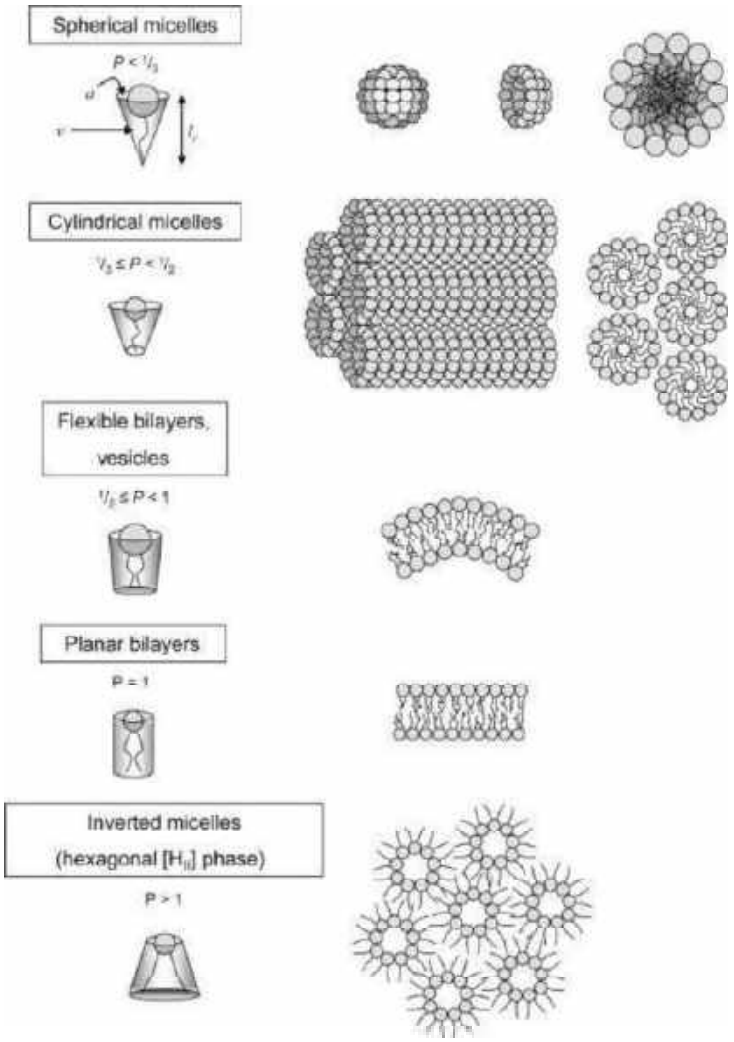

Figure 1.9. Micelle shapes varying due to critical packing parameter. Reproduced from [44].

The micelle behaviour of the chosen surfactants in water has been extensively studied in literature. CTAB and SOS have also been investigated in literature as a binary mixture, as summarised in phase diagrams in Figure 1.10.

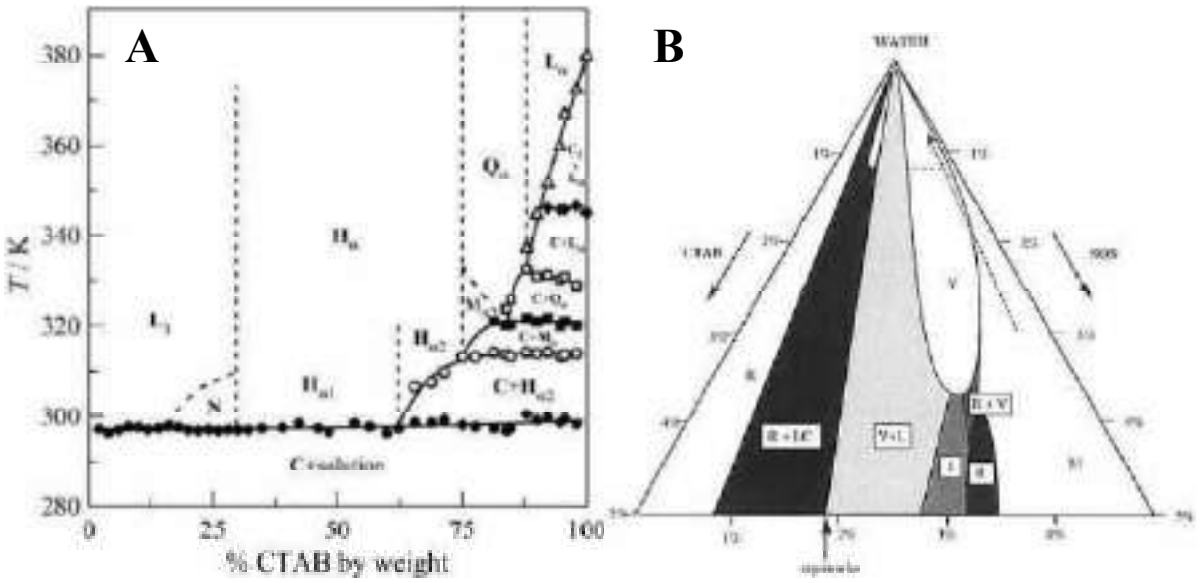

Figure 1.10. A) Phase diagram for CTAB-water, reproduced from [45] and B) CTAB-SOS-water at 25 ℃, reproduced from [46].

Phases formed during self-assembly in CTAB range from micelles at low concentrations of the surfactant to lamellar, hexagonal and cubic phases at higher concentrations and temperatures. In SOS, a lesser range of phases are observed. Only vesicles and micelles are observed in SOS-water binary systems. For CTAB, the Krafft temperature, minimum temperature micelles formation can begin, of 32°C[45] must be achieved before it can form liquid crystal (LC) phases in water. Phases ranging from SOS-rich vesicles (V), rodlike micelles (R) to SOS-rich micelles (M) are observed in CTAB-SOS-water systems at room temperature. It is also worth noting that only up to 5% SOS and CTAB were included in this phase diagram. This falls well within the concentration range for only micelles. Higher order phases have been observed with CTAB in water[47], but no studies could be found exploring SOS LCPs. The critical aggregation concentration (CAC) for pure SOS was observed to be two orders of magnitude higher than that of pure CTAB and three orders of magnitude higher than that of the mixtures.[39] For $C_{12}E_4$, lamellar phases were observed in water.

1.3.3 Self-assembly in ionic liquids

The driving force behind self-assembly is the energy minimisation obtained via segregation of the water-like and "oil"-like components. Solvophobicity is a summary of the driving forces, which combines all the different solvent properties that are beneficial to self-assembly, such as cohesive energy, solvent structure, polarity and the ability to form hydrogen bonded networks, and is the more general term compared to hydrophobicity which is specific to water.[48]

ILs have garnered a lot of interest in recent years due to many having the ability to support surfactants to self-assemble into 3D structures.[36] Non-aqueous solvents which were known to promote self-assembly were very limited prior to this discovery, with only about 14 known molecular solvents being capable of supporting self-assembly.[36] Since the initial discovery that EAN is a solvent which promotes self-assembly, over 40 PILs have shown their potential to support self-assembly. [10] While ILs can support the self-assembly of higher order phases, such as liquid crystal phases (LCPs), the content of this thesis focuses mostly on micelle formation as they are often the simplest form of self-assembly.

Cationic surfactant self-assembly in IL-water mixtures with up to 20 wt% water was investigated by Javadian et al. in their study looking at CTAB self-assembled structures in aprotic imidazolium-based IL-water mixtures.[47] Larger micelles and higher CMC were observed in the IL-water mixtures than in water and they were able to distinguish that the hydrogen bond was an important factor in defining the solvent properties.[47] Smirnova et al. and Sohrabi et al. explored the anionic surfactant, SDS, in imidazolium-based IL-mixtures for mole fractions 0.1-0.9 of the IL in water and found that small additions of the IL substantially decreased the CMC of SDS, leading to the formation of mixed micelles where IL acts as a co-surfactant.[49-50] Sohrabi et al. hypothesised that the decrease in CMC could be attributed to reduction in electrostatic repulsion between headgroups.[50] He et al. has explored the pluronic polymer P123 in EAN at dilute concentrations, up to 2 M, to compare the effects with a salt and an aprotic IL with similar conclusions and found the formation of mixed micelles at low CMC.[51]

Most of these studies focus on dilute IL-molecular solvent mixtures, where the IL can be considered as acting more as a salt additive than a co-solvent. They also focus on aprotic ILs, which have noticeable differences in bonding and solvation compared to PILs. Only a handful of studies could be found in which micellization was investigated in mixtures of PILs with high IL concentrations. Wakeham et al. reported the behaviour of the non-ionic surfactant $C_{14}E_4$ in binary ionic liquid mixtures and ionic liquid-water mixtures of ethylammonium nitrate and ethanolammonium nitrate.[52] They suggested that the CMC of the surfactant strongly correlated to the solvent composition, with an increase in CMC proportional to the PIL concentration. Bryant et al. has investigated the effect of EAN on cationic and anionic surfactants, in which they concluded that the CMC of cationic surfactants are much higher and micelles much smaller in the IL mixture than in water, whereas anionic micelles were less affected.[34] Lam et al. investigated the cationic surfactant DTAB in IL-water mixtures up to neat EAN, where they determined that at low IL concentration, ILs behaviour is similar to that of a simple electrolyte. Then as IL concentration increases beyond the saturation points of most conventional salts, the IL nanostructure influences micellization, raising the CMC.[13] Due to solubility issues with most anionic surfactants in PILs, no studies could be found exploring anionic surfactant self-assembly in aqueous PILs.

The self-assembly of surfactants can be used to understand the solvent environment in which they form nanostructures. It is difficult to determine the concentrations at which the IL and water are dominating the self-assembly process, particularly due to a lack of consistency in concentration units, with mol% and wt% both commonly used.

We also cannot make conclusions regarding the trends due to the variety of ions and how differently they influence self-assembly. To expand on the findings by Bryant et al. mentioned earlier, they explored the difference in self-assembly in EAN and EtAN. The only difference between the two ILs chemically is the extra hydroxyl group in EtAN. When the CMC of a non-ionic surfactant in the two

ILs are observed in the presence of water, it can be noted that the CMC behaviour in EAN is wildly different to EtAN. As depicted in Figure 1.11, in EAN the CMC linearly increases as the concentration of the IL increases in the binary solvent mixture. It is worth noting that in the study weight percentages were used, which does not allow for a direct comparison between ILs, which can only be done by using mol%.

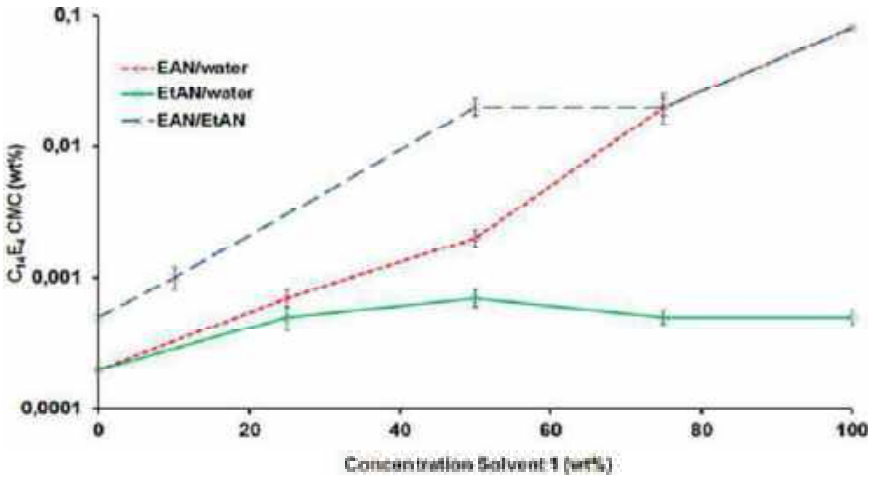

Figure 1.11. The critical micelle concentrations of the non-ionic surfactant $C_{12}E_4$ in binary mixtures of EAN, EtAN and water. Reproduced from 52.

Lam et al. have observed surfactant self-assembly in ethylammonium nitrate, ethanolammonium nitrate and propylammonium nitrate aqueous solvent mixtures with a cationic surfactant, dodecyltrimethylammonium bromide (DTAB).[13] This was also done in wt%, and only 4 concentrations (25, 50, 75 wt% and neat) were explored. They hypothesised that EAN acted as a co-surfactant rather than a co-solvent in mixtures with water, leading to mixed micelles. This was not observed with EtAN due to the presence of the hydroxyl group making it not possible for it to act as an amphiphile. The study on catanionic mixed surfactants by Bryant et al. explored how nanostructure of ILs affected self-assembly of surfactants.[34] They hypothesised that EAN acted as a smaller surfactant rather than a solvent species during their neutron scattering studies and that EtAN and EtAF are better suited as self-assembly media due to their non-amphilicity.

1.3.4 Characterisation of self-assembly

To understand self-assembly in ILs and IL mixtures, the characterisation process requires the use of different techniques. The complexity of the ILs at the molecular level necessitates the use of a combination of both experimental and simulation techniques. This thesis explores using surface tensiometry and small angle x-ray scattering (SAXS) to investigate micelle formation in ILs and IL-water mixtures experimentally. Cross polarised microscopy was also used to assess whether the mixtures investigated can form higher order phases. Other methods such as small angle neutron scattering (SANS) could also be used for this purpose. However, due to the circumstances during which this thesis was completed with multiple lengthy lockdowns during Covid, neutron facility access was unavailable.

1.3.4.1 Characterising self-assembly using surface tensiometry

Micelle formation during self-assembly causes changes to the surface tension of the bulk solvent environment it occurs in. These changes to the surface tension can be used to understand the concentrations at which micellization first occurs. Surface tensiometry measures the surface tension of liquids and surfaces. In this study, it was used to measure changes in surface tension of the solvent-surfactant samples as the amphiphile first begins to self-assemble or aggregate. There are various ways to measure surface tension. The technique used during this study uses the Du Noüy–Padday method, where a probe is inserted into a liquid and the force required to remove it from the surface was used to measure the surface tension.

At very dilute amphiphile concentrations, as the number of surfactants increases, they dissolve in the solvent and begin to aggregate at the air-solvent interface. This leads to a decrease in surface tension. Above a transition concentration, self-assembly of the surfactants begins and the decrease in surface tension plateaus to a constant value. The concentration at which this occurs is referred to as the critical

micelle concentration (CMC). The change in surface tension during the self-assembly process is illustrated in Figure 1.12.[53]

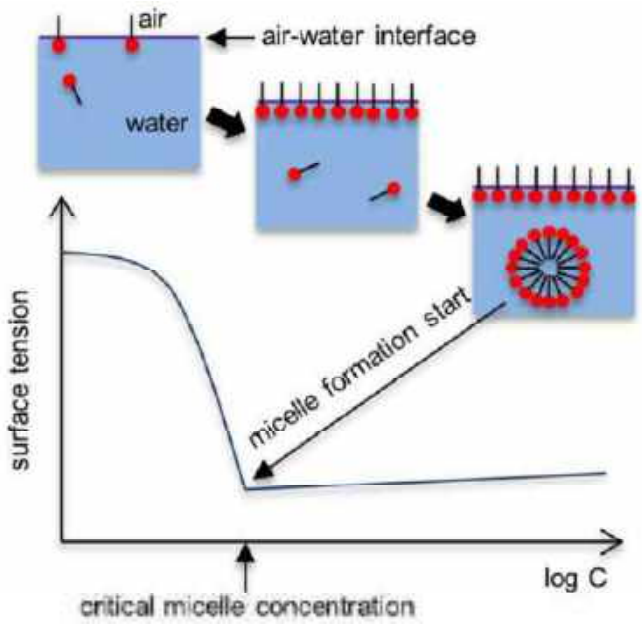

Figure 1.12. Schematic of the change in surface tension observed during micelle formation. Reproduced from [53].

The surface tension measurements and the CMC allow us to gain insight into the interactions occurring in the solvent environment due to self-assembly. The maximum surface excess concentration, Γ_{max}, at the air/liquid interface can be calculated by Equation 1.4, where the quantity inside the brackets is the negative gradient at surfactant concentration just below the CMC,

$$\Gamma_{max} = -\frac{1}{2.303RT}\left(\frac{d\gamma}{d\log(\text{amphiphile concentration})}\right) \quad (1.4)$$

where R is the gas constant and T is the temperature. The surface excess concentration gives insight regarding the position of surfactants in the system and the force exerted by them on the surface. Accumulation of surfactants at the interface leads to positive surface excess concentrations, whereas negative values indicate the surfactants are more likely to be found in the bulk.[54] Using the surface

excess concentration, the minimum molecular areas of the surfactants absorbed at the interface, A_{min} can be calculated,

$$A_{min} = \frac{10^{20}}{N_A \Gamma_{max}} \quad (1.5)$$

where N_A is the Avogadro's constant.

The standard free energy of micellisation, ΔG_m^o, and the standard free energy of adsorption, ΔG_{ad}^o, can also be calculated using the CMC and A_{min} using Equations 1.6 and 1.7,

$$\Delta G_m^0 = RT \ln(CMC) \quad (1.6)$$

$$\Delta G_{ad}^0 = \Delta G_m^0 - (\gamma_o - \gamma_{CMC}) \times A_{min} \quad (1.7)$$

where γ_0 is the initial surface tension and γ_{CMC} is the surface tension recorded at the CMC. [55]

Positive free energy parameters indicate the process requires an external input of energy, whereas negative values are expected for a spontaneous process such as self-assembly. These parameters are useful for comparing the energies and micellization process of surfactants in different solvent environments.[33]

1.3.4.2 Micelle confirmation using Small Angle X-ray Scattering

To interrogate the size and shape of self-assembled structures, scattering techniques can be used. Small Angle X-ray Scattering (SAXS) is a structural analysis technique, capable of providing information such as size and shape of particles as well as internal structural information of systems by measuring the fluctuations of electronic densities in the matter. SAXS involves elastic scattering of hard X-rays

(0.07 – 0.2 nm) from a sample and recording the scattering at small angles (0.001 - 1°). The experimental process for observing micelles using SAXS is summarised in Figure 1.13.

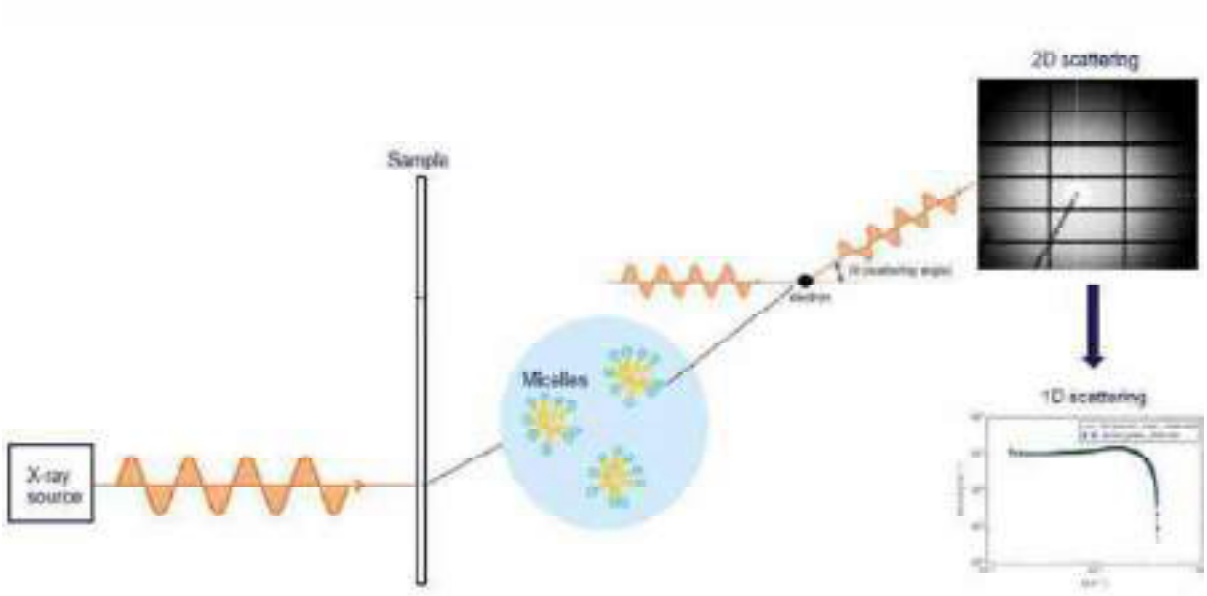

Figure 1.13. Schematic of experimental workflow of SAXS on micelle samples, from scattering to mathematical fitting.

The contrast in the micelle mixtures during SAXS arises due to their electron scattering length density (SLD) differences. SLD can be computed from the scattering lengths and material densities. For x-rays, the scattering arises from the interaction between the incident wave and the electron clouds of the atoms in the material and varies based on the composition of the surfactant components.

The scattering information can be fitted to mathematical models to determine physical properties such as size and shape of the particles in the sample. For example, if a sample contained dilute spherical structures the scattering intensity function I(q) can be described by the Equation 1.8:[56]

$$I(q) = \frac{scale}{V} \cdot \left[\frac{3V(\Delta\rho)\big(\sin(qr) - qrcos(qr)\big)}{(qr)^3}\right]^2 + bkg \quad (1.8)$$

Where scale is a volume fraction, V is the volume of the scattering particle, r is the radius of the sphere and bkg is the background level. The 2-dimensional scattering is also described by Equation 1.8, regardless of the orientation of the q vector. Fitting the scattering curves of gathered experimental data to similar models will allow for determination of the nanoscale structural properties. Structure factors were not necessary for these fits during the current study as all systems were dilute.

1.3.4.3 Cross polarised optical microscopy

Cross polarised microscopy (CPOM) has been extensively used in the literature to qualitatively observe higher order phases during self-assembly. It is a technique where samples are placed between crossed polarisers. In birefringent samples, the polarised light interacts strongly with the sample, leading to a non-zero intensity, with patterns characteristic of different phases. Due to the alignment of the surfactants in various nanostructures during self-assembly, the birefringence of the sample changes as the phases change. Figure 1.14 showcases common liquid crystal phases (LCP) observed in PIL-surfactant systems with cross polarised microscopy.

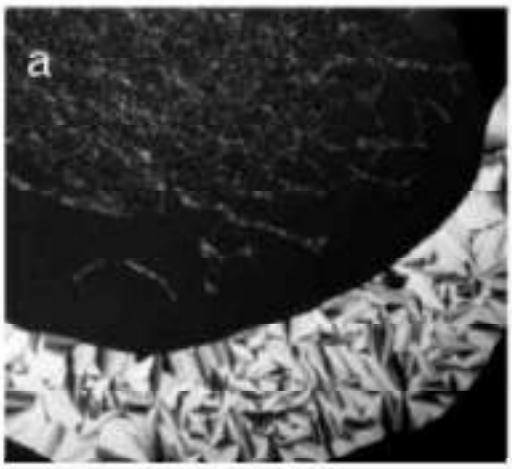

Figure 1.14. Cross polarised optical microscopy images of penetration scans of propanolammonium formate and CTAB showing anisotropic hexagonal, isotropic cubic and anisotropic lamellar phases. Reproduced from [57].

As the surfactant concentration increases, the likelihood of forming higher order phases increases. In EAN and EtAN, there are three common liquid crystal phases which are observed: H_1: hexagonal phase, V_1: Cubic phase, as well as L: Lamellar phase. Both EAN and EtAN have previously been shown to promote LCP with cationic surfactants such as CTAB and DTAB.[58] There is less information in the literature regarding anionic and non-ionic surfactant higher order self-assembly in PILs.[37]

1.4 Modelling of molecular dynamics of PILs with solutes

While it is possible to hypothesise the interactions between solutes and the solvent environment based on experimental techniques, simulations allow us to approximate and validate these results. There are a host of simulation techniques which can emulate physical systems in varying timescales and length scales, ranging from density functional theory (DFT) simulation to Monte Carlo. Molecular dynamics (MD) simulations can simulate all atoms in system with millions of atoms for timescales up to milliseconds, as illustrated in Figure 1.15.

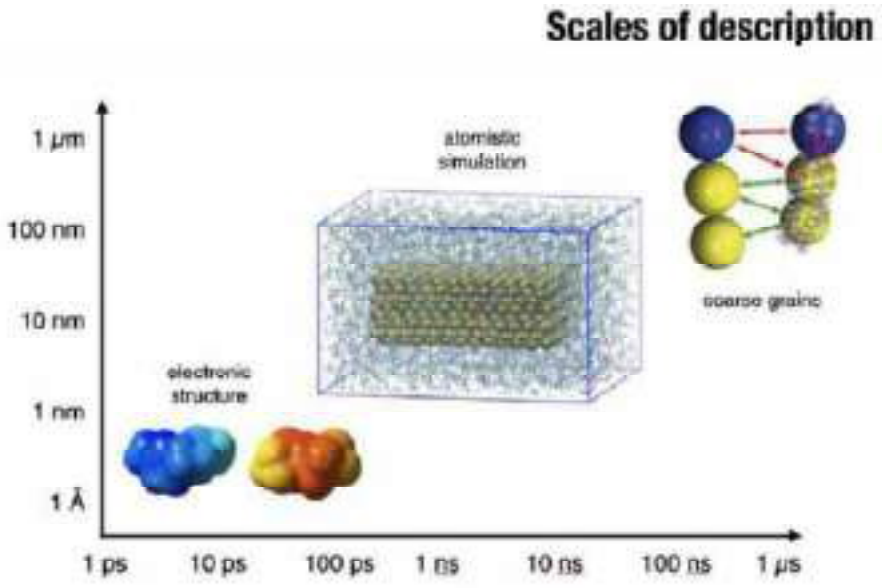

Figure 1.15. Scales of descriptions in simulations situating where molecular dynamics simulations capacities lie in comparison to other methods. (Schematic provided by: Agilio Padua)

MD simulations have been used extensively for AILs in literature. Sprenger et al. has reported that the generalised AMBER force field can simulate a variety of ionic liquids and accurately predict thermodynamic and transport properties.[59] Doherty et al. has also used OPLS (Optimized Potentials for Liquid Simulations) based force fields to simulate imidazolium, pyridinium and choline based ionic liquids with properties for densities, viscosities, diffusion coefficients and surface tensions comparable to experimental results.[60] The main issue associated with classical force fields such as OPLS is that they do not account for polarizability. These models describe electrostatic interactions in terms of a fixed charge, which is not the case in experiments. OPLS based force fields attempt to account for this by scaling the charges of the atoms to mimic polarisation and charge transfer effects. However, this could potentially lead to degradation of intermolecular interactions at short ranges.[60] The classical models are unable to model diffusion correctly, which is an important property for simulating liquids and their interactions.

1.4.1 Molecular dynamics simulations

MD simulations are used to understand the movement and interactions of systems at an atomic or molecular level. MD simulations use Newton's second law of motion,

$$F = ma \tag{1.9}$$

where F is the force acting on a particle, calculated by its mass, m, and acceleration, a. Every atom in an MD simulation is assigned a random initial velocity and the force acting on this atom in a specific timestep is used to calculate the new position and velocity. The projected trajectory of the atoms and molecules over a specified time period is calculated by repeating this process.

Forcefields are energy functions which describe the geometry of a molecule and allow for the calculation of the potential energy of the system. Forcefields are defined for each different type of

molecule present in an MD simulation. The energy function is derived from Newton's equations for motion. These energy functions have two components: bonded and non-bonded terms. The bonded terms contain information about the bond lengths, angles and dihedrals. The functional form of the OPLS forcefields used in the thesis for IL and surfactant simulations is shown in Equation 1.10,

$$PE = E_{bonds} + E_{angles} + E_{dihedrals} + E_{nonbonded} \tag{1.10}$$

where:

$$E_{bonds} = \sum_{bonds} K_r(r - r_0)^2 \tag{1.11}$$

$$E_{angles} = \sum_{angles} K_\theta(\theta - \theta_0)^2$$

$$E_{dihedrals} = \sum_{dihedrals} K_\phi(1 + \cos[n\phi - \gamma])$$

$$E_{nonbonded} = \sum_{i<j}^{atoms} \varepsilon_{ij}\left[\left(\frac{r_m}{r_{ij}}\right)^{12} - 2\left(\frac{r_m}{r_{ij}}\right)^{6}\right] + \frac{q_i q_j}{4\pi\varepsilon_0 r_{ij}}$$

The bonds and angles are modelled as simple harmonic oscillators and described by Hooke's law where K is the force constant, r is bond length and θ is bond angle. The energy terms for dihedrals are expressed by a cosine series expansion where n is the number of minima as the bond rotates and γ is the phase factor, which determines the minimum value of the dihedral.

The non-bonded term includes the van der Waals forces and electrostatics. The van der Waals forces are modelled using the Lennard-Jones 6-12 term, which is a simplified model for describing interaction between two particles at a specific distance. The electrostatics are expressed via Coulomb's law where each atom is given a partial charge and their energy is determined as a sum of interactions of point

charges. The non-bonded terms are more computationally expensive and the cut-off for non-bond interactions range from 8-15 Å, with a longer cut off resulting in greater accuracy at the cost of longer computational time. Generally, long-range electrostatics beyond the cut-off are approximated by an Ewald mesh approximation.[61] MD simulations are usually performed under two conditions: NVT (constant volume and temperature) and NPT (constant pressure and temperature). The thermostat used in simulations allows particles to move via the kinetic energy corresponding to the set temperature while the barostat allows the system to equilibrate to the correct density. The constraint algorithm LINCS (Linear Constraint Solver) can be used to fix the bond lengths and allow for larger timesteps.

1.4.2 MD of ILs

While there have been efforts to establish forcefields for PILs, especially EAN, only very recently has a polarised forcefield for EAN been published.[62] Due to the hydrogen bonding prevalent in EAN and other PILs, it has been shown to be difficult to design and implement MD simulations of PILs and mixtures.[62] While most effort has been concentrated on establishing forcefields, there is currently a gap in literature when it comes to combining the available PIL forcefields with molecular solvents and solutes. OPLS based force field for EAN has been revised to provide better reproduction of the experimental density and dielectric constant.[14] These solvent models, along with the OPLS force field for surfactants, have been used to simulate mixtures of micelles in IL-water mixtures in this thesis.

Mixtures of PILs with molecular solvents have not been explored extensively in literature using simulations, perhaps in part because it is important to fully understand the force fields being used for different constituents of a molecular dynamics simulation before they can be simulated together. Most notable studies exploring PIL mixtures using MD simulations include a study by Docampo-Álvarez et al., wherein they investigated the self-assembly of EAN in solutions of water, ethanol and methanol. [63] Their EAN model was an OPLS-AA based force field and a TIP5P water model was used. The compatibility of these two force fields is unclear, which could have resulted in inconsistencies.[63] Huang

et al. has also explored OPLS based EAN in different concentrations of water, which was described by the TIP3P water model.[64] Again, the lack of consistency of the force fields for IL and molecular solvent raises the need for a comprehensive comparison of different water models and IL force fields.

1.5 Scope of the research

The overall objective of this thesis was to understand the behaviour of protic ionic liquids, with a focus on EAN as a representative PIL, in mixtures with water and various amphiphilic solutes using both experimental and computational tools. Due to the wide variety of techniques used during this project, the details of the methods are included in each chapter, rather than as a separate methods chapter.

Specific aims included:

1. Understanding solvent properties of IL-molecular solvent mixtures.
    a. Viscosity and ionic conductivity of neat ILs were explored using machine learning models.
    b. Surfactants were used as probes to understand mixtures of IL-water.
2. Creating machine learning models to investigate physicochemical property relationships of ionic liquids.
    a. Based on literature values, multiple linear regression and artificial neural network models were created and 10 new ionic liquids were synthesised and characterised experimentally to verify the models.
3. Understanding the interaction of IL mixtures and various ionic and non-ionic solutes.
    a. Three surfactants were chosen as model solutes and their interactions in ethylammonium nitrate (EAN) and ethanolammonium nitrate (EtAN) were explored in the presence of water.
4. Optimising molecular dynamics simulations to understand the interactions of ILs in mixtures at a molecular level.

a. To confirm the presence of micelles in surfactant-IL-water simulations, molecular dynamics simulations were used.
b. How the solvation of the micelle varies as the concentration of the IL present changes was observed.

Chapter 2 examines using machine learning as an advanced analysis technique for understanding trends in physicochemical properties of PIL, taking into consideration their water content. It also examines the capacity of machine learning to extend beyond the capabilities of an analysis technique and looks at the feasibility of using machine learning for predicting the physical properties of viscosity and ionic conductivity of new ILs.

To extend the understanding of PIL-water mixtures obtained in Chapter 2, the representative PIL of EAN was chosen for further experimental investigation in **Chapter 3. Chapter 3** investigates the effect of ionicity of surfactants on the self-assembly of three surfactants in mixtures of PIL-water solvent systems. This chapter systematically examined the effect of changing the ionicity of the surfactant across the IL-water concentration range to understand the solvation effects of ILs in systems where self-assembly is occurring. The CMC of the IL-water-surfactant systems were obtained using surface tensiometry measurements and the formation of micelles was confirmed using SAXS measurements. Cross polarised optical microscopy was used to identify higher order liquid crystal phases in the solvents.

Chapter 4 looks at furthering our understanding of using MD simulations to investigate mixtures of ILs and water. This chapter focuses on choosing the optimal water model for use in conjunction with existing force fields for ILs, which was used for multi-component systems of PIL-water-solutes.

Chapter 5 verifies the experimental results from Chapter 3 using the preliminary results for MD simulations gathered in Chapter 4. Finally, molecular dynamics simulations were performed for EAN-water-surfactant systems to understand the interactions at a molecular level of the experimental results from Chapter 3.

Chapter 6 includes concluding remarks and recommended future work.

2 Machine learning for investigating IL-mixtures

This chapter has contributed largely to the publication: Dung Viet Duong, Hung-Vu Tran, **Sachini P K Pathirannahalage**, Stuart Brown, Michael Hassett, Dilek Yalcin, Nastaran Meftahi, Andrew J Christofferson, Tamar L Greaves, Tu C Le. *Machine Learning Investigation of Viscosity and Ionic Conductivity of Protic Ionic Liquids in Water Mixtures*. J. Chem. Phys. 156, 154503 (2022). This chapter details the experimental work, and the interpretation of the machine learning models I completed in support of the publication. Full publication can be found in the Appendix.

2.1 Introduction

Ionic liquids (ILs) are designer solvents consisting of a vast sample space of possible cations and anions, with an estimated $10^{14\text{-}18}$ configurations of possible ionic liquids. To thoroughly understand the structure-property relationships of ILs and develop new methods for predicting properties of new ILs, novel data analysis techniques are necessary to investigate the existing body of experimental data. In addition, to investigate the vast number of IL possibilities, high throughput experimental methods have been used to screen various ILs solvent properties which has rapidly increased the data available. Therefore, there are large datasets for the thermal and physical properties of neat ionic liquids which have been built up over time from research in many different groups.[2, 16-17]

The use of ILs combined with a co-solvent is also increasing in recent years, and new methods are required to obtain and interrogate data from multivariable systems. Thus, it can be difficult to extract structure-property relationships from IL data using conventional analysis techniques, and there is an urgent need for advanced data analysis methods. Previously, machine learning (ML) has been used to interrogate the IL solvents properties for an experimental dataset in order to understand the relationship between the surface tension and liquid nanostructure and the solvent composition of non-stoichiometric aqueous protic IL solvents.[30] This work suggested that high quality machine learning models can be

developed to interrogate IL properties using multiple linear regression (MLR) and artificial neural network (ANN) methods.

Using statistical systems, ML can provide insights into structure-property relationships, while also allowing for predictions of properties of new ILs. While ML has been used extensively in fields such as drug discovery, IL researchers have only scratched the surface of the capabilities of using statistical analysis for IL property prediction. A recent review by Koutsoukos et al. summarises the studies conducted so far in the area of IL discovery using ML and demonstrates the newfound interest in our field regarding the capabilities of ML.[21]

Existing literature on using ML for ILs focuses on a few physical properties of ILs in the development of their machine learning models and extracts information relevant to these properties from databases. Beckner et al. recently devised an adaptive learning and design strategy using a combination of neural network training, genetic algorithm search and molecular dynamics.[22] They focused on heat capacity (C_p) and density (ρ) and used experimental information contained in the ILThermo database as a starting point for training the neural networks. Both Keshavarz et al. and Paduszynski have devised models for predicting ρ,[23-24] while Paterno et al. and Zhao et al. have developed QSPR (quantitative structure-property relationship)[25] models for modelling C_p.[26-27] Ionic liquid toxicity and CO_2 solubility have also been predicted with machine learning models.[28-29]

There is a noticeable lack of literature when it comes to PILs in the ML literature for IL discovery.[9] This is certainly a topic worth investigating because unlike aprotic ILs, it is easier to produce PILs in a high throughput manner due to the more straightforward synthesis and purification process, which can then be characterised using automated approaches. An example of this was done using automated robotic system Chemspeed to create PILs.[4] This enables the collection of experimental data from libraries of PILs, which allows us to make ML models with consistent datasets under the same

experimental settings. The quality of the input data is one of the main factors in producing a good ML model with a high R^2 value.

This chapter of the thesis is dedicated to using existing literature data to develop ML models which can predict the viscosity and conductivity of PILs, with a focus on understanding how the presence of water impacts these properties. New PILs were then synthesised and characterised to test the accuracy of the created MLR and ANN models. This work has contributed to a publication.[65]

2.2 Method

2.2.1 Computational method

Experimental values of viscosity and conductivity for PILs which had been reported previously in a review paper was used as the data for creating ML models.[1] Attempts to compile data and construct models for thermal properties were also made but the available data was not sufficient to generate meaningful models. The viscosity dataset comprised 91 data from 83 unique ILs, with 8 additional values at different water contents for the same ILs. These 83 ILs contained 39 different cations and 16 anions. The conductivity dataset comprised 106 data from 97 unique ILs, again with 8 additional values from ILs with multiple water contents. These 97 ILs contained 48 cations and 17 anions. It is noted that the viscosity and conductivity of some PILs were measured at different temperatures and/or water concentrations, and these were used as input descriptors in the models.

The set of PILs was not identical for the viscosity and conductivity data, and hence some cations and/or anions were present for one property and not the other, and these are distinguished in Figures 2.1 and 2.2, respectively.

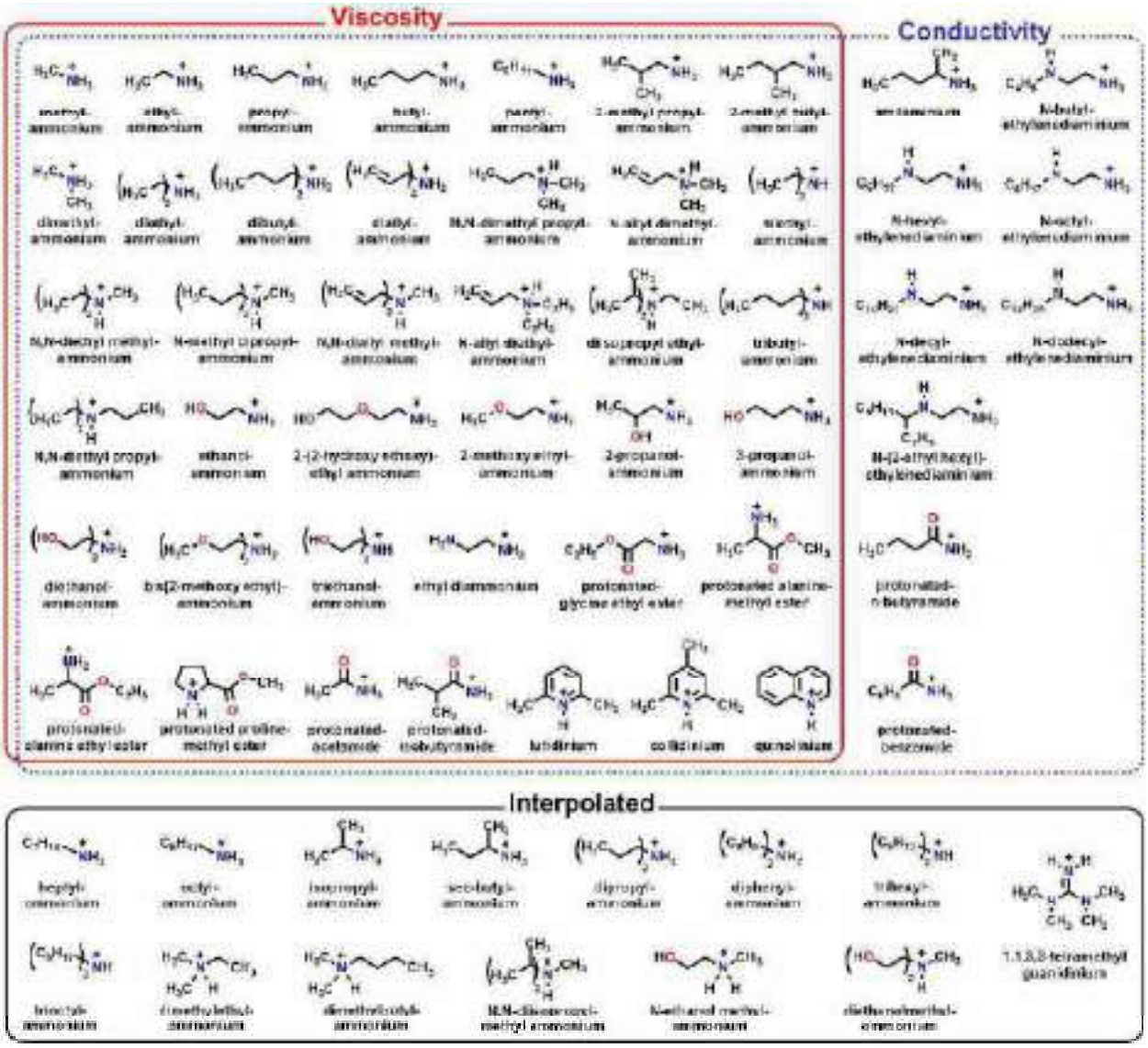

Figure 2.1. Chemical structures of the cations used in this study, along with their names. The cations are categorized as those present in the training sets for viscosity and/or conductivity. The interpolated are related ions that had viscosity and conductivity.

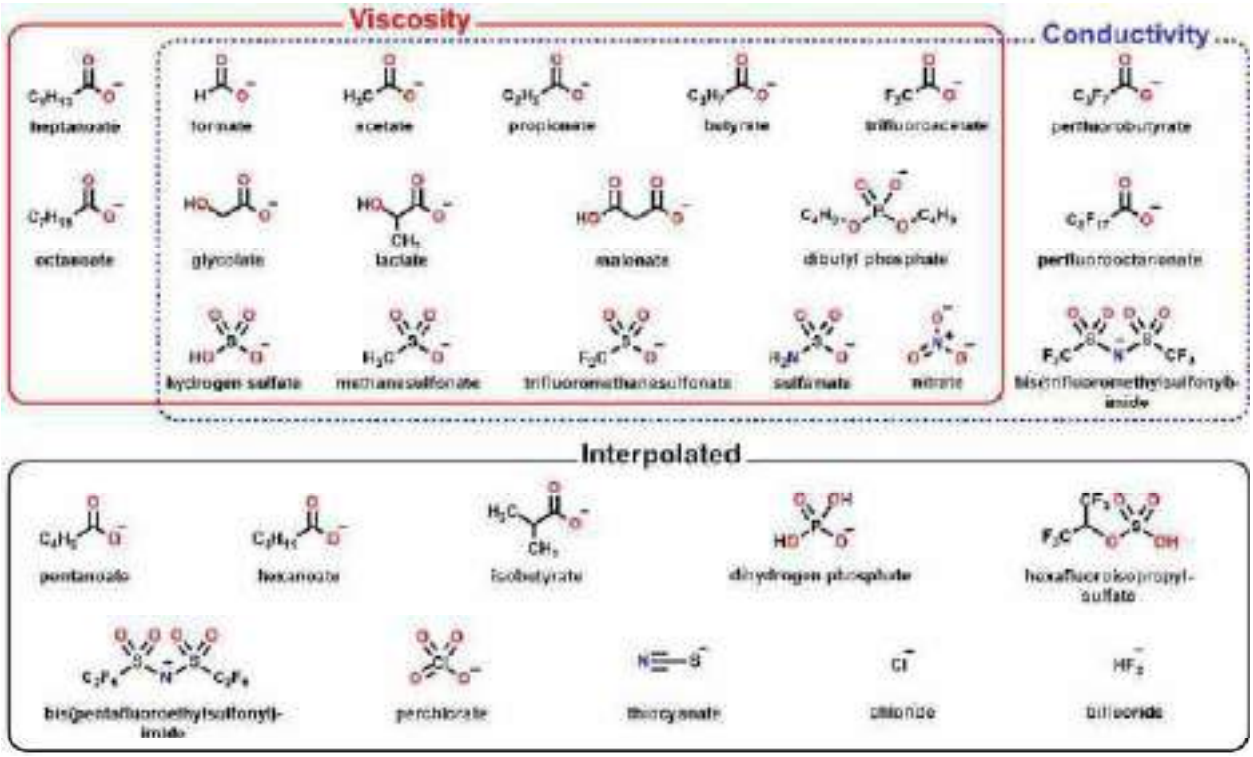

Figure 2.2. Chemical structures of the anions used in this study, along with their names. The anions are categorized as those present in the training sets for viscosity and/or conductivity. The interpolated are related ions that had viscosity and conductivity predictions made for the interpolated set of PILs.

After the data sets were collected, all viscosity and conductivity values, as well as water concentrations were converted into standardized units of measurement if needed (cP for viscosity, mS/cm for conductivity, and wt% for water concentration) during the data processing step. The viscosity values are between 0.0258 to 5647 cP, with water concentrations from 0.005 to 4.35 wt%, and temperatures in the range of 20-130 °C. The conductivity values are between 0.0149 to 51.1 mS/cm, with water concentrations between 0.001 to 4.35 wt%, and temperatures between 20 to 150 °C. Due to the big differences between these ranges, the viscosity, conductivity, and water concentration data was transformed using the log function. Hence log(viscosity), log(conductivity), and log(water concentration) were used in all machine learning models.

Descriptors are numerical values of molecular properties which are essential in quantitative structure–property relationship modelling. To generate the descriptors in this study, Avogadro software was used

to draw molecular structures of the precursor acid and base corresponding to the cation and anion for each IL, as shown in Figures 2.1 and 2.2.[58] Then the Avogadro files of these components were saved in MOL format to use as input files for generating molecular descriptors in the Dragon software.[59] The molecular descriptors correlate with constitutional properties (e.g., the numbers of atom of a specific type of element, the molecular weight) and structural properties (e.g., the numbers of a specific type of functional group or atom-centred fragments that show the number of atoms within a specific distance, molecular properties-related indices such as H-donor, H-acceptor, and topological surface area).[60,61] To distinguish the effects of anions and cations on the viscosity and electrical conductivity of PILs, descriptors of anions and cations were independently generated. Since this project was mainly focused on providing guidance for experimental scientists to design new PILs, only the chemically interpretable descriptors from the pool of generated descriptors were used. The use of more complex descriptors such as those from quantum mechanical calculations may improve the predictability of the models[62] but bring challenges to the reverse engineering process of designing new compounds.

A k-means clustering algorithm was used to partition the dataset into a training set (80% of the dataset) to develop the model, and a test set (20% of the dataset) to evaluate the predictive ability of the machine learning models. In comparison to randomly dividing data, the k-means clustering algorithm chooses the test set within the domain of applicability of the trained model. Moreover, it will allow others to reproduce exactly the model we report here. In this study, the quantitative relationship between the input descriptors and properties of PILs containing small amounts of water was derived by applying linear algorithm MLREM (multiple linear regression with expectation maximization) and non-linear algorithm BRANNLP (Bayesian regularized artificial neural network with Laplacian prior) implemented in the BioModeller program.[63–65] The neural networks had three layers, consisting of input, hidden, and output layers. The number of nodes in the input layer was equal to the number of descriptors, while the hidden layer had 2 nodes and the output layer had one single node corresponding to the viscosity or conductivity of PILs. Importantly, because MLREM and BRANNLP are sparse

feature selection algorithms, they pruned out the irrelevant descriptors allowing retention of only the most relevant descriptors.

After developing the robust QSPR models by MLREM and BRANNLP algorithms, the obtained models were used to interpolate the viscosity and conductivity values for a variety of PILs containing small amounts of water. Relevant descriptors obtained by the training models were used to construct these models. A library of new PILs was designed by pairing all possible cations and anions listed in Figures 2.1 and 2.2, followed by removing the PILs in the original data set. Then each of these new potential PILs was combined with five different water concentrations. Specifically, 8605 viscosity values and 8580 conductivity values of interpolated PILs containing small amounts of water have been predicted. Since all the cations and anions were used in these predictions, it is important to note that there were some predicted ILs that have a cation and/or anion that was not present in their training set.

2.2.2 Experimental method

A selection of 13 acids and 26 amines were screened to characterise new ionic liquids with a range of viscosities. Each precursor was used as received, with formic acid (98%) obtained from Merck, and all other chemicals from Sigma-Aldrich including trihexylamine (96%), trioctylamine (98%), tributylamine (98.5%), octylamine (99%), 2-methoxyethylamine (99%), acetamide (99%), amylamine (99%), benzamide (99%), butylamine (99.5%), allylamine (98%), diethylamine (99.5%), triethylamine (99%), trimethylamine (45%), methylamine (40%), ethylamine (70%), ethanolamine (95%), diethanolamine (98%), triethanolamine (99%), diethylmethylamine (97%), diisopropylmethylamine (98%), 1,1,3,3-tetramethylguanidine (99%), collidine (99%), lutidine (98%), propylamine (98%), propanolamine (99%), quinoline (98%), glycolic acid (99%), butyric acid (99%), methanesulfonic acid (99%), propionic acid (99.5%), trifluoroacetic acid (99%), acetic acid (99%), thiocyanic acid (99%),

hexanoic acid (98%), lactic acid (85%), perchloric acid (70%), trifluoromethanesulfonimide (95%), and trifluoromethanesulfonic acid (99%).

The screening process involved combining approximately equal volumes of less than 0.1 ml of all possible acid-base combinations of the precursors listed above into Eppendorf tubes. If these all underwent a full proton transfer then this would have generated a library of PILs consisting of all possible combinations of the 13 anions and 26 cations shown in Figures 2.1 and 2.2, respectively. This was a coarse screening process, with no cooling during addition, and no calculated stoichiometry. Each resulting combination was visually observed to identify candidates likely to be liquid at room temperature after synthesis and drying. Combinations were excluded that were highly viscous or solid at room temperature, or where the acid and base did not appear to react. From the remaining ILs, a selection of 10 were made with diversity of cations and anions.

Larger batches of the chosen ILs were made using an acid-base titration with a stoichiometric ratio of the acid to the base. The acid was slowly added to the base, during which the temperature was maintained at 12 °C using an ice bath, as previously reported.[66] Water was removed from the resulting ILs using a Heidolph Hei-VAP Core rotatory evaporator, followed by a LabconcoFreeZone 4.5 Litre freeze dryer. The water contents of the ILs were measured using a Mettler Toledo Coulometric Karl Fischer after freeze drying. From these, ILs with water contents ranging from 0.1-1 wt% were investigated during the study and characterized to compare against the ML predictions.

The viscosity of these new ILs was measured under SLC using an AND vibro viscometer. Conductivity measurements were taken using a Mettler Toledo Seven Excellence S470 pH/Conductivity Meter under SLC. Density was determined in triplicate measurements using a 2 mL volumetric flask.

2.3 Results and Discussion

Models using MLREM and BRANNLP were developed for previously reported viscosity and conductivity data of PILs containing small amounts of water. The correlations between the experimental and predicted values of viscosity and conductivity for MLREM and BRANNLP models are illustrated in Figure 2.3. For both properties, 80% of the data was used for training the predictive models and 20% for testing. This led to 73 data points in the training set and 18 in the test set for viscosity, and 84 data points in the training set and 21 in the test set for conductivity.

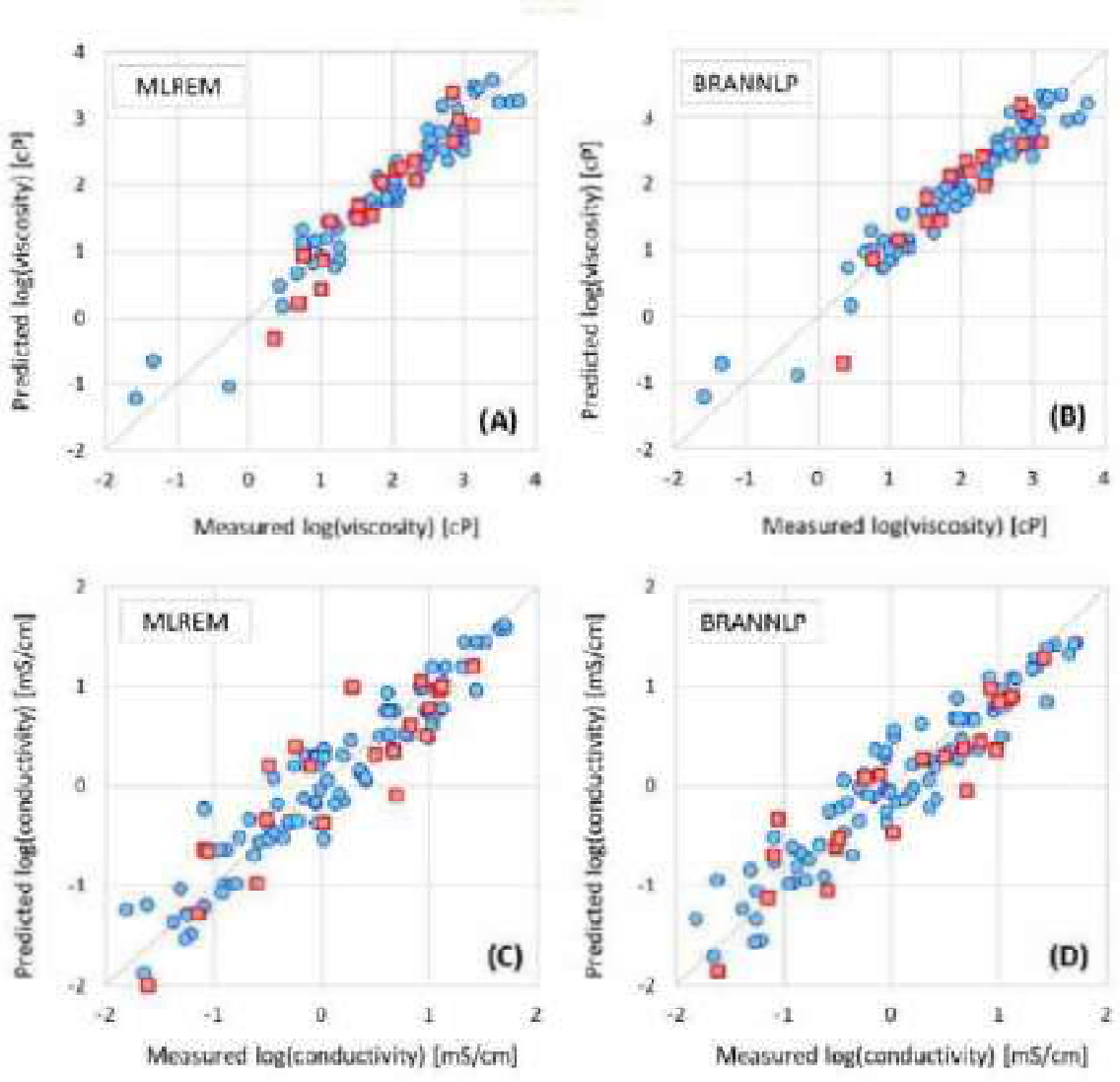

Figure 2.3. Experimental vs. predicted viscosity (A, B) and conductivity (C, D) of PILs containing small amounts of water according to MLREM (A, C) and BRANNLP (B, D) models. Blue circles and red squares denote the training and test data sets, respectively.

Both models also worked well for the conductivity prediction, with R^2 and Q^2 values higher than 0.78 for both the MLREM and BRANNLP models. For the conductivity output, the number of effective weights was 18 for MLREM and 23 for BRANNLP models. Similar to the viscosity prediction, the BRANNLP model also performed better than the MLREM model in the prediction of conductivity for the investigated PILs containing small amounts of water, with higher Q^2 (0.853 for BRANNLP vs. 0.785 for MLREM, respectively) and smaller SEP (0.350 vs. 0.409 cP, for BRANNLP and MLREM, respectively).

Table 2.1. Statistical Results for MLREM and BRANNLP Models of Investigated PILs Containing Small Amounts of Water.

Output	**Data points**	**Model**	**Effective weights**	**Training set**		**Test set**	
				R^2	**SEE**	**Q^2**	**SEP**
Viscosity (cP)	*Training:* 73	MLREM	20	0.921	0.314	0.917	0.310
	Test: 18	BRANNLP	29	0.925	0.240	0.893	0.365
Conductivity (mS/cm)	*Training:* 84	MLREM	18	0.889	0.300	0.785	0.409
	Test: 21	BRANNLP	23	0.873	0.272	0.853	0.340

Next, all the data (not partitioned into training and test sets) was used to produce MLREM and BRANNLP models for viscosity and conductivity which will be used for exploring structure-property relationship and predicting properties of new PILs. The statistical results of the best QSPR models for the new library are shown in Table 2.2. Consistent with Table 2.1, all the models had high R^2 and small SEE, showing good predictive capability. These models were used to predict the viscosity and conductivity of all possible combinations of the 63 cations and 29 anions, leading to 1827 cation-anion pairs.

Table 2.2. Statistical Results for MLREM and BRANNLP Models of the Interpolated PILs Dataset.

Output	Training Data points	Model	Effective weights	Training set	
				R^2	SEE
Viscosity (cP)	91	MLREM	27	0.935	0.290
		BRANNLP	33	0.949	0.202
Conductivity (mS/cm)	105	MLREM	38	0.935	0.265
		BRANNLP	37	0.915	0.217

To validate the predictions from the models, a selection of new PILs were synthesized and characterized to compare to the outputs of the models. An experimental screen was firstly conducted of 26 amines and 13 Brønsted acids to visually observe which combinations were likely to form ILs, and of those which were likely to be liquid at room temperature after drying. As described in the methods, this was a coarse screening method with equal volumes of the precursors used for simplicity, rather than stoichiometric quantities. It was important to note that amine precursors which contained a large proportion of water, such as ethylamine, led to significantly lower viscosities, and acid-base combinations with one having a particularly high or low molecular weight led to the lowest accuracy since the screening was done by equal volumes. The nitrates were deliberately omitted from this screening study due to the risk of an explosion through the heat generated from the reaction. The results are summarised in Table 2.3.

Table 2.3. Heat map generated from combining volumetrically equal portions of the precursor acid and base to screen for protic ionic liquids likely to be liquid at room temperature. The cations are listed in the first column, and the abbreviations are given for the anions in the first row, which are the same as those in Figure 2.1. The values correspond to increasing viscosity from 1 to 5, where those classified as '1' have very low viscosity, and those classified as '5' are extremely viscous. The samples classified a '6' were solid at room temperature.

Cation	F	A	P	B	HX	G	L	MsO	SCN	PC	TfA	TfO	Tf2N
methylammonium	1	1	1	2	2	1	3	3	1	1	1	5	1
ethylammonium	1	1	1	2	2	1	1	1	1	1	1	6	1
propylammonium	1	1	3	3	3	3	2	6	2	6	2	6	1
butylammonium	1	1	3	3	4	4	3	6	1	5	1	6	1

amylammonium	2	2	3	3	4	3	3	6	1	6	3	6	1
octylammonium	1	1	3	3	4	3	5	6	1	6	3	6	2
diethylammonium	1	1	2	1	2	3	2	2	5	6	6	6	3
trimethylammonium	1	1	1	1	1	1	1	1	1	6	1	1	1
triethylammonium	1	2	1	1	1	1	1	4	1	1	1	1	2
tributylammonium	1	1	1	2	2	3	3	4	1	6	2	6	1
trihexylammonium	1	1	1	2	2	1	3	3	3	1	1	1	3
trioctylammonium	1	1	1	2	2	3	3	2	3	5	1	1	4
ethanolammonium	1	4	4	4	4	1	3	6	1	1	5	6	4
propanolammonium	3	5	4	4	2	1	4	3	2	2	3	3	1
diethanolammonium	2	4	4	3	2	1	4	4	4	1	5	6	4
triethanolammonium	4	4	3	2	2	1	4	6	4	1	4	4	4
2-methoxyethylammonium	1	4	4	4	2	1	3	4	1	1	2	6	1
diethylmethylammonium	1	1	1	2	1	1	2	2	3	1	1	1	3
diisopropylmethylammonium	1	1	2	1	1	1	3	3	3	6	1	6	3
1,1,3,3,-tetramethylguanidinium	1	4	4	4	6	1	4	3	2	1	3	3	1
acetamide (protonated)	1	1	1	1	1	2	1	1	1	1	1	1	1
benzamide	6	6	1	1	1	6	3	1	6	1	6	1	1
allylammonium	1	1	3	2	3	3	2	6	2	6	2	6	1
collidinium	1	2	1	1	1	2	4	3	2	1	1	2	1
lutidinium	1	1	1	1	1	1	4	3	2	1	1	6	1
quinolinium	1	1	2	2	1	1	3	6	2	6	6	6	1

Of the 338 acid-base combinations, 39 formed solids, 46 had high viscosities, and the remaining 253 had low to medium viscosities. This latter group was identified as the combinations most likely to result in a PIL after careful stoichiometric synthesis, and of those, the ones with the lowest viscosities were more likely to be liquid at room temperature. Overall, it could be seen that from the acids and bases trialled, the carboxylic and Tf_2N acids generally led to a large proportion of low viscosity combinations. Similarly, the methylamine, ethylamine, trimethylamine, triethylamine, and acetamide generally led to low viscosity acid-base pairs. Conversely, the perchloric, triflic, and methanesulfonic acids along with quinolinium had a relatively high proportion of solids forming with the amines in this study.

From this screening, a selection of 10 potential PILs was made and synthesized, namely diethanolammonium glycolate (DEtAG), trihexylammonium acetate (THexAA), methylammonium propionate (MAP), triethylammonium lactate (TEAL), N,N-diisopropylmethylammonium hexanoate

(DIPMAH), pentylammonium acetate (PeAA), trioctylammonium formate (TOAF), trioctylammonium methanesulfonate (TOAMS), diethylmethylammonium hexanoate (DEMAH), butylammonium propionate (BAP). The water content, surface tension, density, viscosity, refractive index, and conductivity of these 10 PILs are provided in Table 2.4. Many of these have not previously been reported, and literature values where available with known water contents have been included for comparison. These 10 PILs represent a broad range of cation and anion structures across those in the interpolated data and had a broad range of viscosities and conductivities.

It should be noted that some of these ions were not in the training sets used for developing the viscosity or conductivity models, and these are shown inside the interpolated boxes in Figures 2.1 and 2.2. These were deliberately included to test the robustness of the models for predicting the properties of PILs with both, one, or neither ions present in the training sets, while keeping the ions used relatively similar to those in the training sets.

The viscosity of these new ILs was measured under SLC using an AND vibro viscometer. Conductivity measurements were taken using a Mettler Toledo Seven Excellence S470 pH/Conductivity Meter under SLC. Density was determined in triplicate measurements using a 2 mL volumetric flask.

Table 2.4. Experimental physicochemical properties and melting points of 10 PILs prepared for validating the Machine Learning models, including water content, liquid-vapour surface tension (γ_{LV}), density (ρ), viscosity (η), refractive index (n_D) and conductivity (κ). All measurements were made at 22 ^{o}C. Uncertainties are provided in parenthesis.

IL[a]	Water content (wt%)	γ_{LV} (mN/m)	ρ(g/ml)	η (cP)	n_D	κ (mS/cm)
DEtAG	0.0050(5)	[b]	1.15(6)	[b]	1.491	0.100(5)
THexAA	0.011(6)	30.6(1)	0.822(4)	8.51(0.17)	1.437	0.099(5)
MAP	0.322(7)	44.2(6)	0.991(5)	42.0(8)	1.431	12.8(6)
TEAL	0.036(6)	51.8(7)	1.04(5)	483(10)	1.458	0.20(1)
DIPMAH	0.0020(5)	35.6(5)	0.90(4)	44.2(9)	1.443	0.27(1)
PeAA	0.047(7) 0.26[17]	37.4(1.3) 38.9[c,17]	0.91(5) 0.941[17]	473(9)	1.444	0.39(2)

TOAF	0.0027(50)	32.3(6)	0.83(4)	8.5(2)	1.450	0.176(9)
TOAMS	0.0040(10)	36.1(1)	0.89(4)	381(8)	1.460	0.019(1)
DEMAH	0.012(6)	33.1(5)	0.90(5)	26.5(5)	1.436	0.53(3)
BAP	0.67(1)	38.3(1.2)	0.89(4)	452(9)	1.443	0.32(2)

[a] The abbreviations for the ILs are diethanolammonium glycolate (DEtAG), trihexylammonium acetate (THexAA), methylammonium propionate (MAP), triethylammonium lactate (TEAL), N,N-diisopropylmethylammonium hexanoate (DIPMAH), pentylammonium acetate (PeAA), trioctylammonium formate (TOAF), trioctylammonium methanesulfonate (TOAMS), diethylmethylammonium hexanoate (DEMAH), butylammonium propionate (BAP).

[b] Sample had a high viscosity which exceeded the limits of the instrument used. This high viscosity also prevented surface tension from being measured, though the measurements suggest it is above 60 mN/m.

[c] Measurement reported at 20.5 ºC.

Even after multiple days of freeze drying, it was difficult to dry methylammonium proprionate (MAP) beyond the 0.322 wt% water noted in Table 2.4. Both diethanolammonium glycolate (DEtAG) and ethylammonium lactate (EAL) had viscosities exceeding 1000 mPa.s and the viscosity could not be accurately measured using the instrument available to us. The high viscosity of DEtAG also impacted its surface tension and the surface tension value obtained was higher than the calibration standard (water: 72 mN/m).

These experimental viscosity and conductivity values were compared against the predicted values from MLREM and BRANNLP machine learning models to assess the prediction capabilities of the models. The predicted viscosities using the MLREM model for THexAA, TOAF, and TOAMS were all effectively zero.

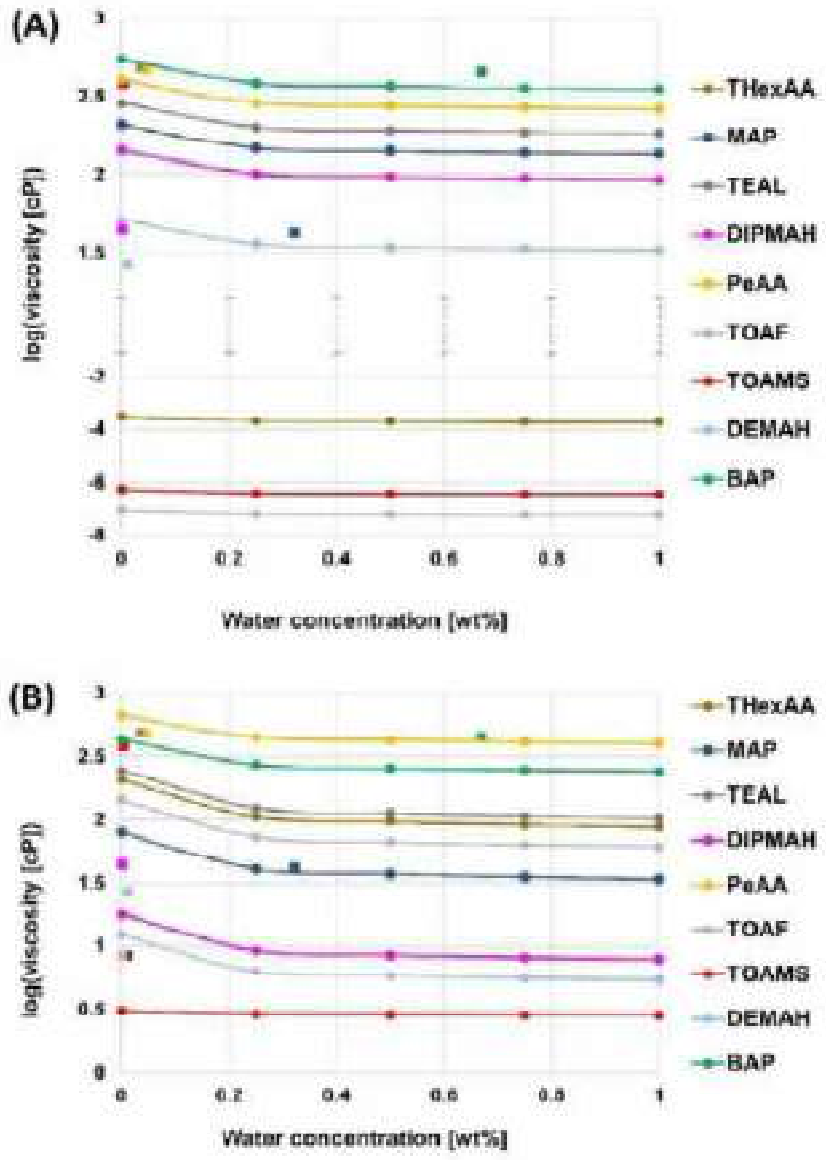

Figure 2.4. Comparison of experimental viscosity values from the PILs in Table 2.5 with the predictions from a) MLREM and b) BRANNLP models, with water contents up to 1 wt %. The predicted data are represented by circles, with the solid lines a guide to the eye. Experimental data is shown by squares with the same colour corresponding to the modelled PILs.

Both models were able to predict that viscosity would decrease with increasing water content. The predicted data for DEtAG has been omitted since the values were significantly higher, with values from the MLREM model from 8299 cP at 1 wt% to 12856 cP at 0.001 wt%, and for the BRANNLP model from 5748 cP at 1 wt% to 9025 cP at 0.001 wt%. These are consistent with the viscosity of DEtAG being too high to measure in this study.

Based on the experimental data the ILs can be grouped into those with very high viscosity (DEtAG), those with an intermediate to high viscosity (TEAL, PeAA, TOAMS, and BAP), and the remainder with relatively low viscosities (DEMAH, DIPMAH, MAP, TOAF, and THexAA). Overall, there was good agreement for both models in grouping the ILs into these three categories, indicating the usefulness of both models for predicting viscosity. Both models clearly distinguished DEtAG as having the highest viscosity. The BRANNLP model identified TEAL, PeAA, TOAMS, and BAP as having viscosities higher than the other ILs, but lower than DEtAG, with moderate agreements to the experimental values, and not in the same order. Similarly, DEMAH, DIPMAH, MAP, TOAF, and THexAA were identified as low viscosity ILs for the BRANNLP model, though had a different order compared to the experimental data. The MLREM model predicted non-feasible values for THexAA, TOAF, and TOAMS of effectively zero, but otherwise performed well. TEAL, PeAA, and BAP were identified as having intermediate to high viscosities. The other ILs were correctly identified as having lower viscosities.

For the PILs in Table 2.1 DIPMAH had neither cation nor anion present in the training set. Similarly, THexAA, TOAF, and TOAMS had cations that were not included in the training set but their anions were, while DEMAH had an anion not included in the training set, but the cation was. This shows that these MLREM and BRANNLP models are sufficiently robust to provide useful predictions of low, intermediate, or high viscosities, even for PILs with structures that are related, but not included in the original set. The PILs which had both cation and anion present in the training set did have better numerical similarity to the predicted values for both models. The BRANNLP model overall performed better, without any non-feasible values close to zero, and with the same general order as the experimental values, when grouping the PILs as having low, intermediate-high, and very high viscosities.

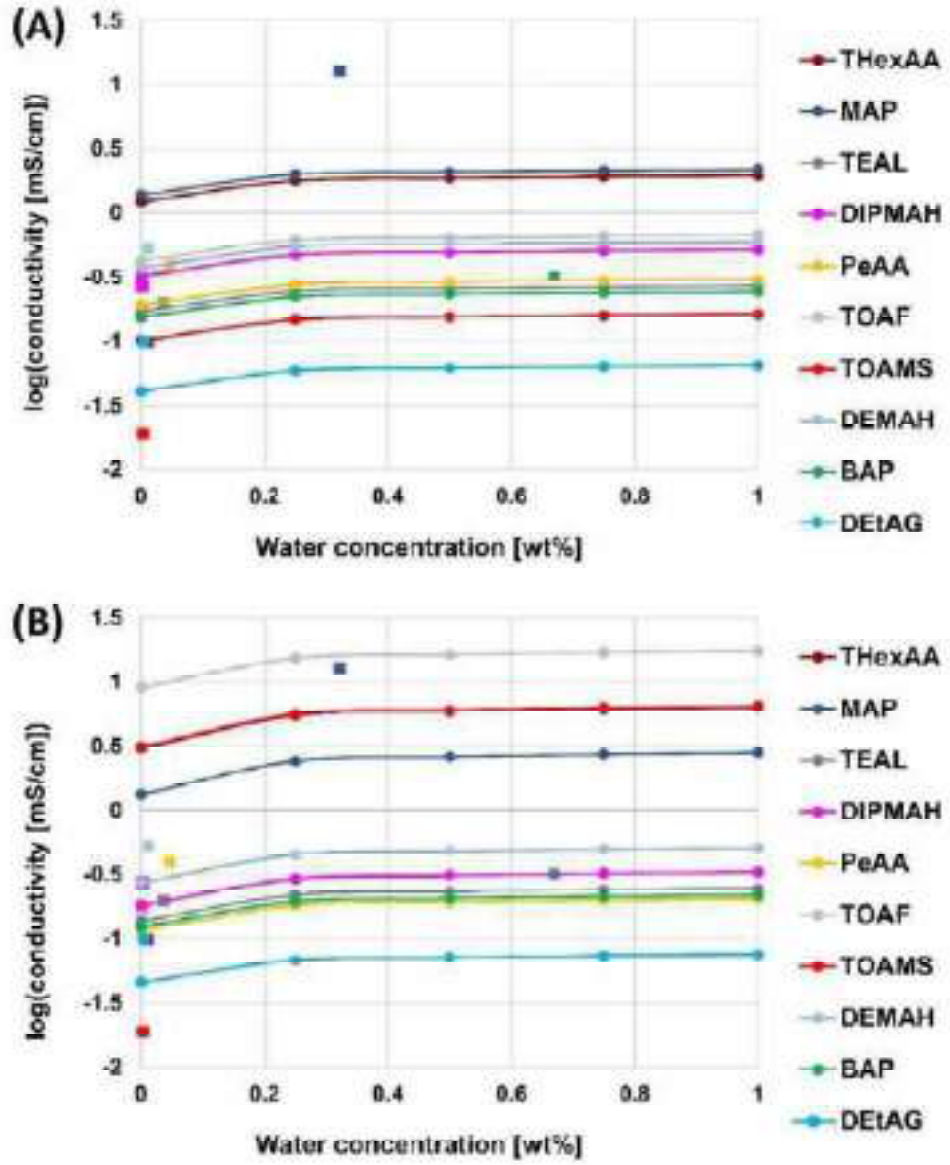

Figure 2.5. Comparison of experimental conductivity values from the PILs in Table 2.5 with the predictions from a) MLREM and b) BRANNLP models, with water contents up to 1 wt %. The predicted data are represented by circles, with the solid lines a guide to the eye. Experimental data is shown by squares with the same colour corresponding to the modelled PILs.

The comparison between the experimental data in Table 2.1 and the models for conductivity is provided in Figure 2.5. As previously mentioned, the MLREM model for conductivity removed water as an important descriptor. However, we have constrained the water concentration as a descriptor and built a MLR model where water concentration together with all descriptors selected as important features were included. As can be seen in Figure 2.5, the predicted values using MLREM or BRANNLP all had

increasing conductivity with increasing water content, which was expected since conductivity is a transport property, and the corresponding decrease in viscosity will increase conductivity. The predicted values using MLREM were similar to those using BRANNLP, except for TOAMS and TOAF. The BRANNLP model predicted high conductivity for these two ILs but the MLREM did not.

The experimental data can be grouped as high for MAP, intermediate for TEAL, DIPMAH, PeAA, EAL, TOAF, DEMAH, and BAP, and low for DEtAG and THexAA. Initially, it appears as though there is relatively poor agreement between the model and the experimental data, with four of the PILs having a factor of 5 difference between the experimental and predicted values at the most similar water contents. However, as described, this was largely dependent on whether the interpolated data entries are within the applicability domain of models or too different. The absence of similar structures or too different water concentration reported in the training set could lead to low accuracy in the prediction. As seen in Figure 2.5, there were moderately good predictions for DEtAG, TEAL, DIPMAH, PeAA, DEMAG, DEMAH, and BAP. However, the models failed to predict the high conductivity for MAP, and gave significantly higher predicted values for THexAA, TOAF, and TOAMS.

For the PILs in Table 2.1, DEtAG, MAP, TEAL, PeAA, and BAP had both their cation and anion present in the training set, and all of these were relatively well predicted by the models, with the exception of MAP. DEMAH had the cation included in the training set, but not the anion, and similarly was well predicted. Both the MLREM and BRANNLP models accurately predicted that DEtAG would have low conductivity, and that many would have intermediate conductivities. The poor agreement of the model with the high experimental value of MAP[68] was indicative of limitations of the available conductivity data for training, since the previously reported values for the structurally similar ILs were very high for MAF (methylammonium formate) (43.8 mS/cm at 0.46 wt%), but low for EAP (ethylammonium propionate) (0.872 mS/cm at 0.42 wt%) and EAF (ethylammonium formate) (12.16 mS/cm at 0.38 wt%), all of which were included in the training set.

In contrast, THexAA, TOAF, and TOAMS all had their anion included in the training set, but not the cation, and all had the poorest agreement between the predicted and experimental values. It was likely that the increased multiple alkyl chains on the cations were significantly decreasing their conductivity through reduced ion mobility and increased van der Waals interactions. The cations in the training set for conductivity which were similar to the trihexylammonium and trioctylammonium cations used in this validation set of PILs were pentylammonium, N-octylethylenediaminium, and dibutylammonium, and hence it was likely that these multiple long alkyl chains were not described well by the model.

2.3.1 Effect of water content on viscosity and conductivity

N,N-diisopropylmethylammonium hexanoate (DIPMAH) was chosen to study the effect of water concentration on viscosity and conductivity experimentally. The results are shown in Table 2.5. These experimental measurements were compared to prediction curves from MLREM and BRANNLP for viscosity and conductivity.

Table 2.5. Experimental measurement for N,N-diisopropylmethylammonium hexanoate with varying water concentrations. The experiments were performed under SLC.

wt% water	Viscosity (m Pa.s)	Conductivity (uS/cm)
0.088	37	291.7
0.229	44	314.6
0.568	41	352.1
0.78	59	357.6
1	57	348.2

As the concentration of water increased, the observed viscosity values of DIPMAH increased. This seemed counterintuitive at first glance and contradicted the trends observed in the ML predicted viscosity curves. Since this IL has never been studied previously in literature, it was difficult to determine why this behaviour was observed. It could potentially be attributed to errors and uncertainty

associated with the values. While great care was taken during experiments to ensure laboratory conditions remained constant, small fluctuations in temperature could have affected the measurements.

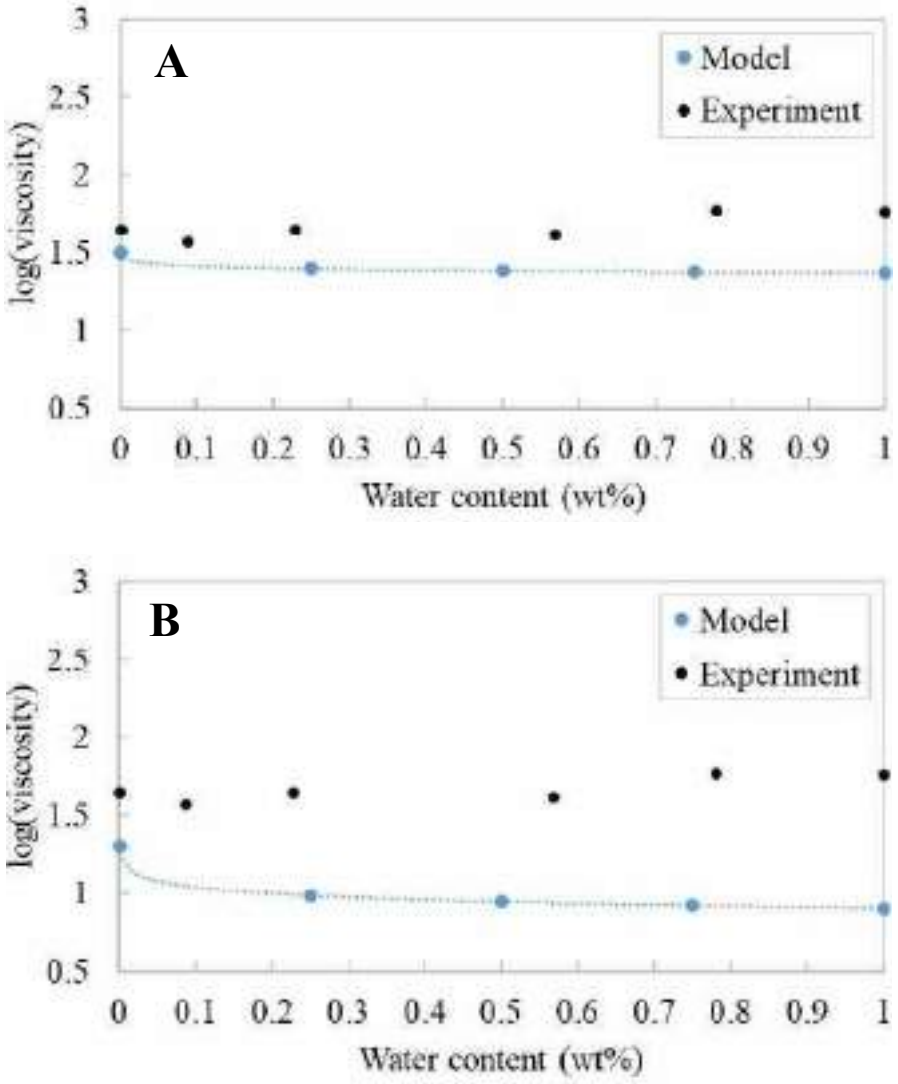

Figure 2.6. A) MLREM and B) BRANNLP predictions for viscosity with varying water concentrations compared against experimental values for viscosity for DIPMAH.

The experimental viscosity data series for DIPMAH had a good general agreement with the predicted trend for MLREM and BRANNLP generated viscosity. However, the trend for this IL with increasing water concentration did not agree with the trend in predicted data, or the general expectation. This was likely due to the ions of DIPMAH not being included in the training data set. The predictions shown in Figure 2.6 were likely made by the model by extrapolating the information it had for the similar ions diisopropylethylammonium, octanoate and heptanoate, with 1, 1 and 2 more carbon atoms respectively,

in the training set. Based on this information, while the trends are not similar, these predictions demonstrate how powerful ML algorithms can be for prediction of new ILs and their properties, even with no prior information regarding the ions being used for synthesis.

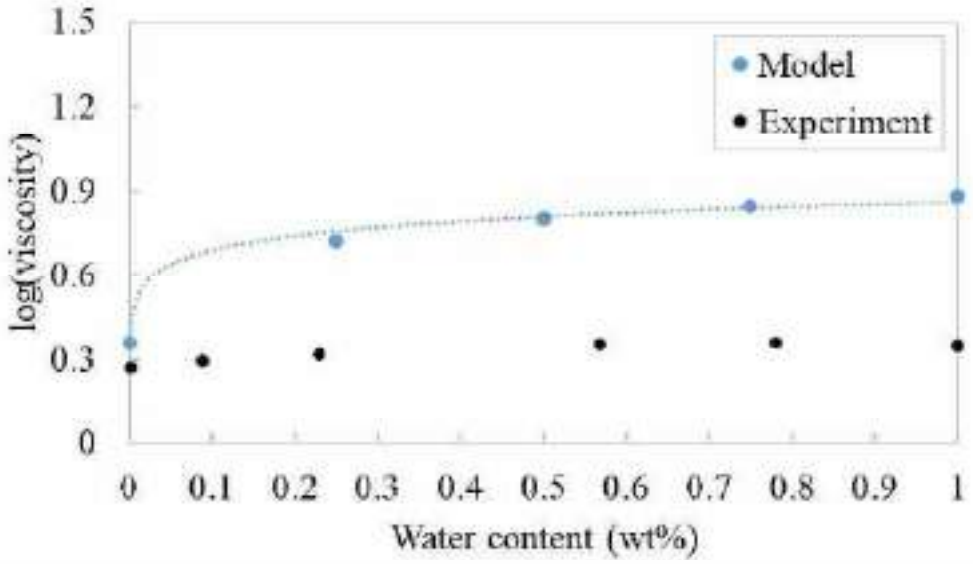

Figure 2.7. BRANNLP predictions for conductivity with varying water concentrations compared against experimental values for conductivity for DIPMAH.

BRANNLP model for conductivity overall suggested an increasing conductivity with increase in water content. DIPMAH experimental values deviated largely from the predicted curve because there were no ILs containing diisopropylmethylammonium or hexanoate in the training set for conductivity. It was concluded more data must be involved in the training set to predict better DIPMAH's conductivity.

Overall, when there was sufficient data in the training set, there was good agreement between the PILs used for validation and the predicted conductivity values from the models. The models did not perform well when the structures of the extrapolated PILs were too different from those used for training.

2.3.2 Further discussion

It is well known that there are vast numbers of possible combinations of cations and anions which can result in ionic liquids, and that these become even larger when combined with a second or third solvent, such as a molecular solvent, another IL, or other additives. While there are high throughput experimental approaches which have been developed to increase the synthesis and characterization of ILs, particularly protic ILs,[17,18] these are not currently able to cover a large proportion of the compositional space. Instead, machine learning methods have the capability to interpolate and extrapolate based on existing data.

In this study, we used reported data that had previously been compiled into a review[1] to produce MLREM and BRANNLP models for viscosity and conductivity. Initially, models were also attempted for thermal properties of glass transitions and melting points. However, these were deemed poor when 80% of the data was used for developing the models and 20% for testing. The other properties, eg. density, refractive index, and surface tension, reported in the review paper were not included in developing models, due to insufficient data reported with known water contents. It was central to developing machine learning models that there was high quality, consistent data available. In particular for ILs, it was essential that the water content was reported. It was also recommended for PILs that the pH at a known concentration in water should also be reported as a quasi-measure of stoichiometry.

The viscosity and conductivity models presented here were developed from relatively scarce data compared to the structure compositional space. There were 91 data points from 83 unique ILs for the viscosity, from 39 cations and 16 anions. These were sufficient to produce useful models for viscosity from both MLREM and BRANNLP for all possible cation and anion combinations in the training sets, along with extrapolation to an additional 24 cations and 13 anions not in the viscosity training data. The comparison to the experimental values for 10 new PILs with either one, both, or neither ion present in

the training set validated both these models, and while the numerical values differed, the models could identify the general order of viscosity.

The conductivity models were developed from 105 data points for 97 unique ILs, including 48 cations and 17 anions. Models were developed to predict conductivity values for all possible cation and anion combinations from the initial training set, along with 15 additional cations and 12 additional anions. In comparison to the experimental values for the new PILs, these showed good agreement when the cation was present in the training set, but poor agreement for the PILs containing the bulky trihexylammonium and trioctylammonium cations which were not present in the training set. Overall, this study demonstrated that the developed models were capable of making useful predictions for interpolated PILs based on the cations and anions in the training set.

These models were able to provide predictions for viscosity and conductivity for 1827 cation-anion combinations, which should provide meaningful guidance about which are likely to be high, low, or intermediate, and how they are likely to vary with up to 1 wt % water present. We expect that these models will undergo significant changes over time as more data becomes available. They are likely to expand to include more cations, anions, and molecular solvents or additives, and in this process the descriptors which are selected as most relevant are likely to change as well.

2.4 Conclusion

It was observed that for both linear and non-linear machine learning algorithms, MLREM and BRANNLP, the quality of the training data greatly impacted the prediction capacities for ILs. BRANNLP models for both viscosity and ionic conductivity outperformed MLREM models with slightly higher R^2 and standard deviation values. A significant finding from the current study was that the water content of the training set affected the accuracy of the predictions to a great degree. The changes in viscosity and conductivity were not linear with incremental increases to the water content

and thus the water content plays an important role in the predicted values for neat ILs. BRANNLP model for conductivity overall suggested an increasing conductivity with increase in water content. This was confirmed with experimental results. The results for viscosity were less conclusive, with the trends observed with the ML models not able to be confirmed with the available experimental results. This was likely due to none of the ions of DIPMAH being included in the training data set for the ML models. To develop high quality machine learning models, there needs to be high quality, consistent data available. In particularly for PILs, it was essential that the water content was reported.

3 Effect of surfactant ionicity on self-assembly in aqueous ionic liquid mixtures

3.1 Introduction

Protic ionic liquids are the largest known solvent class capable of promoting surfactant self-assembly. PILs can act as proton donors or acceptors, and this ability can lead to water-like hydrogen bonded networks.[35, 66-68] These H-bonded networks contribute to the ability of some PILs to promote self-assembly and may contribute to their beneficial solvent properties for applications such as biomolecule preservation.[69-73]

The first report of self-assembly in ILs was by Evans et al. in the early 1980s, where they reported micelle formation in ethylammonium nitrate (EAN).[66, 74] A wide range of ILs have been tested for this property since this discovery, and PILs remain the largest known subclass of solvents capable of supporting self-assembly.[2, 36, 75-76] Reports suggest that the formed micelles tend to be smaller in EAN when compared to water, attributed as due to the higher solubility of hydrocarbons in EAN.[17, 74] In addition to micelles[67, 74, 77], liquid crystal phases, such as lamellar, hexagonal and cubic [17, 58, 76, 78] have been reported in PILs. In general, it has been noted that as the solvophobicity of an IL increases, the likelihood of more diverse liquid crystal phases being supported also increases.[58, 79]

For reasons such as decreasing viscosity, decreasing costs, and increasing surfactant solubility, IL-molecular solvent mixtures have sparked interest in recent years as self-assembly solvents.[3, 14] A broad range of lyotropic liquid crystal phases have been supported in IL-water mixtures, including hexagonal[78], lamellar[58] and cubic phases[76]. However, to date there are few PIL-water-surfactant systems which have been explored. For PIL-water mixtures, the studies have included cationic and nonionic surfactants, such as cetyltrimethylammonium bromide (CTAB)[47], dodecyltrimethylammonium bromide (DTAB)[13] and tetradecyltetraglycol ($C_{14}E_4$)[52]. Some insights into the role of the IL during self-assembly

can be gathered from these publications. Wakeham et al. suggested that the CMC of the surfactant strongly correlated to the solvent composition, with an increase in CMC being proportional the PIL concentration based on their study of $C_{14}E_4$ self-assembly in mixtures of EAN-water and EtAN-water. Bryant et al. reported that the CMC of cationic surfactants are orders of magnitude higher, and micelles much smaller, in EAN than in water, whereas anionic micelles were less affected.[34] Lam et al. reported IL behaviour is similar to that of a simple electrolyte based on their study of DTAB in EAN-water mixtures at low EAN concentrations. However, at IL concentrations beyond the saturation points of most conventional salts, the IL nanostructure influences micellization and acts as a co-solvent rather than a salt, raising the CMC.[13] No studies could be found exploring anionic surfactant self-assembly in PIL-water mixtures.

For aprotic ILs, the micellization behaviour of cationic, anionic and non-ionic surfactants have been investigated in IL-water solvents, but not all in the same study, or with consistent ILs or surfactants. Cationic surfactant self-assembly of CTAB in aprotic imidazolium-based IL-water mixtures, with up to 20 wt% water, was investigated by Javadian et al., using ILs with 1-Butyl-3-methylimidazolium (BMIm) and 1-Hexyl-3-methyl-imidazolium (HMIm) cations paired with Cl, Br and BF_4 anions.[47] The CMC observed in all IL-water mixtures were higher than the values recorded in water, and they determined that the hydrogen bond was an important factor in defining the solvent properties. In contrast, Sohrabi et al. explored the anionic surfactant, sodium dodecyl sulfate (SDS), in $C_n$mim, BMIm and HMIm based IL-mixtures and found that at low concentrations of the ILs, the CMC of SDS decreased, leading to the formation of mixed micelles.[49-50] Sohrabi et al. also hypothesised that the decrease in CMC could be attributed to a reduction in the electrostatic repulsion between headgroups.[50]

The effect of conventional salts on surfactant self-assembly has also been investigated in depth.[80-82] Typically the saturation concentrations of conventional salts which can be dissolved in water is 5 mol%[80]. At these concentrations, the salt was noted to decrease the critical micelle concentrations of

surfactants in water.[80-81] Here, the ILs are not solubility limited, as was the case with conventional salts, and therefore we can investigate the effect on the critical micelle concentrations of having high ion concentrations present in the solvent. In salts, the high ionic strength screened the headgroup charges of anionic and cationic surfactants, leading to decreased effective headgroup area compared to in water.[17, 83]

The solvation behaviour of solutes in IL-water solvent mixtures is complex, with possible contributions including specific ion effects, hydrogen bonding and Van der Waal interactions.[3, 14, 75] Recently, Yalcin et al. explored the chemical environment of binary IL solvents using dyes as probe molecules. The results indicated that the solvation parameters of the binary mixtures deviated considerably from the ideal solvation behaviour. This suggested preferential solvation was solute-dependent and the results demonstrate that some PIL-molecular solvent combinations can enhance the solvation capabilities.[14] Surfactant self-assembly will be strongly affected by these solvation properties, and the proportion of IL cations, IL anions and water are likely to be different in the bulk solvent relative to the proportions found around cationic, anionic and non-ionic surfactants. Therefore, there is a need to have a systematic study to directly compare the micellization behaviour of these three amphiphile classes in the same IL-water environments.

In this chapter the micellization behaviour of a cationic, anionic and non-ionic amphiphiles in PIL-water mixtures, across the full PIL-water composition range were investigated. This is the first comprehensive study of the effect of ionicity on the self-assembly of all three classes of surfactants in PIL-water solvents. Surface tension measurements were used to obtain the CMC, surface excess concentration, Γ_{max}, minimum molecular areas at the air-liquid interface, A_{min}, standard free energy of micellization, ΔG_m^O and standard free energy of adsorption, ΔG_{ad}^O of the surfactants in each PIL-water composition. Small angle X-ray scattering (SAXS) was performed to confirm micelle formation in the anionic surfactant, sodium octylsulfate. The presence of higher order phases were visually observed in

the mixtures using cross-polarised optical microscopy. It is anticipated that this knowledge on the self-assembly behaviour can provide insights regarding the solvent environment in which it occurs, which will be applicable to a broader range of solutes, such as biomolecules.

3.2 Method

The surfactants of $C_{12}E_4$ (Sigma Aldrich), sodium octyl sulfate (Sigma Aldrich) and cetylrimethylammonium bromide (Sigma Aldrich) were used as received. The ionic liquid precursors of ethylamine (Sigma Aldrich), ethanolamine (Sigma Aldrich) and nitric acid (Sigma Aldrich) were used as received.

The ionic liquids used in this study, EAN and EtAN, were prepared using a previously reported method.[10] The reaction was an acid-base titration during which the temperature was maintained 12 °C using an ice bath, as previously reported.[7] The resulting PILs were first dried using a rotary evaporator for 24 hours and then freeze dried up to 3 days to ensure low water content. A Karl Fischer titration (Mettler Toledo, Titrator Compact C10SD) was performed to ensure the water content was less than 0.05 wt%. PILs were mixed with water to obtain solvent mixtures with concentrations of 5, 14, 25, 33, 50 and 75 mol% PIL.

The surfactants were dissolved in PIL-water mixtures at concentrations between 0.0001 wt% to 15 wt% for CMC determination. The full list of the concentrations used for each surfactant in each PIL-water composition are available in the Supporting Information Section 8.2.

Air-liquid surface tension measurements were made using a Kibron Delta-8 multi-channel tensiometer. The samples were loaded in 96 well plates, with 40 µl of sample in each well. MilliQ water was loaded

into one column of each plate and was used for calibration before measuring the surface tension of the samples.

Small angle x-ray scattering was performed at the Australian Synchrotron small and wide-angle X-ray scattering beamline (SAXS/WAXS). Samples were loaded into 0.5 mm capillaries and the experiment was performed with a q-range of 0.014 to 1.3 $Å^{-1}$ at 25°C. Measurements were taken for 1 s and the obtained 2D scattering patterns were converted to 1D patterns using Scatterbrain software, provided by the Australian Synchrotron. To fit the 1D scattering patterns to various mathematical models of micelle scattering patterns, SASView software (Version 4.2.0) was used.

Cross polarised microscopy was used to obtain penetration scans for liquid crystal phases across the PIL/water concentration range for the three surfactants. The surfactants were compressed between microscope slides and coverslips before the PIL-water solvent was added to the edge of the coverslip. The solvent was allowed to penetrate through the surfactant, creating a concentration gradient. The prepared samples were heated at 2-10 °C/min in a Mettler FP82HT hot stage controlled by a FP90 central processor to temperatures up to 90 °C. This was performed for all three surfactants in mixtures of EAN and water ranging from 5 mol% to neat IL.

3.3 Results and Discussion

3.3.1 Micelle formation in EAN

Surface tension measurements, SAXS patterns and cross polarised optical penetration scans were taken of non-ionic, cationic, and anionic amphiphiles in EAN-water mixtures to observe the effect of changing the IL concentration on the CMC, and other self-assembly properties.

Air-liquid surface tension measurements were made for the three surfactants in each of the EAN-water solvents, which contained 5, 14, 25, 33, 50 and 75 mol% of EAN, as well as in neat water and EAN. The concentration range selected included the characteristic decrease in surface tension due to micelle formation. In each EAN-water solvent the surface tension was observed to decrease approximately linearly with increasing surfactant concentration, over some concentration range, before reaching a plateau. The intersection between the linear decrease and the constant surface tension was taken as the CMC.

Representative plots of surface tension versus surfactant concentration are provided in Figure 3.1, 3.2 and 3.3. The plots for the other EAN-water concentrations are provided in Figures in the Appendix 8.2.

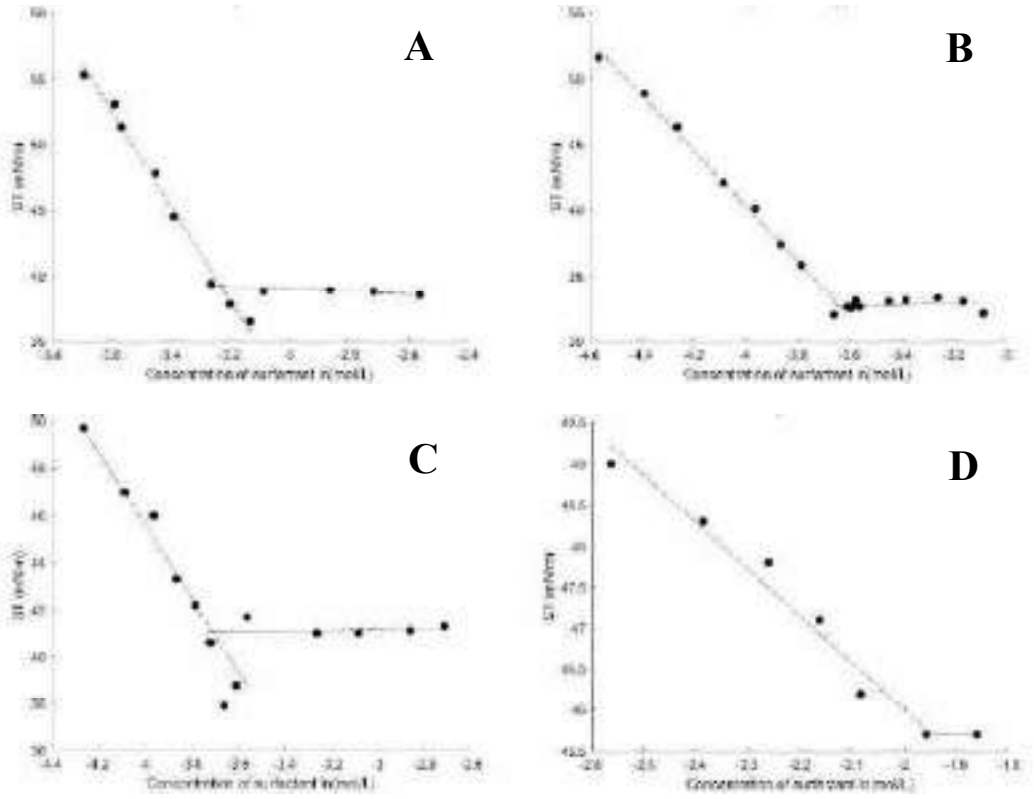

Figure 3.1. The surface tension versus CTAB concentration plots in solvents containing a) water, b) 14 mol% EAN/water, c) 25 mol% EAN/water and neat EAN.

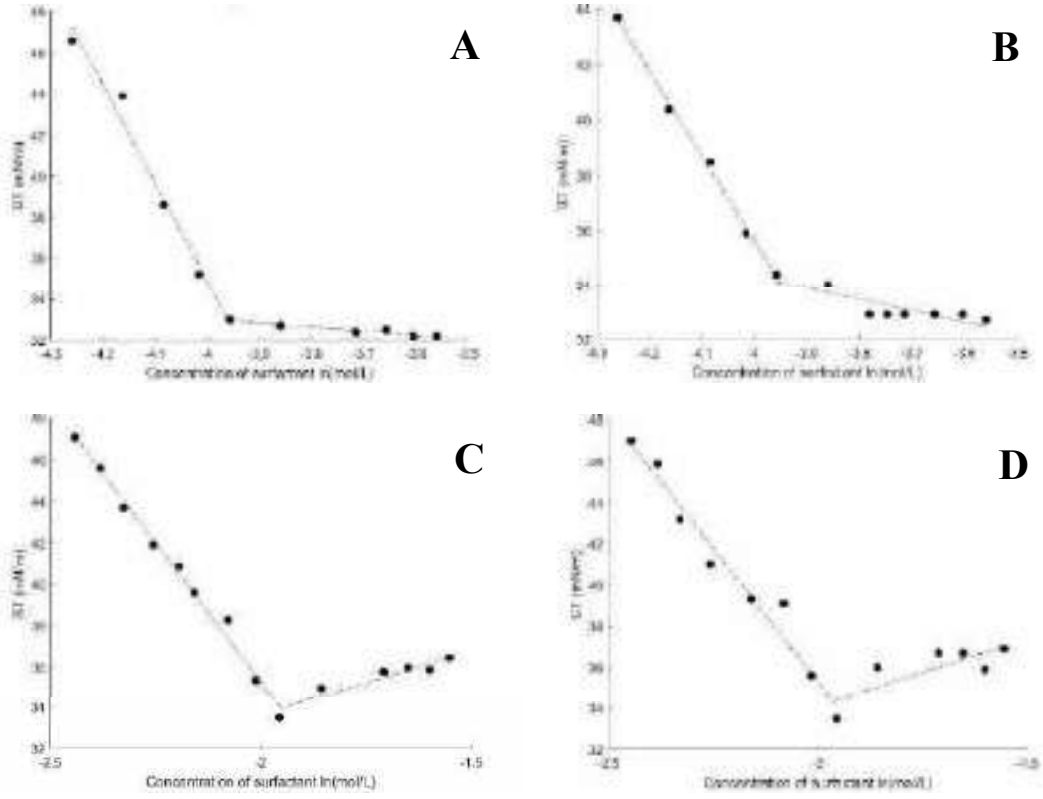

Figure 3.2. Surface tension vs $C_{12}E_4$ concentration plots in a) water b) 5 mol% EAN/water c) 75 mol% EAN/water and d) neat EAN.

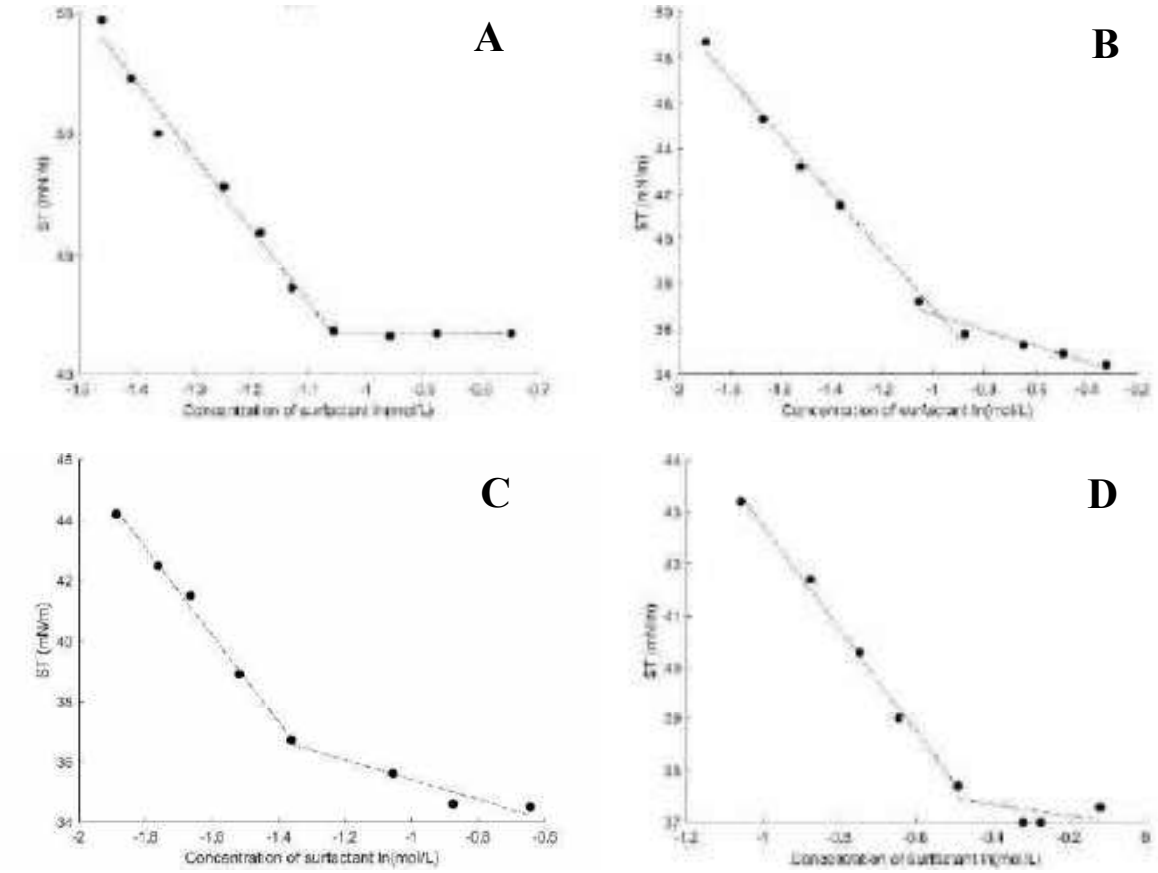

Figure 3.3. The surface tension versus SOS concentration plots in solvents containing a) water, b) 25 mol% EAN-water, c) 33 mol% EAN-water and d) 75 mol% EAN-water.

SOS was used instead of the widely used sodium dodecyl sulfate (SDS) as the anionic surfactant due to poor solubility of SDS in the chosen protic ionic liquid at room temperature. It was not possible to dissolve enough SDS to reach the CMC in EAN during initial testing. The shorter alkyl chain length of SOS increases the solubility of the surfactant in the protic ionic liquid. The CMC of SOS was reported to be an order of magnitude larger than that of SDS in water and we also observed similar differences in values in EAN-water mixtures.[84]

To observe the trends in micellization across the three surfactants across the EAN/water concentration range, the CMC was compared. CMC values obtained for the surfactants in solvents ranging from water to neat IL are shown in Figure 3.4 relative to the EAN proportion in the solvent. The CMC values of SOS in EAN-water mixtures were 2 orders of magnitude larger than that of CTAB in the same mixtures,

which was consistent with reported findings in water. It was reported that SOS micelle formation occurs at concentrations 2 orders of magnitude higher in comparison to CTAB in neat water.[39] The CMC values of the non-ionic surfactant $C_{12}E_4$ were similar to that of the cationic surfactant, CTAB, and also varied from SOS CMC values by approximately 2 orders of magnitude. This indicated that it was more energetically favourable for CTAB and $C_{12}E_4$ to form aggregates at lower concentrations than the anionic surfactant. This could be partly due to the general lack of solubility, as observed with SDS.

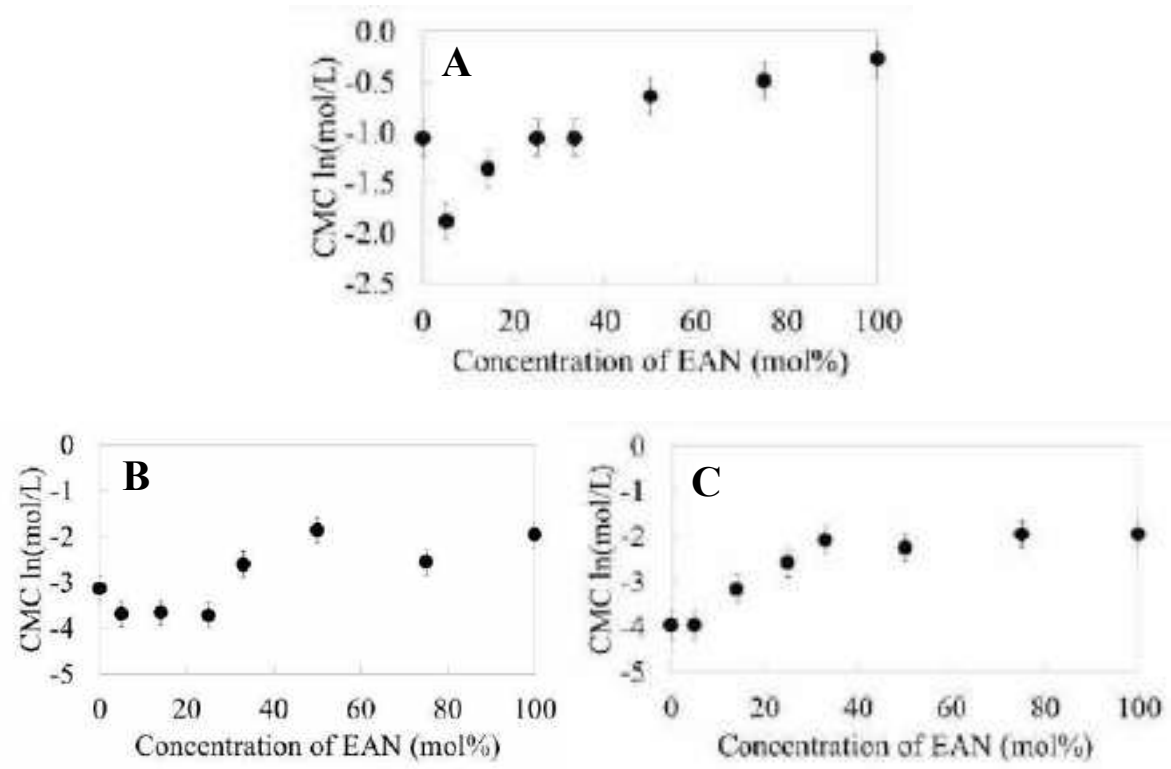

Figure 3.4. The CMC of a) SOS, b) CTAB and $C_{12}E_4$ relative to the EAN concentration in EAN-water mixtures.

The CMC in 5 mol% EAN was lower relative to the CMC in water for CTAB and SOS, and the same in $C_{12}E_4$. The decrease in the CMC for 5 mol% EAN for the ionic surfactants was attributed as due to head group shielding, with the ILs exhibiting similar properties as conventional salts. This was consistent with the results observed by Lam et al.[13] for the cationic surfactant DTAB in EAN/water mixtures at similar low concentrations.

The increase in the CMC with increasing EAN concentration began at 33 mol% for CTAB, whereas this ascent began at 5 mol% in both $C_{12}E_4$ and SOS. This suggests that water may be dominating the self-assembly process for CTAB up to 33 mol% EAN, whereas EAN has more influence on the self-assembly for $C_{12}E_4$ and SOS from 5 mol% EAN. Similarly, the relatively constant CMCs of CTAB and $C_{12}E_4$ above 50 mol% and 33 mol% EAN respectively suggests that EAN was acting as the dominant solvent for these higher concentrations and having a greater influence on the self-assembly than water. In contrast, there was a more linear increase in the CMC of SOS, with increasing EAN, suggesting EAN and water were both having an active solvent role.

Interestingly, significantly larger concentrations of SOS were required to form micelles, in comparison to the cationic and non-ionic surfactants. Initially SDS was explored as an option, but it reached the solubility limit before the CMC for EAN-water compositions. This gave insight regarding the difficulties in observing the self-assembly of longer chained anionic surfactants as there is likely a compromise between the solubility limits of anionic surfactants and the minimum concentration of surfactants required for self-assembly. The trend in the CMC for SOS with EAN concentration showed the largest initial decrease with 5 mol% EAN present.

The maximum surface excess concentration, Γ_{max}, at the air/liquid interface was calculated from Equation 3.1, where R is the gas constant, T is the temperature, and $d\gamma/dC$ is the gradient of the surface tension vs log(concentration) curve at concentrations just below the CMC:

$$\Gamma_{max} = -\frac{1}{2.303RT}\left(\frac{d\gamma}{d\log(C)}\right) \qquad (3.1)$$

Using the surface excess concentration, the minimum molecular areas of the surfactants absorbed at the interface, A_{min}, was calculated from Equation 3.2, Where N_A is the Avogadro's constant.

$$A_{min} = \frac{10^{20}}{N_A \Gamma_{max}} \quad (3.2)$$

The standard free energy of micellisation, ΔG_m^o, and the standard free energy of adsorption, ΔG_{ad}^o, were calculated using Equations 3.3 and 3.4, respectively[55]. These required the previously obtained CMC and A_{min}, along with γ_0, the initial surface tension, and γ_{CMC}, the surface tension at the CMC.

$$\Delta G_m^0 = RT \ln(CMC) \quad (3.3)$$

$$\Delta G_{ad}^0 = \Delta G_m^0 - (\gamma_o - \gamma_{CMC}) \times A_{min} \quad (3.4)$$

The surface tension at the CMC, calculated free energy parameters and packing factors are provided in Tables 3.1, 3.2 and 3.3 for SOS, CTAB and $C_{12}E_4$ in each EAN-water mixture, respectively.

Table 3.1. Free energy parameters and packing factors for the anionic surfactant SOS in EAN-water mixtures, as calculated from surface tension measurements. Parameters include, CMC, surface tension of the solvent, $\gamma_{solvent}$, and at the CMC, $\gamma_{solvent}$, surface excess concentration, Γ_{max}, minimum molecular area at the air-liquid interface, A_{min}, standard free energy of micellization, ΔG_m, and standard free energy of adsorption, ΔG_{ad}.

Conc EAN (mol%)	$\gamma_{solvent}$ ± 2 (mN/m)	CMC (mol/L)	γ ± 2 (mN/m)	Γ (mol/m²)	A (Å²)	ΔG_m (kJ/mol)	ΔG_{ad} (kJ/mol)
0	72	88±2x10^{-3}	42	5390±4x10^{-9}	31±2	-6±0.1	-0.94±0.01
5	59	13±5x10^{-3}	34	2970±70x10^{-9}	56±2	-11±0.2	-2.14±0.01
14	63	44±5x10^{-3}	34	1740±20x10^{-9}	96±2	-8±0.1	-3.61±0.01
25	56	88±4x10^{-3}	37	2420±9x10^{-9}	69±3	-6±0.1	-2.40±0.01
33	51	44±3x10^{-3}	37	2540±10x10^{-9}	65±3	-8±0.2	-2.31±0.01
50	51	230±20x10^{-3}	38	1040±10x10^{-9}	160±3	-4±0.1	-5.51±0.004
75	51	320±10x10^{-3}	38	1770±7x10^{-9}	94±4	-3±0.1	-3.23±0.003
100	50	530±10x10^{-3}	38	1850±5x10^{-9}	60±3	-2±0.1	-3.15±0.002

Table 3.2. Free energy parameters and packing factors for the cationic surfactant CTAB in EAN-water mixtures, as calculated from surface tension measurements. Parameters include, CMC, surface tension of the solvent, $\gamma_{solvent}$, and at the CMC, $\gamma_{solvent}$, surface excess concentration, Γ_{max}, minimum molecular area at the air-liquid interface, A_{min}, standard free energy of micellization, ΔG_m, and standard free energy of adsorption, ΔG_{ad}.

Conc EAN (mol%)	$\gamma_{solvent}$ ± 2 (mN/m)	CMC (mol/L)	γ ± 2 (mN/m)	Γ (mol/m^2)	A (Å^2)	ΔG_m (kJ/mol)	ΔG_{ad} (kJ/mol)
0	73	55±10x10^{-5}	39	1720±30x10^{-9}	97±2	-18±0.4	-3.16±0.02
5	60	21±3x10^{-5}	34	3770±20x10^{-9}	44±0.3	-21±0.3	-1.70±0.02
14	56	22±4x10^{-5}	32	2780±30x10^{-9}	60±0.7	-21±0.4	-2.41±0.02
25	55	19±3x10^{-5}	41	1200±30x10^{-9}	138±3	-21±0.3	-4.36±0.02
33	56	192±3x10^{-5}	37	1470±30x10^{-9}	113±2	-15±0.3	-3.93±0.02
50	51	1380±60x10^{-5}	42	1460±70x10^{-9}	114±5	-11±0.8	-3.47±0.01
75	51	2750±1x10^{-5}	45	1140±70x10^{-9}	146±8	-15±0.1	-3.97±0.01
100	51	1100±3x10^{-5}	46	1010±40x10^{-9}	164±7	-11±0.5	-4.32±0.01

Table 3.3. Free energy parameters and packing factors for the non-ionic surfactant $C_{12}E_4$ in EAN-water mixtures, as calculated from surface tension measurements. Parameters include, CMC, surface tension of the solvent, $\gamma_{solvent}$, and at the CMC, $\gamma_{solvent}$, surface excess concentration, Γ_{max}, minimum molecular area at the air-liquid interface, A_{min}, standard free energy of micellization, ΔG_m, and standard free energy of adsorption, ΔG_{ad}.

Conc EAN (mol%)	$\gamma_{solvent}$ ± 2 (mN/m)	CMC (mol/L)	γ ± 2 (mN/m)	Γ (mol/m^2)	A (Å^2)	ΔG_m (kJ/mol)	ΔG_{ad} (kJ/mol)
0	72	11±2x10^{-5}	33	846±3.33x10^{-8}	20±0.1	-22±0.4	-0.788±0.02
5	63	11±2x10^{-5}	34	547±3.33x10^{-8}	30±0.2	-22±0.4	-1.16±0.02
14	55	69±10x10^{-5}	33	352±2.50x10^{-8}	47±0.3	-18±0.3	-1.85±0.02
25	56	262±10x10^{-5}	32	313±0.975x10^{-8}	53±0.2	-15±0.1	-2.16±0.01
33	51	830±10x10^{-5}	33	603±2.38x10^{-8}	28±0.1	-12±0.3	-1.04±0.01
50	53	553±10x10^{-5}	35	292±4.44x10^{-8}	57±0.9	-13±0.5	-2.10±0.01
75	51	1110±20x10^{-5}	34	476±3.35x10^{-8}	35±0.2	-11±0.4	-1.36±0.01
100	51	1110±20x10^{-5}	34	460±3.35x10^{-8}	36±0.3	-11±0.4	-1.40±0.01

The surface excess concentration, $\Gamma_{max.}$ gives insight regarding the position of surfactants in the system and the force exerted by them on the surface. Accumulation of surfactants at the interface leads to positive surface excess concentrations, whereas negative values indicate the surfactants were more likely to be found in the bulk.[54] This was observed across all three surfactants, as shown in Tables 3.1 to 3.3. The trends in A_{min} and G_m which prove to be more complex are discussed below.

The average area per surfactant at the interface, A_{min}, can give insights regarding the arrangement of the surfactants during the critical micelle concentration. The energy of micellisation, G_m, can give insights regarding the arrangement of the surfactants during the critical micelle concentration. To understand the trends observed across the three surfactants, Figure 3.5 depicts the trends in A_{min} and G_m across the surfactants.

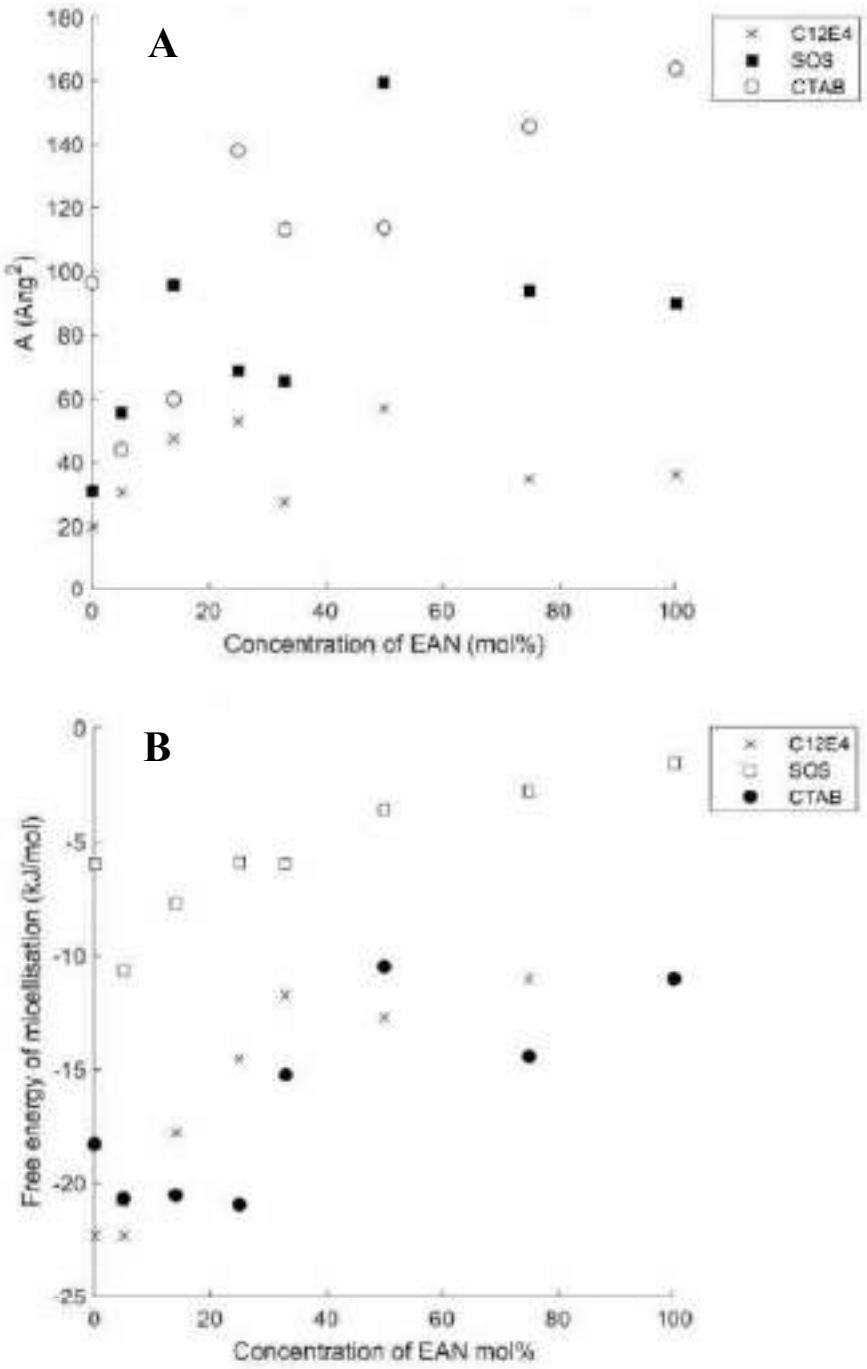

Figure 3.5. a) The area per surfactant at the interface, A_{min}, and b) the energy of micellisation, G_m, of the surfactants SOS, CTAB and $C_{12}E_4$ as calculated from the CMC curve from surface tension.

In general, there is an initial increase in the A_{min} across all the surfactants as the EAN concentration increases, but this increase becomes less pronounced beyond 50 mol% EAN for the anionic and non-ionic surfactant. The A_{min} value fluctuates but remains at a similar order of magnitude for $C_{12}E_4$ and SOS beyond 50 mol%. CTAB shows a different behaviour where the A_{min} stays constant at 33 mol% and 50 mol% but continued to increase at higher EAN concentrations. This could indicate that surfactants were laying flatter at the interface as the EAN concentration increased for $C_{12}E_4$ and SOS, and as the proportion of EAN in the solvent further increased with EAN being dominant, this effect plateaus and A_{min} no longer continues to increase. In the case of the cationic surfactant, CTAB, the separation between the surfactants could also have been increased by the interaction of the anions with the surfactants, leading to a constant increase in A_{min} even at higher concentrations of EAN.

Positive free energy parameters indicate the process requires an external input of energy, whereas negative values were expected for a spontaneous process such as self-assembly.[55] With regards to trends observed in G_m in Figure 3.5B, we see an initial decrease in the energy required for micellization across all surfactants at very low EAN concentrations, followed by a linear increase and a plateau beyond 33 mol% EAN. The energy of micellization was observed to be 2 times larger for the anionic surfactant, in comparison to the cationic and non-ionic surfactants, likely due to solubility limitations associated with anionic surfactants in ILs.

To understand the relationship between solvophobicity of the mixtures and the self-assembly process, the Gordon parameters for the solvents were calculated. In the field of amphiphile self-assembly, the cohesive energy density can be approximated by the Gordon parameter, G, as given in Equation 3.5, where γ is the surface tension at the liquid-air interface and V_m is the molar volume[48]:

$$G = \frac{\gamma}{V_m^{\frac{1}{3}}} \qquad (3.5)$$

While there are other methods for solvent cohesive energy density, these are applicable to volatile solvents. Figure 3.6 depicts the Gordon parameter calculated for varying EAN-water concentrations.

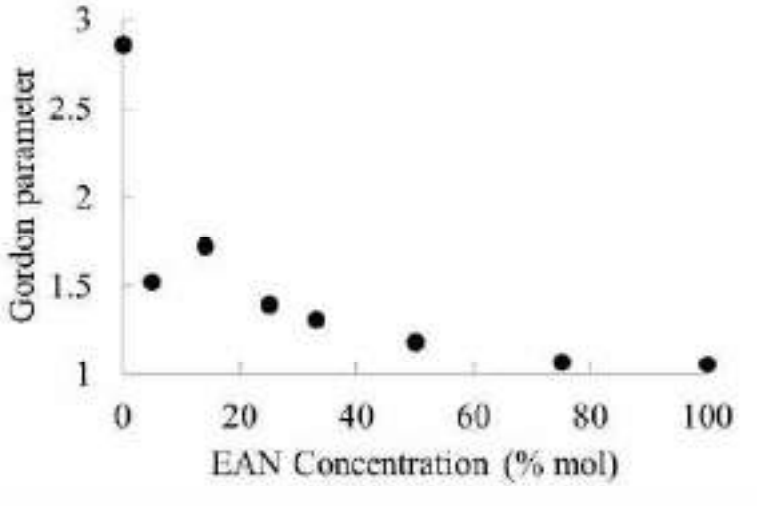

Figure 3.6. Gordon parameters calculated for EAN-water mixtures.

The decreasing trend in Gordon parameter suggests a lower cohesive energy density in EAN rich compositions and indicates that micellization was less favourable as the EAN concentration increased. For the non-ionic surfactant of $C_{12}E_4$, the free energy of micellization showed an inverse relationship to the Gordon parameter, as shown in Figure 3.5. Charge screening effects were not relevant for the non-ionic surfactant, and hence this was consistent with the hypothesis that an increased Gordon parameter led to higher solvophobicity, therefore requiring less energy for micellization. At low EAN concentrations, the water was likely preferentially solvating the surfactants, leading to a higher cohesive energy density, before the IL-water interactions becomes the major influencer of the CMC. This also confirms that solvent-solvent interactions in the system dominate the self-assembly process, with minimal solvent-solute interactions.

Another interesting observation was that the polarity response of the coumarin dye observed by Yalcin et al., which provided insight regarding the change in solvation preferences of the dye in EAN-water mixtures, had an inverse trend in comparison to the change in CMC of $C_{12}E_4$.[14] This consistency in

trends observed further suggests that the changes observed in CMC of non-ionic surfactants are in fact a result of the solvophobic effect. Polarity measurements made via coumarin suggested that with increasing water concentration, the IL-water mixture becomes more polar and solvophobic. [14] This was consistent with the low CMC values observed at low EAN concentrations and further justifies the hypothesis that surfactant-solvent interactions were more prominent at low EAN concentrations.

3.3.2 Micelle characterisation of SOS in EAN-water solutions using SAXS

Since SOS self-assembly has not been previously reported in ILs or IL mixtures, small angle x-ray scattering (SAXS) was performed to confirm the presence of micelles in EAN mixtures. However, in EAN and EAN-water mixtures no scattering could be observed from SOS using SAXS, despite trialling multiple SOS concentrations. This has been attributed as most likely due to contrast issues between the micelles and the solvent. Previous studies on similar systems in neat EAN found that the shell-solvent interface had poor contrast and there was effectively no scattering for many surfactant samples, and instead the contrast observed arose from the core-shell.[37, 67, 79] The x-ray scattering length densities (SLD) of EAN and the shell of the SOS micelle are very close in values, as shown in Table 3.4. These values were approximated using the SLD calculator on the SASView software.[85]

Table 3.4. Electron scattering length densities (SLD) of the solvents and the anionic surfactants for x-rays.

	X-ray SLD (10^{-6}/Å^2)
Water	9.46
EAN	10.9
EtAN	12.5
SOS core	9.3
SOS shell	9.12

As shown in Table 3.4, the difference in electron scattering length densities of the solvents and surfactants is minute. During SAXS, the scattering relies on the contrast between the solvent and solute, which is determined by the SLD difference. The contrast between SOS and water can be predicted to be the worst of all three solvents, as shown by the extremely similar SLD values. Due to the similar SLD values between water and SOS, scattering was not observed during our experiments.

With EAN, due to the slightly better contrast, we were optimistic about observing scattering from the samples. However, consistent x-ray scattering was also not observed with the SOS-EAN samples. A reason for the lack of contrast could also stem from EAN lodging itself into the micelle, causing the contrast between the micelle and the solvent to be even harder to distinguish. Bryant et al. observed this with EAN and mixed micelles of anionic and cationic surfactants. They found that EAN, due to its cationic nature, participates in the micelle formation and acts as a surfactant rather than a solvent during self-assembly. They were able to observe this based on neutron scattering, which allows for higher contrast between the surfactants and solvents. [34]

Neutron scattering would be a better experimental method for these systems due to the different scattering length densities for neutrons, which allow for greater contrast between solvents and surfactants. Due to circumstances detailed in the COVID-19 statement that was not feasible. Instead, to continue with this investigation, we chose EtAN as the solvent to investigate SOS micelles in PIL systems.

3.3.3 SOS micelles in EtAN-water mixtures

EtAN, a less cationic PIL, was chosen as the PIL to investigate the micelle formation of SOS. As demonstrated in Table 3.4 in Section 3.3.2, EtAN has a higher SLD, which leads to better contrast with SOS during x-ray scattering investigations. Another important difference between EtAN and EAN is

that it lacks the amphiphilic nature of EAN[34]. It is unlikely EtAN would lead to contrast issues during micellization due to cationic ions participating in the shell of the micelle.

CMC of SOS in mixtures of EtAN were measured using surface tensiometry, following the same method as for EAN. Figure 3.7 summarises the CMC of SOS micelles observed across the EtAN-water concentration range. The trend in CMC of SOS in EtAN mixtures was quite similar to the trend observed with SOS in EAN mixtures. The initial lowering of CMC at 5 mol% was observed across both PILs, along with the steady increase in CMC beyond the concentrations during which the PIL has a more dominant role in the bulk solvent. After 33 mol%, the CMC hovered around a constant value, which was also observed with EAN.

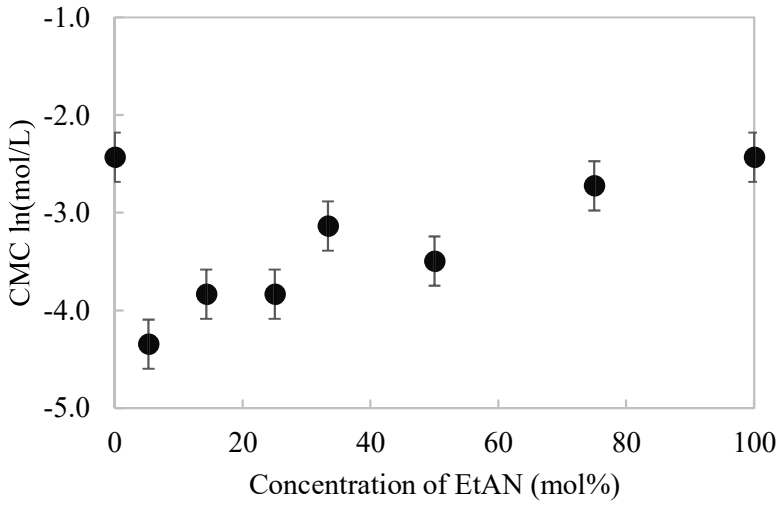

Figure 3.7. The critical micelle concentration (CMC) of SOS in EtAN-water mixtures ranging from water to neat EtAN.

To confirm the presence of micelles in these mixtures, SAXS experiments were performed at the Australian Synchrotron SAXS/WAXS beamline. Figure 3.8 depicts the observed experimental SAXS scattering and the model data for SOS in EtAN and water mixtures.

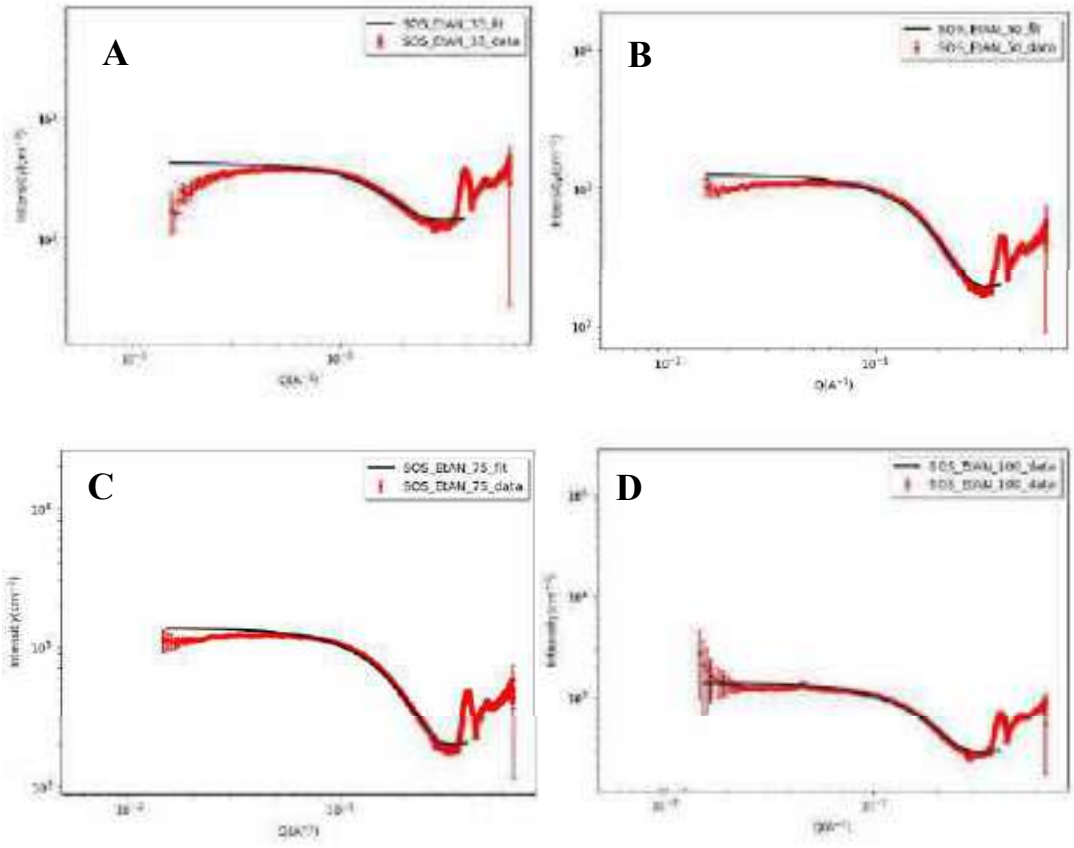

Figure 3.8. Small angle x-ray scattering of SOS in a) 33 mol%, b) 50 mol%, c) 75 mol% and d) Neat EtAN with the mathematical scattering fit for spherical micelle. Red points indicate experimental scattering data and black line indicates the SASView mathematical fit for a sphere.

Overall, the scattering observed for SOS in EtAN mixtures in Figure 3.8 were consistent with micelles, or more generally, spherical aggregates. The upturn at the lowest q values in Figure 3.8D was attributed to small aggregates, and the decrease at low q in the neat EtAN sample was attributed to over subtraction of the buffer. This was the best subtraction we could manage given the scattering issues associated with the samples. Low q also indicated that the scattering occurred close to the beamstop, which usually leads to less reliable data. It should be noted that the peak at 0.3 A^{-1} was due to Kapton tape, and weak scattering, due to poor contrast, made it difficult to subtract the background adequately. Even with the changeover in solvent to EtAN, the data quality was not optimal, and we attribute it to a similar poor contrast as EAN. While EtAN is not amphiphilic, it is also possible that EtAN cations could have aggregated among the headgroups of SOS, also leading to worse contrast than hypothesised. Overall, in the case of EtAN, the contrast was sufficient to obtain scattering to confirm micelles.

Comparison of experimental scattering data and SASView mathematical models indicated the presence of spherical micelles in EtAN-water mixtures above 33 mol% EtAN. Core-shell spheres and ellipsoid models were also tested to confirm the shape of the micelles. While it was hypothesised that the core-shell model would fit the description of a micelle best, the spherical model was able to best approximate the experimental scattering patterns, though we note the fits are poor for what is usually achievable for micelles. Table 3.5 summarises the fitting parameters for the micelles, as performed on SASView.

Table 3.5. The models and corresponding fitting parameters for micelles formed by SOS at varying EtAN concentrations. $SLD_{surfactant}$ was set to $10x10^{-6}/Å^2$ and $SLD_{solvent}$ was set to $9x10^{-6}/Å^2$.

Concentration of EtAN (mol%)	Model	Scale	Background	Radius (Å)
33	Sphere	239.5	143.5	14.2
50	Sphere	1142	190.6	13.1
75	Sphere	1229	200.3	13.2
100	Sphere	973.3	285.7	14.0

To understand the radii values observed, we approximated the size of the fully extended carbons chains contained in the core of a SOS micelle.[55] This value was 12.6 Å, which is very similar to the observed values. The lack of contrast between the core and shell of the micelles, arising from very similar SLDs, led to a lack of distinction between the core-shell boundary. It is likely we have gained scattering information at the SOS core-shell interface during this experiment. This once more highlighted the challenges faced with using x-rays for characterising micelles in PIL mixtures.

No scattering was observed in solvents ranging from water to 25 mol% EtAN, likely due to contrast issues. The SLD of the surfactant tail and core were very similar to the SLD of water. With the water rich environment at low concentrations of the PIL, the boundary between the micelles and solvent was likely not obvious enough with x-ray scattering. With the observed micelles, there were many features in the scattering pattern which could give more structural detail about the micelles. It was difficult to approximate information regarding the core and shell lengths of the micelles based on the obtained scattering.

3.3.4 Higher order liquid crystal phases

To determine the self-assembly behaviour above the CMC concentrations, penetration scans of the three surfactants in varying EAN-water concentration mixtures were characterised using a cross-polarised microscope within a temperature range from 25-90 ℃. This method provides information regarding the higher order phases the surfactant could form in the solvent mixtures and the temperature ranges during which they occur. However, they do not give insight into the exact concentrations of the surfactant at which phase formation occurs. Representative images of CTAB and $C_{12}E_4$ phases observed in EAN-water solvent mixtures are shown in Figure 3.9 and the full list of phases are shown in Table 3.6.

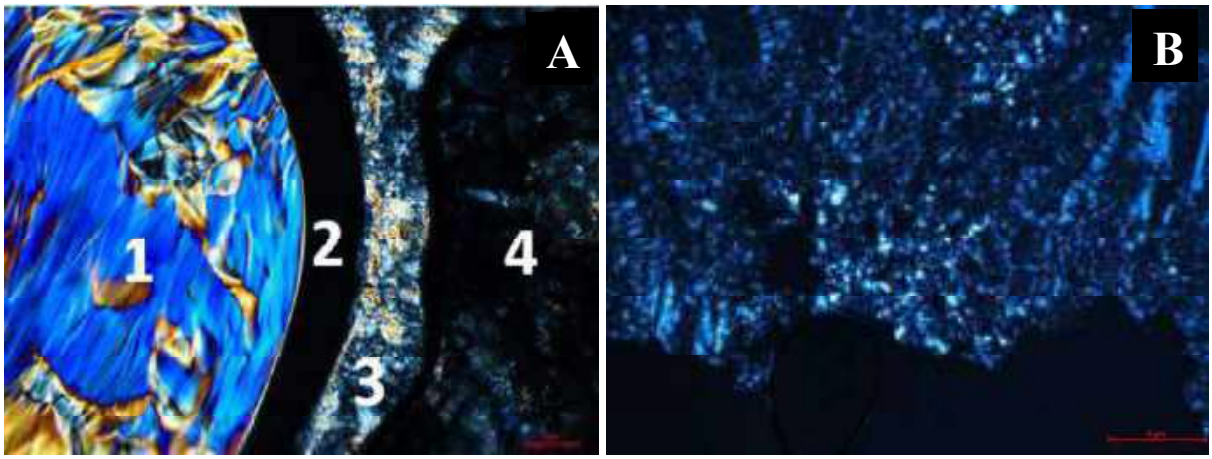

Figure 3.9. Cross polarised optical microscopy images of penetration scans of A) CTAB in 75 mol% EAN at 90 ℃ and B) $C_{12}E_4$ in water at 25 ℃. The numbers in A) represent the following phases: 1. Hexagonal, 2. Cubic, 3. Lamellar and 4. Neat surfactant. In B) only the lamellar phase was observed.

A wide variety of phases were observed for CTAB, whereas only the lamellar phase was observed in $C_{12}E_4$ at limited temperatures and EAN concentrations. SOS was unable to form any higher order phases which could be observed with optical microscopy at any of the solvent concentrations. This was likely due to the short alkyl chain of SOS, leading to poor chance of higher order phase, and the low solubility of anionic surfactants in general. In CTAB across the full EAN concentration range a wide variety of higher order phases were observed. Initially during the heating process hexagonal phases appeared after 30-60 ℃, which evolved into cubic and lamellar phases as the heating continued to 90 ℃. This was consistent with values reported in literature.[38] The higher order phase formation in the non-ionic $C_{12}E_4$ was limited to the lamellar phase, which was observed at room temperature during the initial contact

between the solvent and surfactant. The likelihood of $C_{12}E_4$ forming the lamellar phase decreased with increasing EAN concentration and temperature. The approximate results of the temperature ranges for the higher order phases at varying EAN concentrations across the three surfactants are summarised in Table 3.6.

Table 3.6. The approximate temperature ranges for higher order liquid crystal phases of CTAB, $C_{12}E_4$ and SOS in a range of EAN/water concentrations.

Surfactant	**Conc EAN (mol%)**	**Temperature range (°C)**		
		Hexagonal	Cubic	Lamellar
CTAB	0	33->90	55->90	70->90
	5	33->90	60->90	77->90
	14	49->90	58->90	74->90
	25	51->90	65->90	86->90
	33	49->90	66->90	90->90
	50	45->90	69->90	86->90
	75	43->90	78->90	90->90
	100	60->90	76->90	88->90
$C_{12}E_4$	0			20->70
	5			22->32
	14			22->29
	25			22->28
	33		No phases	
	50			
	75			No phases
	100			
SOS	0			
	5			
	14			
	25			
	33		No phases observed	
	50			
	75			
	100			

The experimental methods employed during this chapter proved to be insufficient to make conclusions regarding the behaviour of anionic surfactants in PIL-water mixtures due to a variety of contrast and solubility issues. CTAB was observed to have the most phases present, which could be attributed to several reasons. Cationic surfactants tend to perform better in self-assembly studies in comparison to anionic and non-ionic surfactants, likely due to their good solubility. It could also have led to a wider variety of phases due to having the longest alkyl chain of C16, which led to a higher driving force for self-assembly. Both $C_{12}E_4$ and SOS were molecules with a smaller carbon chain. Computational methods could potentially provide insights regarding the experimental data which was not conclusive regarding the solvent environment the anionic surfactants experience in the presence of EAN.

3.4 Conclusion

The self-assembly of a cationic, anionic and non-ionic surfactant were investigated in aqueous solutions of two ionic liquids, EAN and EtAN, to gain insight into the role of solvent species, and effect of solvent ionicity on the self-assembly process. For CTAB and SOS, at low concentrations of the PIL (< 5 mol%), the ionic liquids acted as free ions, decreasing the CMC due to charge screening effects reducing head group repulsion, similar to conventional salts. This effect was not observed in $C_{12}E_4$ due to it being non-ionic. Micelle formation of the anionic amphiphile was found to be more complex than initially hypothesised in ionic liquids. It was discovered that EtAN, the less cationic ionic liquid, was able to facilitate self-assembly of SOS, whereas in EAN mixtures micelles could not be confirmed using x-ray scattering due to contrast issues. It was hypothesised that the ethylammonium cation was actively participating in the micellization as a smaller surfactant, rather than just existing in the bulk solvent. The “surfactant-like” behaviour of the ethylammonium cation led to the formation of a micelle akin to a catanionic micelle, which was difficult to observe using x-rays due to lack of contrast between the micelle and the solvent interface. To observe higher order phases in the surfactants, CPOM was utilised. CTAB and $C_{12}E_4$ were able to form LCPs, whereas the anionic surfactant was not observed to have LCPs forming in EAN containing solvents.

4 Comparison of water models for simulations

The work in this chapter has been published: **Sachini P K Pathirannahalage**, Nastaran Meftahi, Aaron Elbourne, Alessia C G Weiss, Chris F McConville, Agilio Padua, David A Winkler, Margarida Costa Gomes, Tamar L Greaves, Tu C Le, Quinn A Besford, Andrew J Christofferson, Systematic Comparison of the Structural and Dynamic Properties of Commonly Used Water Models for Molecular Dynamics Simulations. J. Chem. Inf. Model. 2021, 61, 9, 4521–4536 (2021). Full publication available in the Appendix.

4.1 Introduction

Water is used extensively in simulation studies as a solvent yet the effect of mixing water with other constituents and the changes this induces on the bulk properties of the solvent are not well understood. Water models are widely used to explore many mixtures, including but not limited to, other polymers, biomolecules and interfaces.[86-88] This thesis investigates the interactions between water and protic ionic liquids. While experimental methods allow us to make hypotheses regarding how PILs and water interact based on their structural properties, molecular dynamics simulations allow us to gain an insight into the dynamics at the molecular level. For this, it is important for the bulk properties of the water model used to reflect experimental values when used with MD settings we use for the simulations of the mixtures. This allows us to make conclusions regarding the interactions between the PILs and water with certainty that the changes stem from the mixing, rather than the simulation settings.

To understand how bulk properties of water changes with the addition of another solvent in simulations, we can refer to a study by de Jesús-González et al. on mixing acetone with water.[89] They examined the changes to the dielectric constant, which is an indication of miscibility of molecules, with varying polarizability, with the water model TIP4P. They were able to conclude that to obtain a satisfactory dielectric constant at room temperature in mixtures of acetone and water, the forcefields for the constituents first need to give a good description of the bulk properties of the pure components.[90] Therefore, it is important to test the bulk properties of the pure components before building simulations of the mixtures.

While there are many types of water models available for MD simulations, both implicit and explicit, this study will focus on explicit water models. This thesis specifically discusses rigid and flexible fixed charge models, as well as a polarisable model. As the initial publications of water models report physical properties using settings available to them at the time of inception of the model, which ranges from 1980s to 2020, the aim of the current study was to explore how changing these settings to enable simulations of mixtures changes the predicted physical properties of bulk water.

A prime example of a model that is still widely used is TIP3P, a model first parameterised by Jorgensen in 1981.[91] TIP3P remains a popular choice amongst many due to its simple geometry, low computational cost and relative accuracy. The initial parameterisation of TIP3P truncated the short-range pairwise electrostatic interactions at a cut-off distance of 7.5 Å to produce the properties cited in the original publication. However, due to advances in computational capacities in more recent years, this cut-off distance is often extended as far as 9-12 Å[92-94] in simulations where mixing of water with another forcefield is performed. More modern settings such as long-range electrostatic treatment and dispersion corrections provided by most simulation packages such as AMBER[95] and GROMACS[96] could also not have been accounted for in initial parameterisations. How these changes to settings of the simulations changes the resulting bulk water properties has not been explored. While there have been studies investigating rigid Single Point Charge (SPC) and TIP N-point models with the inclusion of long-range corrections, there has not been an extensive study on a variety of models.[88]

It can also be difficult to determine which water model would suit a specific mixture, considering the sheer variety of water models available. For example, one of the main differences between initial TIP N-point water models and SPC water models is the model geometry, which in the case of SPC mimics a tetrahedral shape of water as present in ice, whereas TIP3P is based on water molecules as they exist in the gas phase. The slight changes in bond lengths and angles allow for SPC based models to reproduce the second peak in the radial peak distribution [97], whereas the second peak is missing entirely from the initial TIP3P potential [91]. It has also been shown that varying the bond length by as little as 10^{-2} Å has

led to up to 30% differences in the calculated self-diffusion constants. [98] This emphasises the sensitivity of the water models to their parametrisation. [87]

Comparing the proficiency of water models based on their original publications also proves to be problematic because initial parameterisations were often performed with a very specific application in mind. For example, SPC is often preferred over TIP3P in simulations of bulk water due to improved self-diffusion coefficients.[87] SPC/E[99] and TIP4PEw[100] are reparametrized versions of SPC and TIP4P for use with Ewald summation to improve water thermodynamics. TIP4P/ε[101] was designed specifically to reproduce the experimental dielectric constant of water. TIP4P/2005[102] was developed based on stability of ice polymorphs. The key goal of OPC[103] was to mimic hydrogen bonding via geometry optimisation. There are also specialised water models such as TIP4P-D[86], developed to more accurately account for London dispersion interactions. New developments in the field, including flexible variations of models such as TIP N-point and SPC, can reproduce experiments such as infrared and Raman spectra.[89, 98, 104] Some of these models are more specialised than others so users should understand the water model and their compatibility before mixing them.

Forcefields have often been parameterised with the assumption that models based on similar parametrization philosophies will be used. Therefore, changing the simulation settings and mixing these models and forcefields could lead to unexpected inconsistencies. A prime example of mismatching forcefields leading to physically impossible simulations was found by Giri et al. where they simulated cluster formation of NaCl in TIP3P water.[105] They tested different ionic forcefields to simulate NaCl and found that the mixing rule of the Lennard-Jones potential of the forcefield needs to be compatible. In cases where the mixing rules were inconsistent, for example where a forcefield with geometric mixing rule was combined with a forcefield with arithmetic mixing rule for the Lennard Jones potential, the crystallisation of the NaCl occurred at much lower concentrations of the salt than is physically observed during experiments.[105] This study highlights the importance of understanding the forcefields for simulations before mixing them with other constituents.

The various considerations involved in the choice of water models led to the need for a systematic study on widely used water models to understand the effect of recent advancements and how they reflect on the bulk water properties of these models. The last study to do a systematic test under standard simulation settings was almost 20 years ago and only included rigid 3-point water models from 3 classes. They were able to conclude that bulk properties of liquid water in molecular dynamics simulations are affected by simulation settings such as the system size, the method used for truncating long-range interactions and the method used for temperature control.[94] The current study builds on work such as this and tests a wider variety of models with a standard, more recent set of parameters to be able to compare them. This is a necessary step towards gaining insight regarding the bulk water properties in PIL-mixtures during simulations. The findings from this study have contributed to a publication.[106]

Table 4.1. Water models examined in this work.

Name	Type	Flexible?	Lennard-Jones on H?	Year Published	Reference
SPC	3-point	No	No	1981	[107]
TIP3P	3-point	No	No	1983	[108]
TIP4P	4-point	No	No	1983	[108]
TIPS3P (mTIP3P)	3-point	No	Yes	1985	[109]
SPC/E	3-point	No	No	1987	[99]
CVFF	3-point	Yes	Yes	1988	[110]
PCFF	Class II	Yes	Yes	1994[a]	[111]
COMPASS	Class II	Yes	Yes	1998[b]	[112]
TIP3P/Fw	3-point	Yes	No	1999	[113]
TIP5P	5-point	No	No	2000	[114]
TIP3P-Ew	3-point	No	No	2004	[115]
TIP4P-Ew	4-point	No	No	2004	[116]
Tip5P-Ew	5-point	No	No	2004	[117]
TIP4P/2005	4-point	No	No	2005	[118]

TIP4P/Ice	4-point	No	No	2005	[119]
SPC/Fw	3-point	Yes	No	2006	[120]
SWM4-NDP	Polarizable	No	No	2006	[121]
TIP4P/2005f	4-point	Yes	No	2011	[122]
TIP4P/ε	4-point	No	No	2014	[101]
OPC	4-point	No	No	2014	[123]
TIP3P-FB	3-point	No	No	2014	[124]
TIP4P-FB	4-point	No	No	2014	[124]
TIP4P-D	4-point	No	No	2015	[86]
SPC/ε	3-point	No	No	2015	[125]
OPC3	3-point	No	No	2016	[126]
a99SB-disp	4-point	No	No	2018	[127]
TIP5P-2018	5-point	No	No	2018	[128]
TIP3P-ST	3-point	No	No	2019	[129]
TIP4P-ST	4-point	No	No	2019	[129]
FBA/ε	3-point	No	No	2020	[130]

[a]PCFF water forcefield parameters were published as part of the INTERFACE forcefield.[131]
[b]Approximate COMPASS water parameters without cross-terms were published as part of the INTERFACE forcefield.[131]

4.2 Method

Thirty different water models were compared using NPT and NVT simulations. The simulations were performed using Large-scale Atomic/Molecular Massively Parallel Simulator (LAMMPS) 5Jun19 release. LAMMPS was chosen as it can run models with LJ functional form 12-6 (Class I), as well as 9-6 (Class II), and polarizable models easily, with input files generated by CHARMM-GUI or Visual Molecular Dynamics (VMD).[132] Moreover, LAMMPS provides the option of running 4-point water models as explicit 3-point models with the offset partial charge of the oxygen calculated internally. This allows 4-point models to be used from structure files that contain only 3-point water. The simulations were performed with periodic boundary conditions in a cubic box with side length 40.0 Å. This box

contained 2000 water molecules and was constructed using PACKMOL version 18.169,[133] and converted to LAMMPS data files using TopoTools[134] release 1.7 in VMD version 1.9.3. The long-range interactions were cut-off at 12.5 Å across all simulations. The simulations were repeated three times for statistical analysis.

The simulations began with an initial energy minimisation wherein the simulation box was under NVT condition before the SHAKE algorithm was enforced to keep the molecules rigid. The initial velocities during the equilibration step of 5 ns were randomly generated and the temperature was set to a constant 298 K. All 3-point and implicit 4-point models used the same initial structure, with a conjugate gradient energy minimization step in LAMMPS to optimize the initial geometry for each model, using force constants of 500 kcal/Å^2 for the O-H bond and 50 kcal/radian^2 for the H-O-H angle with the rigid models, while flexible models used their default parameters. Explicit 4-point models, which were necessary for the calculation of dielectric constants, were constructed individually using PACKMOL, as were the 5-point models. The polarizable SWM4-NDP model was constructed as an explicit 4-point model using PACKMOL, with the Drude oscillator added by the Python tool polarizer.py.[135] Data was collected for 25 ns.

For analysis, the PYLAT program was used to calculate dielectric constant, mean square displacement (MSD) and coordination numbers[136]. The slope of the linear section of the MSD vs time plot of the oxygen atoms was used to estimate the self-diffusion coefficient. The geometries and interaction parameters for 3-point, 4-point and 5-point models are given in Tables 4.2, 4.3 and 4.4, respectively.

Table 4.2. Parameters from original publications for 3-point models. Full list of publications and reference provided in Table 4.1.

Model	O sigma (Å)	O epsilon (kcal/mol)	O charge (e)	H charge (e)	O-H bond (Å)	H-O-H angle (°)
SPC	3.166	0.15535	-0.82	0.41	1.0	109.466667
TIP3P	3.15061	0.1521	-0.834	0.417	0.9572	104.52
TIPS3P	3.1506	0.1521	-0.834	0.417	0.9572	104.52
	H: 0.4	H: 0.046				
SPC/E	3.166	0.15535	-0.8476	0.4238	1.0	109.466667
CVFF	3.16552	0.155416	-0.82	0.41	0.96	104.5
PCFF	3.608	0.274	-0.7982	0.3991	0.97	103.7
	H: 1.098	H: 0.013				
COMPASS	3.84	0.08	-0.82	0.41	0.9572	104.52
	H: 1.087	H: 0.008				
TIP3P/Fw	3.1506	0.1522	-0.834	0.417	0.96	104.5
TIP3P-Ew	3.188	0.102	-0.83	0.415	0.9572	104.52
SPC/Fw	3.165492	0.155425	-0.82	0.41	1.012	113.24
TIP3P-FB	3.178	0.155865	-0.84844	0.42422	1.0118	108.15
SPC/ε	3.1785	0.168704	-0.89	0.445	1.0	109.45
OPC3	3.17427	0.163406	-0.89517	0.447585	0.97888	109.47
TIP3P-ST	3.19257	0.143858	-0.85112	0.42556	1.023	108.11
FBA/ε	3.1776	0.18937	-0.845	0.4225	1.027	114.7
TIP3P/Fw	3.1506	0.1522	-0.834	0.417	0.96	104.5

Table 4.3. Parameters from original publications for 4-point models. Full list of publications and reference provided in Table 4.1.

Model	O sigma (Å)	O epsilon (kcal/mol)	M charge (e)	H charge (e)	O-H bond (Å)	H-O-H angle (°)	O-M bond (Å)
TIP4P	3.15365	0.155	-1.04	0.52	0.9572	104.52	0.15
TIP4P-Ew	3.16435	0.16275	-1.04844	0.52422	0.9572	104.52	0.125
TIP4P/2005	3.1589	0.185207	-1.1128	0.5564	0.9572	104.52	0.1546
TIP4P/Ice	3.1668	0.210839	-1.1794	0.5897	0.9572	104.52	0.1577
TIP4P/2005f	3.1644	0.185207	-1.1128	0.5564	0.9419	107.4	0.15555
TIP4P/ε	3.165	0.18481	-1.054	0.527	0.9572	104.52	0.105
OPC	3.16655	0.212801	-1.3582	0.6791	0.8724	103.6	0.1594
TIP4P-FB	3.1655	0.179082	-1.05174	0.52587	0.9572	104.52	0.10527
TIP4P-D	3.165	0.223841	-1.16	0.58	0.9572	104.52	0.1546
a99SB-disp	3.165	0.238764	-1.18	0.59	0.9572	104.52	0.1546
TIP4P-ST	3.1661	0.176936	-1.04344	0.52172	0.9572	104.52	0.0989

Table 4.4. Parameters from original publications for 5-point models and polarizable model. Full list of publications and reference provided in Table 4.1.

5-point model	O sigma (Å)	O epsilon (kcal/mol)	O charge (e)	H charge (e)	L charge (e)	O-H bond (Å)	H-O-H angle (°)	O-L bond (Å)	L-O-L angle (°)
TIP5P	3.12	0.16	0.0	0.241	-0.482	0.9572	104.52	0.70	109.47
TIP5P-Ew	3.097	0.178	0.0	0.241	-0.482	0.9572	104.52	0.70	109.47
TIP5P-2018	3.145	0.188815	-0.641114	0.394137	-0.07358	0.9572	104.52	0.70	109.47
Polarizable model	**O sigma (Å)**	**O epsilon (kcal/mol)**	**O charge (e)**	**H charge (e)**	**M charge (e)**	**Drude charge (e)**	**O-H bond (Å)**	**H-O-H angle (°)**	**O-M bond (Å)**
SWM4-NDP	3.18395	0.210939	1.71636	0.55733	-1.11466	-1.71636	0.9572	104.52	0.24034

4.3 Results and Discussion

Thirty water models with varying structures were simulated with consistent conditions and parameters to obtain structural and dynamic properties. Each simulation was run for 25 ns across three separate simulations and results were compared against each model and to experimental properties of water. The radial distribution function (RDF) analysis was investigated to confirm the structural characteristics of the simulated water. A representative RDF for the 3-point water model, OPC, is shown in Figure 4.1, along with the anticipated experimental RDF for water. Refer to Section 8.3 in the Supplementary Information for all RDFs.

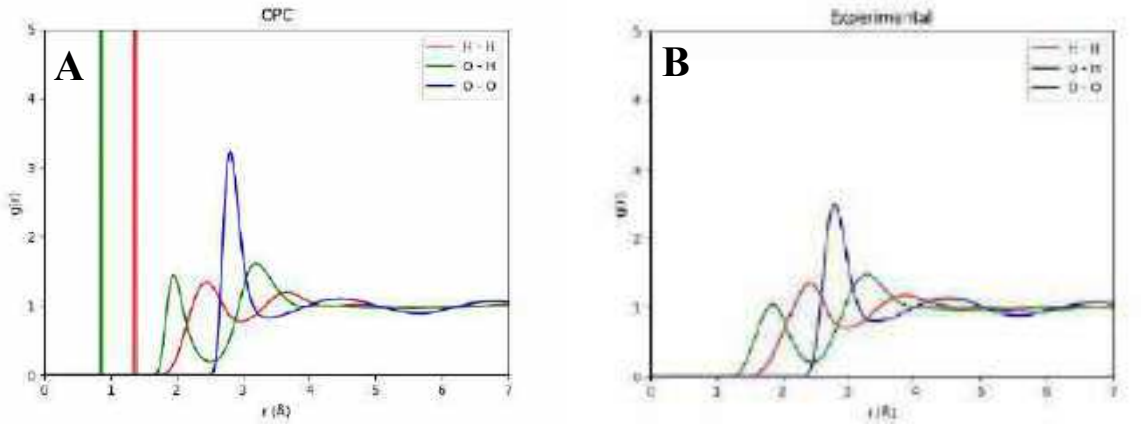

Figure 4.1. A) Radial distribution function (RDF) of 3-point water model OPC and B) experimental RDF for water reproduced from [137].

As shown in the case of OPC, the majority of water models showed satisfactory agreement between their simulated RDF and the experimental RDF for water. The largest discrepancy between the experimental and simulated models was seen in the second peak of the partial RDF which corresponded to the Hydrogen atoms of the same water molecule. The magnitude of this peak varied across the different models, likely resulting from the specified bond angles and lengths differing from one model to another. An overall summary of the calculated structural and dynamic properties across all the tested water models are provided in Table 4.5.

Table 4.5. Calculated dielectric constant, MSD, surface tension, coordination number and density of 30 water models and the associated uncertainties.

Model	Density (g/cm^3)	Coordination number	Surface tension (mN/m)	Dielectric constant	Self-diffusion coefficient ($\times 10^{-5}$ cm^2/s)
SPC	0.972 ± 0.006	5.585 ± 0.001	50.3 ± 0.2	65 ± 1	4.32 ± 0.04
TIP3P	0.980 ± 0.006	6.239 ± 0.001	47.0 ± 0.2	95 ± 3	5.72 ± 0.04
TIP4P	0.994 ± 0.006	5.14 ± 0.001	52.2 ± 0.2	51.3 ± 0.5	2.57 ± 0.04
TIPS3P	1.007 ± 0.006	7.5 ± 0.3	51.1 ± 0.2	106 ± 1	5.55 ± 0.06
SPC/E	0.993 ± 0.006	4.9 ± 0.2	57.6 ± 0.2	73 ± 1	2.60 ± 0.03
CVFF	0.978 ± 0.006	6.4 ± 0.3	47.3 ± 0.4	135 ± 3	5.95 ± 0.05
CVFF(cm)	0.989 ± 0.006	5.761 ± 0.001	49.8 ± 0.4	151 ± 2	5.2 ± 0.2
PCFF	1.008 ± 0.005	13.5 ± 0.4	69.5 ± 0.4	159 ± 2	7.7 ± 0.2
COMPASS	0.958 ± 0.006	4.953 ± 0.001	40.7 ± 0.4	118 ± 2	6.4 ± 0.1
TIP3P/Fw	1.027 ± 0.006	5.3 ± 0.3	55.2 ± 0.4	197 ± 2	3.8 ± 0.1
TIP5P	0.985 ± 0.006	4.991 ± 0.001	48.9 ± 0.2	94 ± 3	2.79 ± 0.03
TIP3P-Ew	0.996 ± 0.006	4.7300 ± 0.0004	47.1 ± 0.2	92 ± 1	4.11 ± 0.05
TIP4P-Ew	0.996 ± 0.005	4.6900 ± 0.0005	59.2 ± 0.2	65 ± 1	2.54 ± 0.01
TIP5P-Ew	1.003 ± 0.006	5.143 ± 0.001	52.2 ± 0.2	100 ± 2	2.92 ± 0.04
TIP4P/2005	0.997 ± 0.005	4.7053 ± 0.0001	63.5 ± 0.2	58 ± 1	2.18 ± 0.04
TIP4P/Ice	0.993 ± 0.006	4.634 ± 0.001	73.4 ± 0.2	63 ± 2	1.21 ± 0.03
SPC/Fw	1.007 ± 0.006	4.743 ± 0.001	58.6 ± 0.4	80 ± 3	2.57 ± 0.06
SWM4-NDP	0.990 ± 0.005	5.209 ± 0.001	63.1 ± 0.5	75 ± 1	2.57 ± 0.05
TIP4P/2005f	0.996 ± 0.005	5.0 ± 0.2	60.3 ± 0.4	59 ± 2	2.76 ± 0.04
TIP4P/ε	0.996 ± 0.006	4.717 ± 0.001	64.6 ± 0.2	79 ± 2	2.16 ± 0.01
OPC	0.997 ± 0.005	5.1971 ± 0.0005	70.1 ± 0.2	78 ± 1	2.27 ± 0.02
TIP3P-FB	0.990 ± 0.006	4.6786 ± 0.0004	60.3 ± 0.2	79 ± 4	2.14 ± 0.05
TIP4P-FB	0.997 ± 0.006	4.702 ± 0.001	64.7 ± 0.2	77 ± 1	2.10 ± 0.03
TIP4P-D	0.993 ± 0.006	5.149 ± 0.001	70.8 ± 0.2	63 ± 1	2.01 ± 0.07
SPC/ε	0.991 ± 0.005	4.672 ± 0.001	65.3 ± 0.2	80 ± 3	1.55 ± 0.05

OPC3	0.991 ± 0.006	4.9 ± 0.2	61.0 ± 0.2	79 ± 1	2.28 ± 0.02
a99SB-disp	0.996 ± 0.006	5.173 ± 0.001	74.4 ± 0.2	67 ± 1	1.78 ± 0.03
TIP5P-2018	0.997 ± 0.006	5.175 ± 0.001	61.6 ± 0.2	129 ± 2	2.31 ± 0.09
TIP3P-ST	0.993 ± 0.005	4.6009 ± 0.0005	63.8 ± 0.2	81 ± 2	1.24 ± 0.02
TIP4P-ST	0.999 ± 0.006	4.7034 ± 0.0003	64.5 ± 0.2	82 ± 4	2.02 ± 0.01
FBA/ε	0.991 ± 0.005	4.64 ± 0.001	68.0 ± 0.4	75 ± 1	1.56 ± 0.02
Experimental	**0.997**[138]	**4.7**[139]	**71.99**[140]	**78.3**[141]	**2.30**[142]

Interestingly, some 3-point models outperformed 4-point models in terms of simulating specific properties. This demonstrated that more computationally costly models do not necessarily lead to more accurate representations of water in simulations, especially for very specific property.

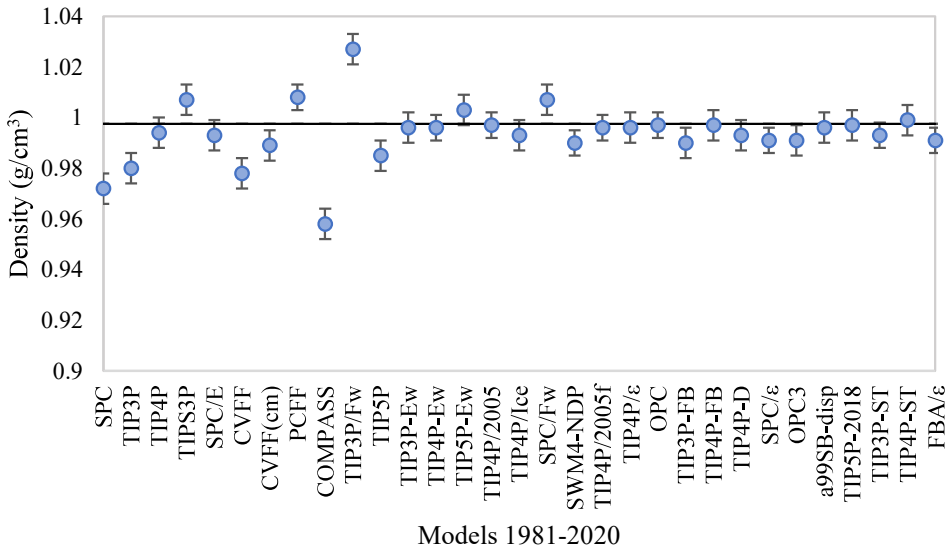

Figure 4.2. Simulated density for water models from 1981 to 2020. The horizontal line corresponds to the experimental density of 0.99753 g/cm^3.

The density across all water models reproduced experimental results very well, as shown in Figure 4.2, with newer models outperforming older models. It was observed that models published after the introduction of particle-particle particle-mesh (PPPM)[143] and particle-mesh Ewald (PME)[144] methods for approximating long-range electrostatics performed better than models published before this

advancement. The model which deviated from the experimental density value the most was COMPASS, published in 1998 without long-range electrostatics approximations, which was likely affected adversely by PPPM which it was not designed to be used with. These findings suggest that testing is required before combining older water models with newer long-range electrostatic treatments available for use today.

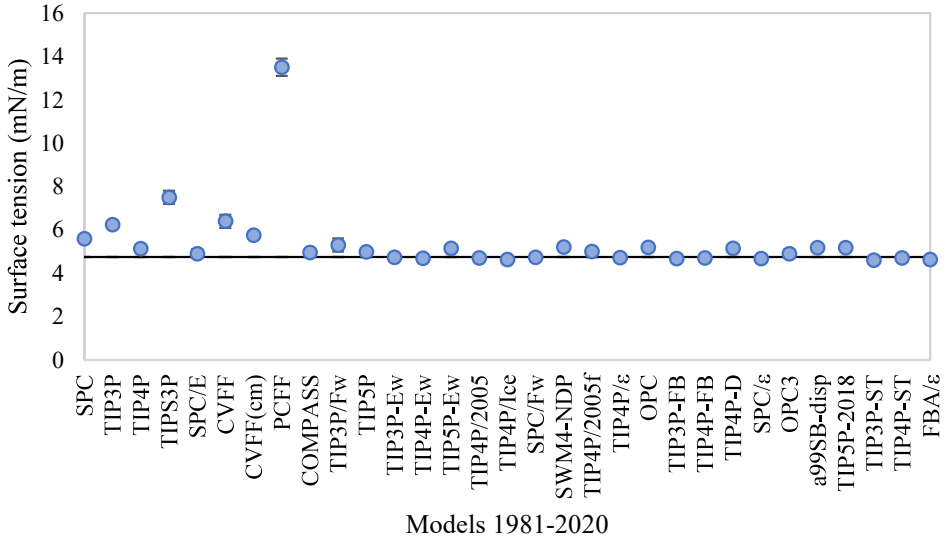

Figure 4.3. Simulated surface tension of water models from 1981 to 2020. The horizontal line corresponds to the experimental coordination number of 4.7.

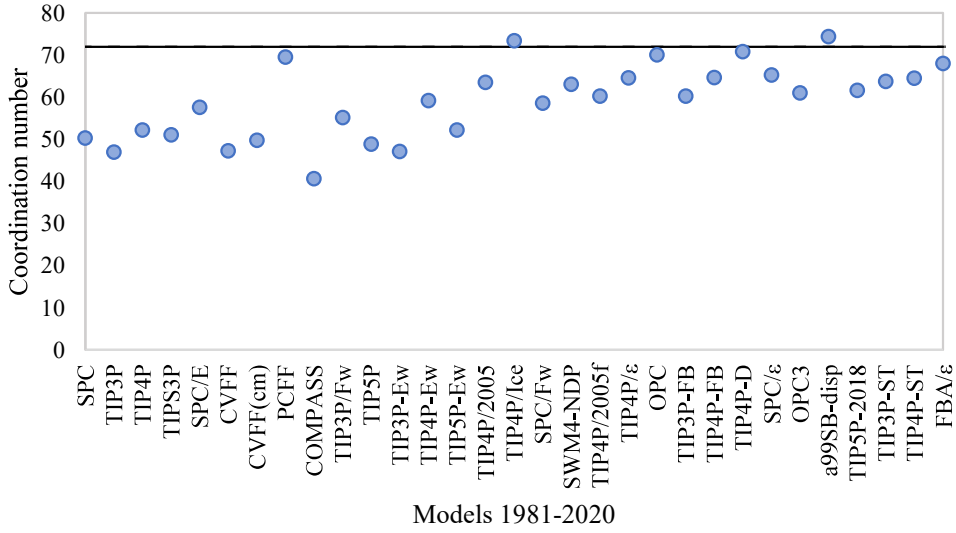

Figure 4.4. Simulated coordination number of first solvation shell of water models from 1981 to 2020. Horizontal line corresponds to the experimental surface tension of 71.99 mN/m.

Until recently the water models were not parameterised to optimise the surface tension values. Unsurprisingly, TIP3P-ST and TIP4P-ST, designed for use in simulations where surface tension is a key property, performed well, as shown in Figure 4.4. The analytical tail correction to the surface tension due to the Lennard-Jones cutoff was not performed in this study, which could explain why some models outperformed TIP3P-ST and TIP4P-ST at first glance. The majority of models published in 2005 and later reproduced the experimental surface tension reasonably well.

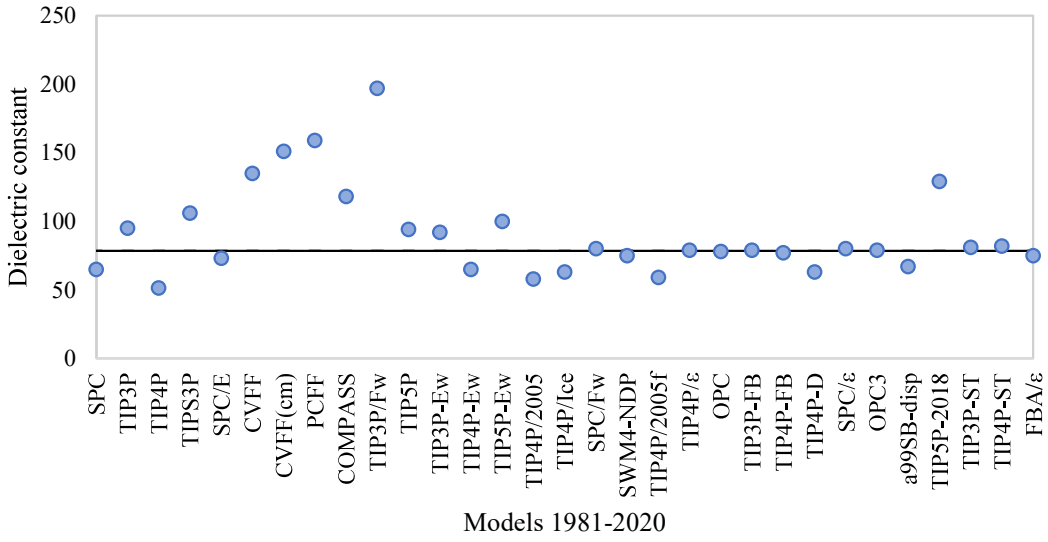

Figure 4.5. Static dielectric constant of water models from 1981 to 2020. The horizontal line corresponds to the experimental dielectric constant of 78.3.

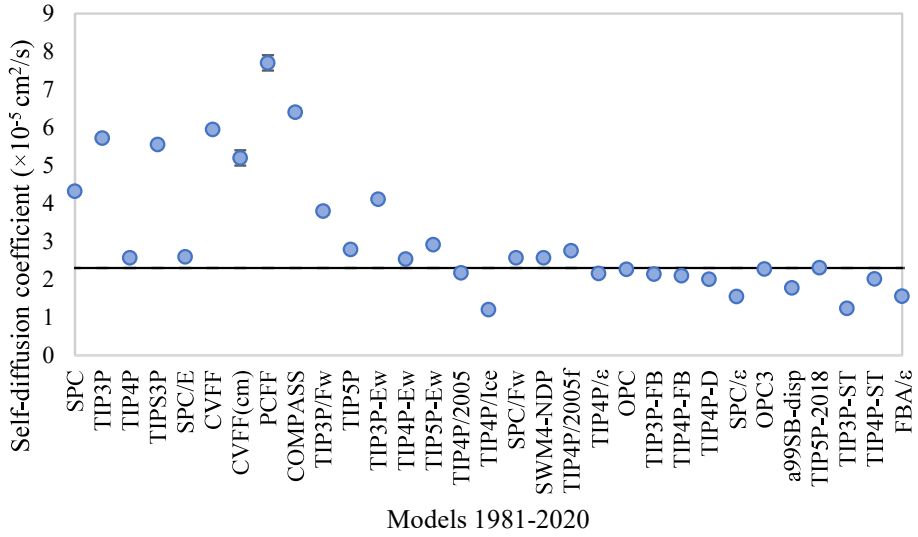

Figure 4.6. Self-diffusion coefficient of water models from 1981 to 2020. The horizontal line corresponds to the experimental self-diffusion coefficient of 2.30×10^{-5} cm^2/s.

As with most other properties discussed, experimental dielectric constant and self-diffusion coefficient improved drastically after 2006. As the field progressed and use of water models in multivariable systems increased, these properties were important for interactions in mixtures and had to be investigated thoroughly during forcefield parameterisation. TIP4P/ε, SPC/ε, and the flexible FBA/ε were all parametrized to optimise the dielectric constant, therefore reproducing the experimental value quite well. Unfortunately, during the parametrisation of SPC/ε, and FBA/ε to increase accuracy of the dielectric constant, the changes led to not so accurate self-diffusion coefficients. The majority of the TIP3P based models, except TIP3P-FB, also had large discrepancies between simulated and experimental diffusion coefficients. This was largely expected since TIP3P based models were initially designed for Monte Carlo simulations.

To compare the models against corresponding experimental values for the properties of water and determine the best option across the wide variety of models available for use in simulations with mixtures, the discrepancy between the calculated values and the experimental values was quantified, and these are provided in Table 4.6.

Table 4.6. Discrepancy between the simulated water model physical property values and the experimental values as a percentage.

	Dielectric constant	**MSD**	**Surface tension**	**Coord number**	**Average**
COMPASS	50%	180%	43%	5%	70%
PCFF	103%	236%	3%	187%	132%
SPC	17%	88%	30%	19%	38%
SPC/E	6%	13%	20%	4%	11%
TIP3P	22%	149%	35%	33%	60%
TIPS3P	35%	142%	29%	60%	66%
TIP4P/2005	26%	5%	12%	0.11%	11%
TIP4P/ε	0.7%	6%	10%	0.36%	4%
a99SB-disp	15%	22%	3%	10%	13%
CVFF	72%	159%	34%	36%	75%
SPC/Fw	1.93%	12%	19%	1%	8%
TIP3P/Fw	152%	67%	23%	13%	64%

TIP3P/Ew	17%	79%	35%	1%	33%
TIP4P-Ew	17%	10%	18%	0.21%	11%
TIP4P/2005f	25%	20%	16%	6%	17%
TIP4P-D	19%	12%	1.70%	10%	11%
OPC	0.1%	1.06%	3%	11%	3.7%
TIP4P	35%	12%	28%	9%	21%
TIP3P-FB	1%	7%	16%	0.46%	6%
TIP4P-FB	2%	9%	10%	0.04%	5%
CVFFcm	93%	126%	31%	23%	68%
TIP4P/Ice	19%	47%	2%	1%	17%
OPC3	0.8%	0.66%	15%	4%	5%
SPC/Epsilon	2%	33%	9%	1%	11%
TIP3P-ST	3%	46%	11%	2%	16%
TIP4P-ST	4%	12%	10%	0.07%	7%
FBA/Epsilon	5%	32%	6%	1%	11%
TIP5P	20%	22%	32%	6%	20%
TIP5P-Ew	28%	27%	28%	9%	23%
TIP5P-2018	65%	0.6%	15%	10%	23%
SWM4-NDP	5%	12%	12%	11%	10%

Overall, the water models with the most accurate predicted properties in comparison to experimental results could be identified. With an average discrepancy of 5% across all properties, the best 3-point model was OPC3. For 4-point model, the OPC description of water also had the best agreement across properties with an average difference of 3.7% between the simulated and experimental properties. TIP5P had the best agreement with experimental results of all the tested 5-point models, with an average difference between experimental and simulated values of 20%. Of all the flexible models tested, SPC/Fw yielded the best results, with an average difference of 8%.

4.4 Conclusion

30 water models were tested to explore how the simulated properties of water change due to widely used, modern settings. The models which had the closest average agreement with experimental results across properties, dielectric constant, surface tension, coordination numbers and density were identified. The best 3-point model was determined to be OPC3, as well as for 4-point models, OPC description of

water also had the best agreement across properties. TIP5P had the best agreement with experimental results of all the tested 5-point models and for the flexible models tested, SPC/Fw yielded the best results. As the field of molecular dynamics have shifted to simulating pure water to mixtures in the early 2000s, properties important for mixtures such as surface tension, dielectric constant and self-diffusion coefficients have become more of a focus during water forcefield parametrisation. This was clearly reflected by the general increase in accuracy across all properties of water models investigated in the current study. For the purpose of investigating PIL-water mixtures, OPC3 was chosen as the suitable water model due to the accuracy of its simulated properties as well as the efficiency in comparison to more computationally costly 4-point, 5-point or polarisable models.

5 Molecular dynamics of micelles in protic ionic liquid mixtures

5.1 Introduction

As discussed throughout this thesis, the presence of the hydrogen available for proton transfer in PILs leads to many of their interesting physicochemical properties, particularly due to a strong H-bond network in the bulk solvent.[74] Much like water, this led to complications when it came to PIL descriptions in molecular dynamics simulation. In the case of water, there was much debate regarding ways to express the molecular structure which leads to accurate physical properties in simulations.[62] In developing forcefields for PILs, a similar conundrum occurred.

While there was interest in designing appropriate forcefields for ILs, the wider field of computational work related to PILs was divided on the nature of the H-bonds and how to best reproduce experimental properties. EAN, a usual starting point for work involving PILs, was at the heart of the debate. There were contradicting opinions in literature regarding whether the H-bonds in EAN should be expressed as linear or with a slight bent. Based on x-ray and neutron structure factors, several literature sources have hypothesised that the bond between NH-O is slightly bent.[145-147] On the other hand, several other authors suggest that this bond was linear in nature, based on DFT trajectories in condensed phase[148] and X-ray diffraction of EAN crystals[149]. It was unclear so far which is the correct interpretation of the H-bonds involved in EAN and it was difficult to make conclusions regarding the molecular structure based on the current experimental information we have on EAN.

There is renewed interest in using computational molecular dynamics simulations to understand molecular interactions in PIL mixtures due to the new polarisable forcefield for EAN. Goloviznina et al. has extended their transferable polarisable forcefield to include EAN, which could allow for accurate representation of EAN in mixtures.[62] This allows for simulations of EAN to simulate diffusion, which

solves the issues of EAN being solid at room temperature in classical MD. While this new force field will prove to be a large step forward, critical properties such as dielectric constant has not been validated yet. As the field of PILs gear up for a new era of simulations which will allow for binary and ternary mixtures with polarisable effects included, it is now possible to combine existing classical forcefields to simulate these systems.

The existing literature in the field of PILs and MD focuses on mixing PILs with forcefields for molecular solvents such as water and other organic solvents. There are some recent examples of PILs, EAN and PAN, being mixed with water and organic solvents.[14] These studies allowed the authors to confirm hypotheses regarding preferential solvation properties of PILs, which were verified via autofluorescence spectroscopy. Since the main focus of the field has been on refining and answering fundamental questions about forcefield development, there is still much room for more studies to understand binary and ternary mixtures of ILs using MD. It was also worth noting that since classical forcefields for PILs come with some caveats, existing MD studies on PILs mostly use MD as a complementary computational technique to understand behaviour and properties of mixtures that they verify experimentally.[14]

There is a distinct lack of any literature on using MD to probe self-assembly of surfactants in PILs or PIL mixtures. An important unanswered question in the wider PIL community is the role of the cation and the anion of the PIL during surfactant self-assembly. As PILs are the largest solvent class capable of promoting self-assembly of surfactants, it is important to understand how the constituents of the PIL are acting during this process. While experimental techniques such as SAXS and neutron scattering allow us to make hypotheses regarding what happens at the molecular level, computational simulations are necessary to truly understand the processes and dynamics of the mixtures. While MD forcefields for PILs are still being refined, they are now at a level where they can be used to probe the molecular structures and dynamics of surfactant self-assembly successfully. Compatible forcefields for surfactants

and molecular solvents with force fields for PILs now exist.[14] While there are no reports in the literature which seek to combine these force fields to simulate ternary mixtures of micelles, the current study aims to show this was in fact possible, opening the door of opportunities for the field of PILs to complement their experimental self-assembly studies with computational MD simulations.

5.2 Method

The molecular dynamics simulations were setup using the simulation package GROMACs. The surfactant forming micelles used during the current study were CTAB, SOS and $C_{12}E_{4.}$ These were chosen to be consistent with previous experimental investigations in Chapter 3. The micelles were constructed using PACKMOL and equilibrated in water for 100 ns. Separately from the micelles, cubic boxes of length 100 Å were packed with solvents. The solvents included binary mixtures of ethylammonium nitrate (EAN) and water. The concentration of EAN varied from 0, 25, 50, 75 mol% to neat EAN. Setting up the simulations with the micelles included in the solvents required a several step process. First, the solvent was equilibrated for up to 10 ns. The micelles were then extracted from the initial water box and packed into the solvent box using PACKMOL. VMD was used to remove the solvent molecules which were closer than 2 Å from the micelle. The charges and the solvent ratios were readjusted by manually adding the appropriate number of cations and anions before submitting the simulation to run. Simulations of the CTAB, SOS and $C_{12}E_4$ micelles in EAN-water mixtures underwent an energy minimisation, followed by equilibration for 5 ns before running for 10 ns. The temperature of the simulation was kept constant at 298 K. Radial distribution functions were calculated for the systems to understand the solvation layers around the micelles.

5.3 Results and discussion

MD simulations were performed for the three surfactants forming micelles in EAN-water mixtures to understand their interactions. Micelles of CTAB, $C_{12}E_4$ and SOS were equilibrated for 100 ns in water before introducing the solvents, EAN and EAN-water mixtures. Figure 5.1 illustrates the equilibrated micelles in water prior to solvating them in the respective EAN-water solvent boxes.

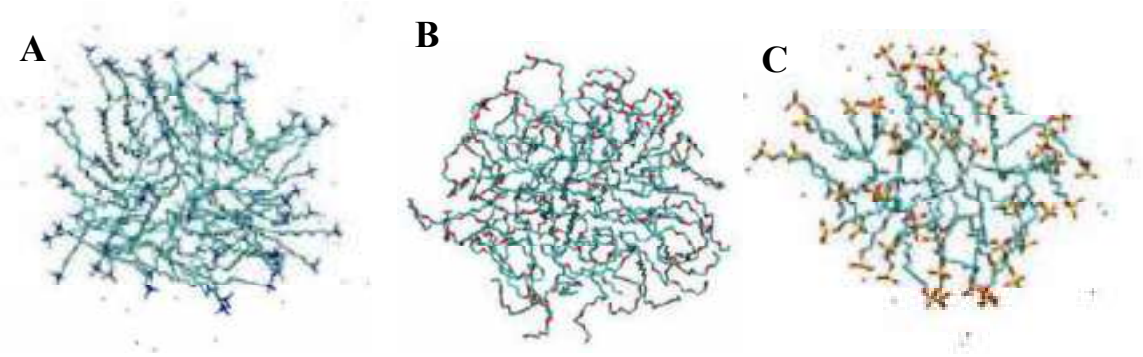

Figure 5.1. Molecular Dynamics simulations of surfactant micelles of A) CTAB, B) $C_{12}E_4$ and C) SOS in water.

In water, the micelles were surrounded by the solvent, with no significant molecular level interactions observed between the solvation layer and the micelles. This changed drastically when EAN was introduced to the anionic and cationic surfactant micelles. As hypothesised in Chapter 3, the experimental results indicated that there could be interactions between the cation of the PIL and the micelle formed by the surfactants.

In the MD simulations, the cation of the EAN, ethylammonium, was seen to form a solvation layer around the micelles with an overall charge. Ethylammonium was lodging itself in the shell layer of the micelle, displaying “surfactant-like” behaviour, as shown in Figure 5.2 and 5.3.

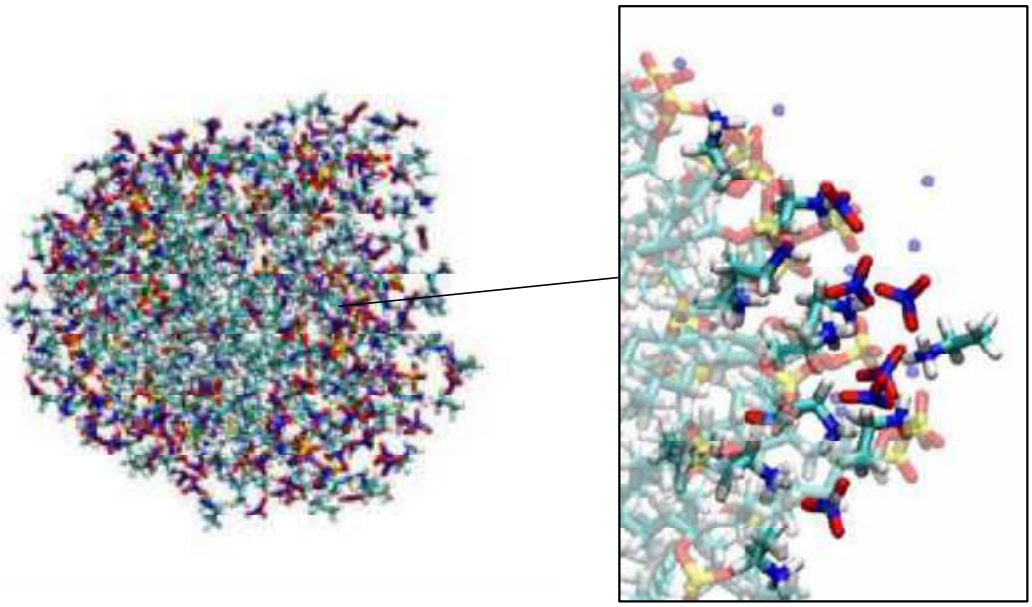

Figure 5.2. SOS micelles solvated by neat EAN. SOS micelle is represented by pale blue and white molecules, while nitrate anions are blue and red.

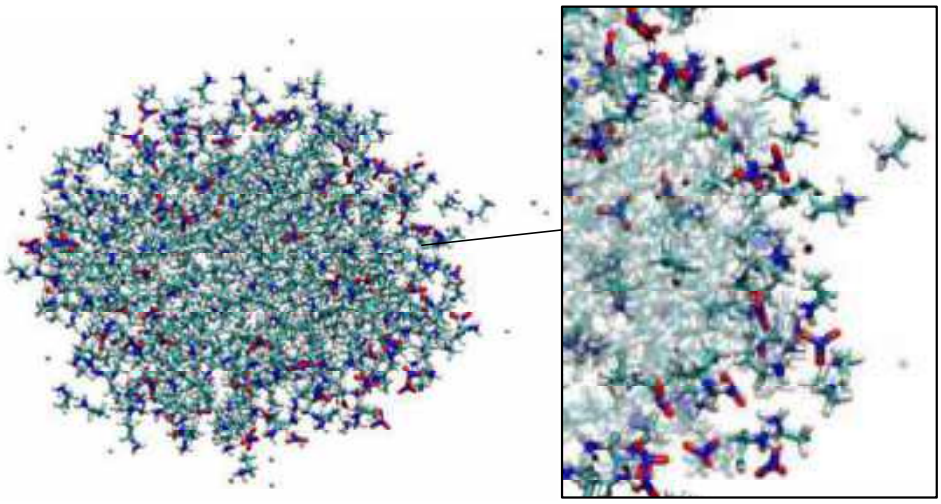

Figure 5.3. CTAB micelles solvated by neat EAN. CTAB micelle is represented by pale blue and white molecules, while nitrate anions are blue and red.

With $C_{12}E_4$, it was noticable that a layer of nitrate ions from the EAN seemed to be closer to the micelle surface, compared to the ethylammonium ions. In general, the "surfactant-like" behaviour of the ethylammonium cation, where it lodged itself into the micelle was not visually observed to the extent it was with the charged micelles, as shown in Figure 5.4.

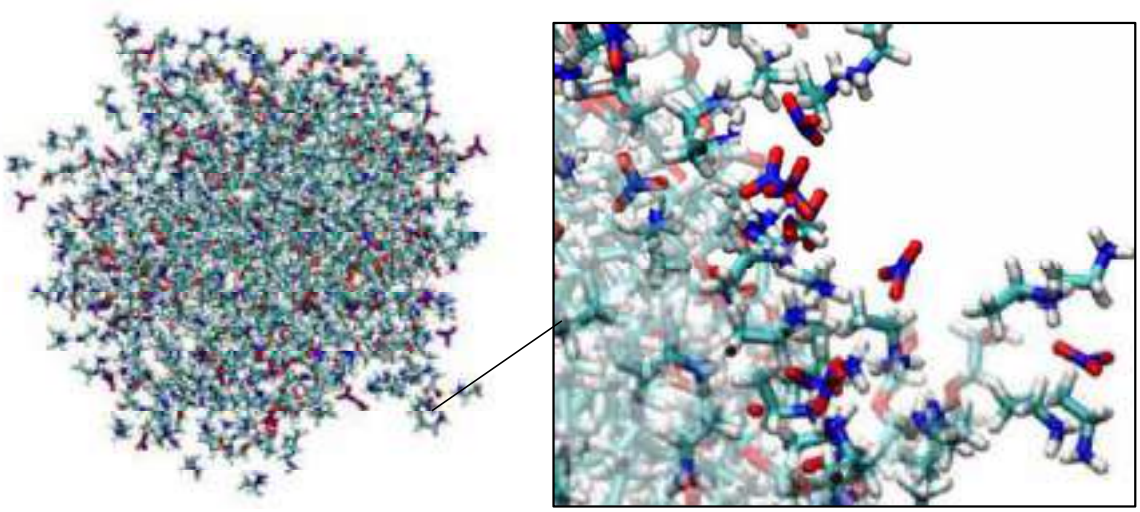

Figure 5.4. C12E4 micelles solvated by neat EAN.

These results show ethylammonium cations participating in the micelle formation as small surfactants, rather than simply solvating the micelles. This was hypothesised by Lam et al. via their neutron scattering studies of DTAB micelles in EAN.[13] Their experimental investigation of DTAB in multiple PILs, including EAN and EtAN, suggested that due to the polar and non-polar constituents of the EA cation, which is similar to the structure of the surfactants themselves, they lodge themselves into the micelle and act as smaller cationic surfactants with DTAB. We were able to demonstrate that this hypothesis holds in the case of the cationic surfactant, CTAB, and also extends to anionic surfactant self-assembly via the current study. Another interesting insight gained from the SOS micelles being solvated by the EAN was that nitrate ions are forming a solvation shell around the anionic micelles, despite both constituents being negatively charged. This was likely due to the cationic ethylammonium ions making the overall charge of the micelle less negative than initially anticipated. To verify these results quantitatively, the radial distribution functions (RDF) were calculated. The RDFs for the three micelles in neat EAN are shown in Figure 5.5.

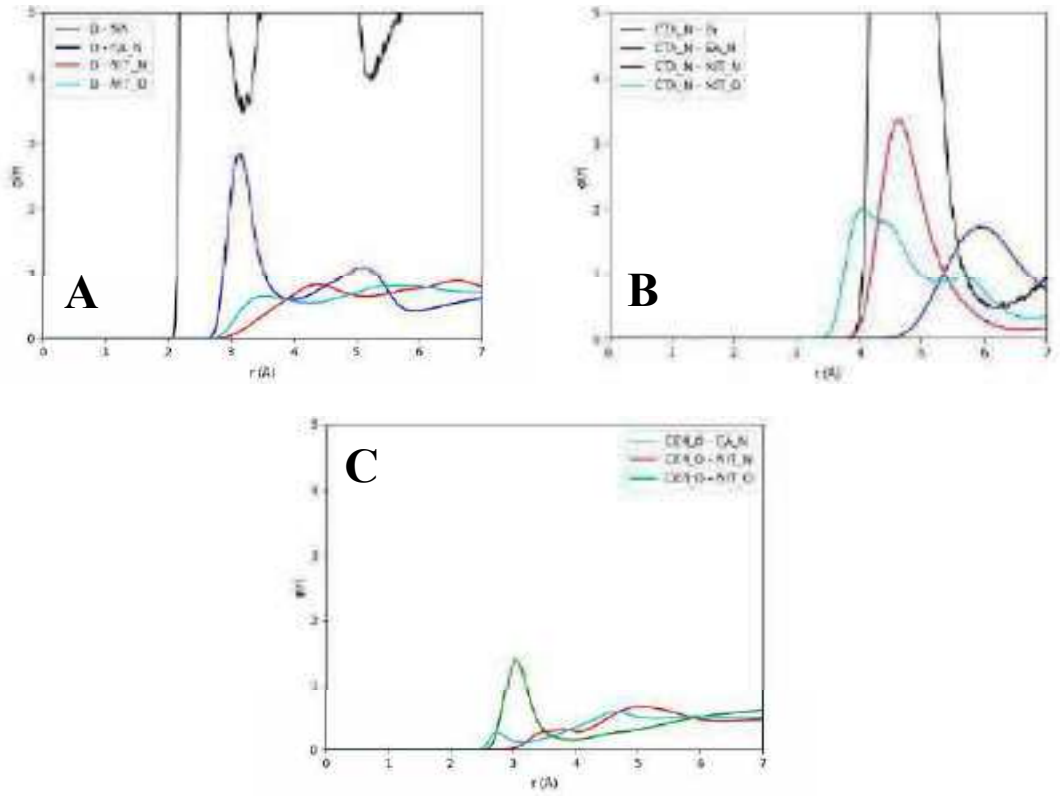

Figure 5.5. Radial distribution functions (RDFs) of A) CTAB, B) SOS and C) $C_{12}E_4$ in neat EAN.

Across the three surfactants, the calculated RDFs showed that the nitrogen from the ethylamine cation from the EAN was interacting closely to the anion of the surfactants. In the case of the positively charged surfactant CTAB, there was a noticeable solvation shell of nitrate anions of the EAN surrounding the micelle, as demonstrated by the RDFs in Figure 5.5. In the case of SOS, the cation of EAN, ethylamine, had a considerably large and close interaction with the outer shell of the micelle. This likely is due to the "lodging" of the cation in the micelle, observed visually in Figure 5.2. For $C_{12}E_4$ micelles, the interactions were less complicated, due to the lack of surface charge of the micelle.

It is important to note that the EAN model used in these simulations does not factor in diffusion, as observed by the very large RDF peaks across all surfactants. This is a limitation of classical force fields which is addressed in polarisable force fields. Due to the time constraints of this project, we were unable

to test and confirm the polarisable force field for EAN to confirm if the trends observed using classical force fields translate to the dynamics observed when diffusion is factored.

The RDFs for the negatively charged micelle, SOS, as the concentration of EAN varies are shown in Figure 5.6. The trends in the RDFs provide insight into the interactions between the different atoms on the surfactant and the solvent. As shown in Figure 5.6, as the ratio of water and EAN varies in the micelle solvent environment, the biggest change to the RDFs was observed in the interaction between the micelle cation and anion. As the EAN concentration increased in the SOS-EAN-water mixtures, the strength of interaction between the micelle cation and anion seemed to increase. The interaction between the micelle cation and the EAN cation also seemed to decrease with increasing EAN concentration. However, the surprising outcome of this was the shapes of the curves did not change with the increasing EAN concentration in the presence of SOS. The water did not appear to displace the EAN or vice-versa.

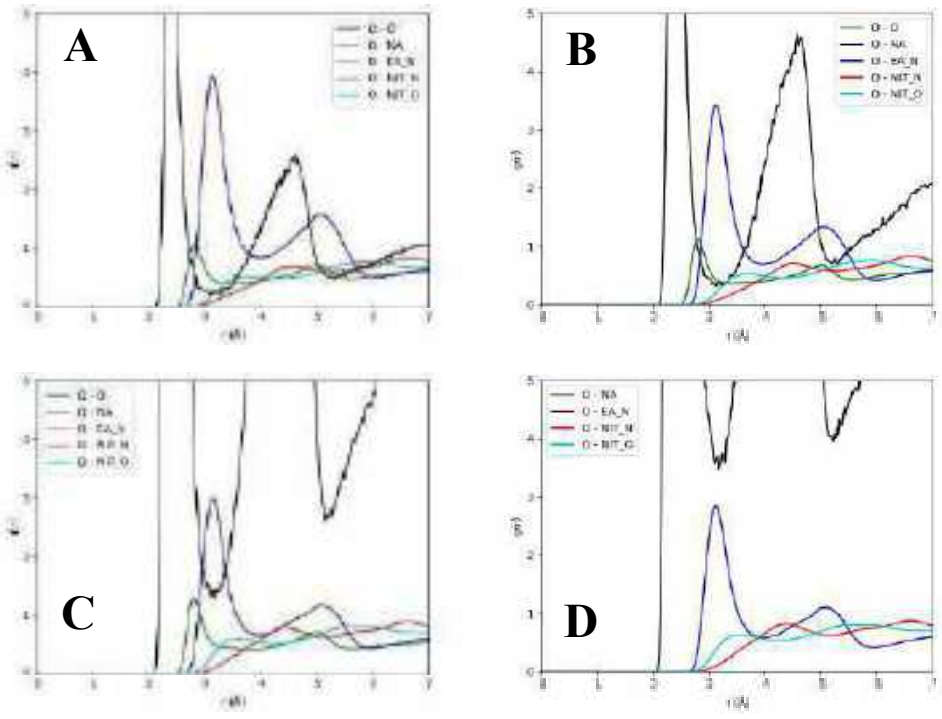

Figure 5.6. Radial distribution functions (RDFs) of SOS in A) 25 mol% EAN, B) 50 mol% EAN, C) 75 mol% EAN and D) neat EAN mixtures.

The RDFs for the micelle formed by positively charged surfactant, CTAB, as the concentration of EAN varies was shown in Figure 5.7. As the EAN concentration increased in the presence of the positively charged micelle, the biggest change observed was in the interaction between the cation and the anion of the CTAB. When the concentration of the EAN increases, it seemed to facilitate the nitrogen of the CTAB anion and the bromide ion to interact to a greater degree.

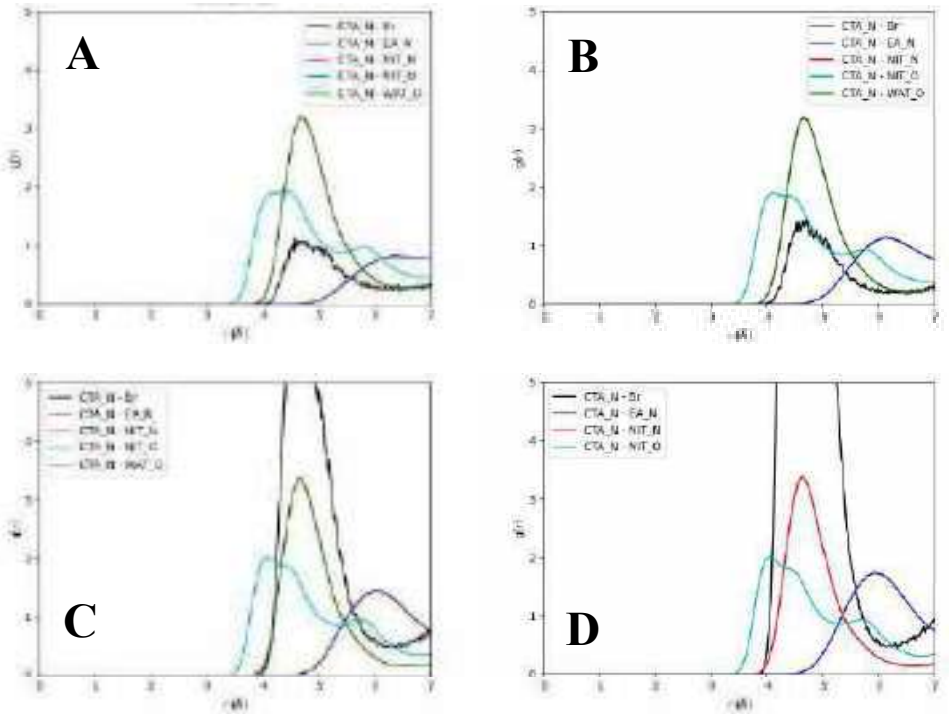

Figure 5.7. Radial distribution functions (RDFs) of CTAB in A) 25 mol%, B) 50 mol%, C) 75 mol% and D) neat EAN mixtures.

Finally, the RDFs formed by the neutral micelle, $C_{12}E_4$, as the concentration of EAN varies was shown in Figure 5.8. At low concentrations of EAN, there was a strong interaction between the $C_{12}E_4$ micelle and the nitrogen of the ethylamine cation. However, as the ratio of EAN increased in the solvent, this interaction was overtaken by the water, as water seems to be forming a solvation layer surrounding the micelle in higher EAN concentrated solvents (above 50 mol% EAN). This can be seen in Figure 5.8 by the decrease in the CE4 – O interaction and the increase in the CE4 – WAT_O.

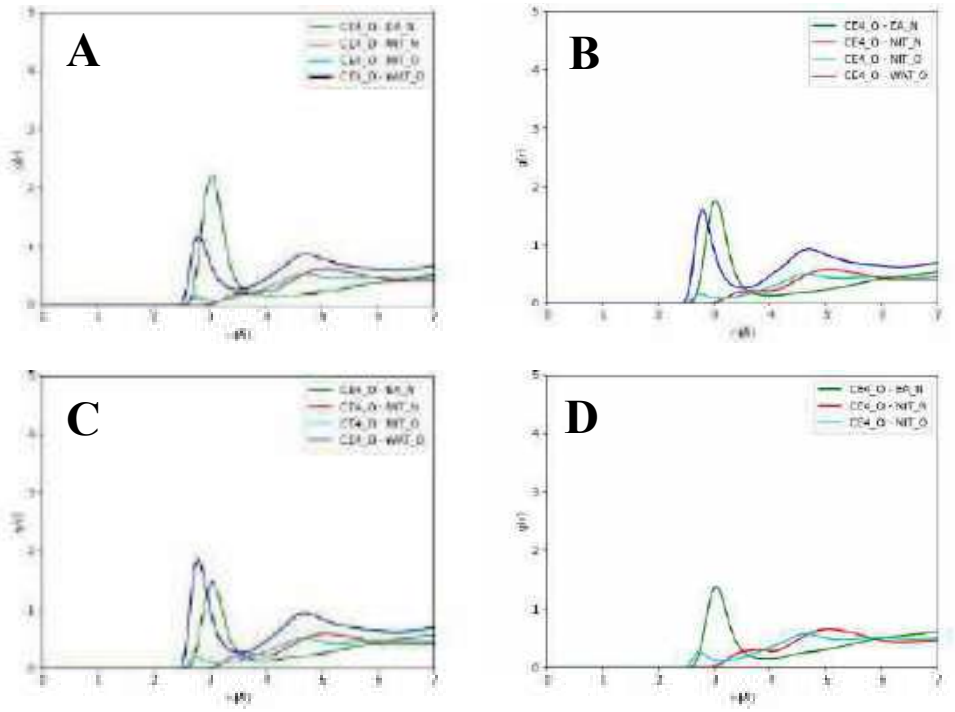

Figure 5.8. Radial distribution functions (RDFs) of C12E4 in A) 25 mol%, B) 50 mol%, C) 75 mol% and D) neat EAN mixtures.

In the literature, there was vast interest in forming mixed catanionic micelles using both cationic and anionic surfactants.[34, 39] It was interesting to observe that this effect was possible by using ILs as a co-solvent and it was possible to make catanionic micelles without necessarily having to use two different types of surfactants.

Overall, the simulations were able to allow us insight into the solvation properties of EAN in mixtures of water and a self-assembling solute. This investigation allowed us to further investigate the hypotheses formed in Chapter 3 regarding how the cation of a PIL could potentially participate in self-assembly as more than just a bulk solvent. However, it would be hasty to make conclusions regarding the surfactant-like qualities of PIL cations based on these simulations alone. As mentioned throughout this thesis, classical simulations come with uncertainties regarding their ability to simulate diffusion correctly. This is a very important property to simulate correctly when investigating complex solutions with PILs. These results must be validated using a polarisable model to fully understand these mixtures computationally and make firm conclusions.

5.4 Conclusion

The hypothesis regarding the behaviour of the cation of EAN acting as a co-surfactant rather than just a co-solvent during the self-assembly process was observed in this chapter using MD simulations. We were able to observe the molecular level interactions of the micelles and the solvation layer, which allowed us insight into the contrast issues observed in Chapter 3 during SAXS experiments on the same systems. The RDFs were able to provide insight regarding the solvation properties of EAN in the presence of cationic, anionic and non-ionic surfactants. Caution must be taken regarding making further conclusions based on the MD simulations performed during this chapter due to the lack of polarizability in the forcefields. While this study was able to provide clarification for our experimental results, the results are at best qualitative. Further investigations are required using polarisable forcefields with more extensive testing to quantitatively assess molecular interactions of PILs in mixtures with micelles.

6 Conclusions and recommended future work

The work summarised in this thesis sought to understand the solvent properties of protic ionic liquids in mixtures with water using a variety of experimental and computational methods. The development of capabilities in applying machine learning algorithms and molecular dynamics simulations to systems which have never been subjected to these techniques was also a focus.

Chapter 2 used machine learning as an advanced analysis technique for understanding trends in physicochemical properties of PIL-water mixtures reported in the literature. Predictive models were generated, and their predictions were tested experimentally. A significant finding from the study was that the water content of the training set affected the accuracy of the predictions to a great degree. The changes in viscosity and conductivity were not linear with incremental increases to the water content and thus the water content plays an important role in the predicted values for neat ILs.

To extend the understanding of PIL-water mixtures obtained in Chapter 2, the representative PIL of EAN was chosen for further experimental investigation in **Chapter 3.** Chapter 3 investigated the effect of ionicity of surfactants on the self-assembly of a cationic, anionic, and non-ionic surfactant in mixtures of PIL-water systems. For CTAB and SOS, at low concentrations of the PIL (< 5 mol%), the ionic liquid acted as free ions, decreasing the CMC due to charge screening effects, similar to conventional salts. This effect was not observed in $C_{12}E_4$ due to its neutral charge. Micelles could not be confirmed using x-ray scattering in EAN mixtures due to a variety of contrast issues. It was hypothesised that the ethylammonium cation was actively participating in the micellization as a smaller surfactant, rather than only existing in the bulk solvent. The “surfactant-like” behaviour of the IL cation probably led to the formation of a micelle akin to a catanionic micelle, which was difficult to observe using x-rays due to lack of contrast between the micelle and the solvent interface. This led to the need to explore computational methods to confirm findings. The ability of SOS to self-assemble in PIL mixtures was confirmed in EtAN, a less cationic PIL with higher contrast with SOS, using SAXS.

Chapter 4 set up the foundation for using molecular dynamics simulations to investigate mixtures of ILs and molecular solvents. This chapter focused on choosing the optimal water model for use in conjunction with existing force fields for ILs, which was used for multi-component systems of IL-water-solutes. 30 water models were tested to explore how the simulated properties of water change due to widely used, modern settings. OPC3 was identified as the best option for use with IL forcefields as a suitable water model due to the accuracy of its simulated properties as well as the efficiency in comparison to more computationally costly 4-point, 5-point or polarisable models.

Chapter 5 verified the experimental results from Chapter 3 using the preliminary results for MD simulations gathered in Chapter 4. Finally, molecular dynamics simulations were performed for EAN-water-surfactant systems to understand the interactions at a molecular level of the experimental results from Chapter 3. The simulations suggested that ethylammonium ions, are not just in the bulk solvent, but are in fact participating in the micelle formation with the surfactants. This provided an explanation regarding the contrast issues which led to inconclusive results from SAXS experiments and was consistent with the hypothesis from the experimental results.

As the properties of PILs are subject to drastic changes with minute changes to their chemical structure, as shown by the example of EAN and EtAN, it was necessary to develop new methods of investigating PIL mixtures. Due to the vast sample space in the field of PILs, it is near impossible to characterise these mixtures only using experimental approaches. The work included in this thesis was able to demonstrate that combining experimental, MD simulations and machine learning methods allow us to approach the problem of characterising PIL mixtures from a fresh perspective. The work done during this thesis will form the basis for future work in the space of MD simulations and machine learning models for PILs and their mixtures.

Future work from this study could branch out to several areas, both experimental and computational:

- Neutron scattering experiments could be performed on the experimental samples from Chapter 3 to verify the hypothesis regarding ethylammonium cation behavior during micelle formation.
- Polarizability should be introduced to the MD forcefields of ILs used for the Chapter 5 study with mixtures. A polarizable forcefield for EAN has recently been published and should be tested for compatibility with existing solvent and surfactant forcefields before using them in mixtures. Testing water and more PILs using MD is a must for the future to understand the interactions of PIL-water mixtures at the molecular level.
- Machine learning models could be trained with the insights gathered during this study regarding how PILs influence surfactant self-assembly to aid the ultimate goal of our field, designing PILs for various applications.

The biggest hindrance during the current study, lack of contrast between observed components in solution, could be resolved using neutron scattering. It is anticipated these experiments would be able to clarify the interactions between the surfactants and the protic ionic liquid mixtures. As scattering tools rapidly progress with the availability of resources such as x-ray free electron lasers, there is no doubt that future experimental work in the field of solvation properties of protic ionic liquids will be able to probe even deeper into the molecular structure and dynamics. However, one of the most prominent challenges faced by the field, the lack of behavioral patterns and predictability with minute changes to ionic liquid chemical structures, cannot be resolved by merely performing "crank the handle" type experiments. It is imperative to embrace computational techniques such as machine learning and molecular dynamics to probe deeper into the trends of large ionic liquid datasets to discern patterns one may not be able perform within the capacity of a single laboratory group. The experimental ionic liquid researchers will need to find ways to collaborate and create databases which can be easily accessible by computational researchers. These ventures will come with many challenges, including verification and standardization of data, but it will create imperative infrastructure for future advancements in the field.

7

References

1. Nuthakki, B.; Greaves, T. L.; Krodkiewska, I.; Weerawardena, A.; Burgar, M. I.; Mulder, R. J.; Drummond, C. J., Protic ionic liquids and ionicity. *Australian Journal of Chemistry* **2007,** *60* (1), 21-28.
2. Greaves, T. L.; Drummond, C. J., Protic ionic liquids: Properties and applications. *Chemical Reviews* **2008,** *108* (1), 206-237.
3. Yalcin, D.; Drummond, C. J.; Greaves, T. L., High throughput approach to investigating ternary solvents of aqueous non-stoichiometric protic ionic liquids. *Physical Chemistry Chemical Physics* **2019,** *21* (13), 6810-6827.
4. Greaves, T. L.; Ha, K.; Muir, B. W.; Howard, S. C.; Weerawardena, A.; Kirby, N.; Drummond, C. J., Protic ionic liquids (PILs) nanostructure and physicochemical properties: development of high-throughput methodology for PIL creation and property screens. *Physical Chemistry Chemical Physics* **2015,** *17* (4), 2357-2365.
5. Greaves, T. L.; Kennedy, D. F.; Kirby, N.; Drummond, C. J., Nanostructure changes in protic ionic liquids (PILs) through adding solutes and mixing PILs. *Physical Chemistry Chemical Physics* **2011,** *13* (30), 13501-13509.
6. Greaves, T. L.; Kennedy, D. F.; Kirby, N.; Mudie, S. T.; Hawley, A.; Shen, Y.; Song, G. H.; Drummond, C. J., Nanostructure of protic ionic liquids. *Abstracts of Papers of the American Chemical Society* **2014,** 248.
7. Greaves, T. L.; Kennedy, D. F.; Mudie, S. T.; Drummond, C. J., Diversity Observed in the Nanostructure of Protic Ionic Liquids. *Journal of Physical Chemistry B* **2010,** *114* (31), 10022-10031.
8. Evans, D. F.; Chen, S.-H.; Schriver, G. W.; Arnett, E. M., Thermodynamics of solution of nonpolar gases in a fused salt. Hydrophobic bonding behavior in a nonaqueous system. *Journal of the American Chemical Society* **1981,** *103* (2), 481-482.
9. Yalcin, D.; Le, T. C.; Drummond, C. J.; Greaves, T. L., Machine Learning Approaches for Further Developing the Understanding of the Property Trends Observed in Protic Ionic Liquid Containing Solvents. *Journal of Physical Chemistry B* **2019,** *123* (18), 4085-4097.
10. Greaves, T. L.; Weerawardena, A.; Fong, C.; Krodkiewska, I.; Drummond, C. J., Protic ionic liquids: Solvents with tunable phase behavior and physicochemical properties (vol 110B, pg 22479, 2006). *Journal of Physical Chemistry B* **2006,** *110* (51), 26506-26506.
11. Yalcin, D. Structure - property relationships for protic ionic liquids and their mixtures. 2019.
12. Lazar, M. A.; Al-Masri, D.; MacFarlane, D. R.; Pringle, J. M., Enhanced thermal energy harvesting performance of a cobalt redox couple in ionic liquid-solvent mixtures. *Physical Chemistry Chemical Physics* **2016,** *18* (3), 1404-1410.
13. Lam, M.; D. Adamson, W.; Miao, S.; Atkin, R.; Warr, G., DTAB Micelle Formation in Ionic Liquid/Water Mixtures is Determined by Ionic Liquid Cation Structure. *Journal of Colloid and Interface Science* **2019,** 552.
14. Yalcin, D.; Christofferson, A. J.; Drummond, C. J.; Greaves, T. L., Solvation properties of protic ionic liquid - molecular solvent mixtures. *Physical Chemistry Chemical Physics* **2020**.
15. Welton, T., Room-temperature ionic liquids. Solvents for synthesis and catalysis. *Chemical reviews* **1999,** *99* (8), 2071-2084.
16. Dong, Q.; Muzny, C. D.; Kazakov, A.; Diky, V.; Magee, J. W.; Widegren, J. A.; Chirico, R. D.; Marsh, K. N.; Frenkel, M., ILThermo: a free-access web database for thermodynamic properties of ionic liquids. *Journal of Chemical & Engineering Data* **2007,** *52* (4), 1151-1159.
17. Greaves, T. L.; Drummond, C. J., Ionic liquids as amphiphile self-assembly media. *Chemical Society Reviews* **2008,** *37* (8), 1709-1726.
18. Silva, W.; Zanatta, M.; Ferreira, A. S.; Corvo, M. C.; Cabrita, E. J., Revisiting Ionic Liquid Structure-Property Relationship: A Critical Analysis. *International Journal of Molecular Sciences* **2020,** *21* (20), 7745.
19. Izgorodina, E. I., Towards large-scale, fully ab initio calculations of ionic liquids. *Physical Chemistry Chemical Physics* **2011,** *13* (10), 4189-4207.

20. Palomar, J.; Torrecilla, J.; Lemus, J.; Ferro, V.; Rodriguez, F., A COSMO-RS based guide to analyze/quantify the polarity of ionic liquids and their mixtures with organic cosolvents. *Physical chemistry chemical physics* **2010,** *12*, 1991-2000.
21. Koutsoukos, S.; Philippi, F.; Malaret, F.; Welton, T., A review on machine learning algorithms for the ionic liquid chemical space. *Chemical Science* **2021,** *12* (20), 6820-6843.
22. Beckner, W.; Pfaendtner, J., Fantastic Liquids and Where To Find Them: Optimizations of Discrete Chemical Space. *Journal of Chemical Information and Modeling* **2019,** *59* (6), 2617-2625.
23. Keshavarz, M. H.; Pouretedal, H. R.; Saberi, E., A simple method for prediction of density of ionic liquids through their molecular structure. *Journal of Molecular Liquids* **2016,** *216*, 732-737.
24. Paduszyński, K., Extensive Databases and Group Contribution QSPRs of Ionic Liquids Properties. 1. Density. *Industrial & Engineering Chemistry Research* **2019,** *58* (13), 5322-5338.
25. Hansch, C.; Maloney, P. P.; Fujita, T.; Muir, R. M., Correlation of biological activity of phenoxyacetic acids with Hammett substituent constants and partition coefficients. *Nature* **1962,** *194* (4824), 178-180.
26. Paternò, A.; Fiorenza, R.; Marullo, S.; Musumarra, G.; Scirè, S., Prediction of ionic liquid's heat capacity by means of their in silico principal properties. *RSC advances* **2016,** *6* (42), 36085-36089.
27. Zhao, Y.; Zeng, S.; Huang, Y.; Afzal, R. M.; Zhang, X., Estimation of heat capacity of ionic liquids using S σ-profile molecular descriptors. *Industrial & Engineering Chemistry Research* **2015,** *54* (51), 12987-12992.
28. Xia, L.; Wang, J.; Liu, S.; Li, Z.; Pan, H., Prediction of CO_2 Solubility in Ionic Liquids Based on Multi-Model Fusion Method. *Processes* **2019,** *7* (5), 258.
29. Zhu, P.; Kang, X.; Zhao, Y.; Latif, U.; Zhang, H., Predicting the toxicity of ionic liquids toward acetylcholinesterase enzymes using novel QSAR models. *International journal of molecular sciences* **2019,** *20* (9), 2186.
30. Yalcin, D.; Le, T. C.; Drummond, C. J.; Greaves, T. L., Machine Learning Approaches for Further Developing the Understanding of the Property Trends Observed in Protic Ionic Liquid Containing Solvents. *The Journal of Physical Chemistry B* **2019,** *123* (18), 4085-4097.
31. Greaves, T. L.; KS, S. M.; Burkart-Radke, R. F.; Harper, J. B.; Le, T. C., Machine learning approaches to understand and predict rate constants for organic processes in mixtures containing ionic liquids. *Physical Chemistry Chemical Physics: PCCP* **2021**. *23*, 2742-2752.
32. Le, T.; Epa, V. C.; Burden, F. R.; Winkler, D. A., Quantitative Structure–Property Relationship Modeling of Diverse Materials Properties. *Chemical Reviews* **2012,** *112* (5), 2889-2919.
33. Greaves, T. L.; Drummond, C. J., Solvent nanostructure, the solvophobic effect and amphiphile self-assembly in ionic liquids. *Chemical Society Reviews* **2013,** *42* (3), 1096-1120.
34. J. Bryant, S.; Jafta, C.; Atkin, R.; Gradzielski, M.; Warr, G., Catanionic and Chain-packing Effects on Surfactant Self-Assembly in the Ionic Liquid Ethylammonium Nitrate. *Journal of Colloid and Interface Science* **2019,** 540.
35. Greaves, T. L.; Weerawardena, A.; Fong, C.; Drummond, C. J., Formation of Amphiphile Self-Assembly Phases in Protic Ionic Liquids. *The Journal of Physical Chemistry B* **2007,** *111* (16), 4082-4088.
36. Greaves, T. L.; Weerawardena, A.; Krodkiewska, I.; Drummond, C. J., Protic ionic liquids: Physicochemical properties and behavior as amphiphile self-assembly solvents. *Journal of Physical Chemistry B* **2008,** *112* (3), 896-905.
37. Chen, Z. F.; Greaves, T. L.; Caruso, R. A.; Drummond, C. J., Effect of cosolvents on the self-assembly of a non-ionic polyethylene oxide-polypropylene oxide-polyethylene oxide block copolymer in the protic ionic liquid ethylammonium nitrate. *Journal of Colloid and Interface Science* **2015,** *441*, 46-51.
38. López-Barrón, C. R.; Wagner, N. J., Structural Transitions of CTAB Micelles in a Protic Ionic Liquid. *Langmuir* **2012,** *28* (35), 12722-12730.
39. Yatcilla, M. T.; Herrington, K. L.; Brasher, L. L.; Kaler, E. W.; Chiruvolu, S.; Zasadzinski, J. A., Phase Behavior of Aqueous Mixtures of Cetyltrimethylammonium Bromide (CTAB) and Sodium Octyl Sulfate (SOS). *The Journal of Physical Chemistry* **1996,** *100* (14), 5874-5879.
40. Warr, G. G.; Atkin, R., Solvophobicity and amphiphilic self-assembly in neoteric and nanostructured solvents. *Current Opinion in Colloid & Interface Science* **2020,** *45*, 83-96.

41. Chen, R.; Lopez-Barron, C.; Wagner, N., Self-assembly of Pluronic triblock copolymers in a protic ionic liquid and polymerization to create wearable electronics. *Abstracts of Papers of the American Chemical Society* **2018,** *255*.
42. López-Barrón, C. R.; Li, D.; Wagner, N. J.; Caplan, J. L., Triblock Copolymer Self-Assembly in Ionic Liquids: Effect of PEO Block Length on the Self-Assembly of PEO–PPO–PEO in Ethylammonium Nitrate. *Macromolecules* **2014,** *47* (21), 7484-7495.
43. Conn, C. E.; Dynamics of structural transformations between lyotropic liquid crystalline phases. Department of Chemistry, Imperial College London **2007**.
44. Godbey, W. T.; *Biotechnology and its Applications*, 2nd Ed. Academic Press **2022**.
45. Yamamoto, T.; Yagi, Y.; Hatakeyama, T.; Wakabayashi, T.; Kamiyama, T.; Suzuki, H., Metastable and stable phase diagrams and thermodynamic properties of the cetyltrimethylammonium bromide (CTAB)/water binary system. *Colloids and Surfaces A: Physicochemical and Engineering Aspects* **2021,** *625*, 126859.
46. Rossi, G.; Fuchs, P. F. J.; Barnoud, J.; Monticelli, L., A Coarse-Grained MARTINI Model of Polyethylene Glycol and of Polyoxyethylene Alkyl Ether Surfactants. *The Journal of Physical Chemistry B* **2012,** *116* (49), 14353-14362.
47. Javadian, S.; Ruhi, V.; Heydari, A.; Shahir, A. A.; Yousefi, A.; Akbari, J., Self-Assembled CTAB Nanostructures in Aqueous/Ionic Liquid Systems: Effects of Hydrogen Bonding. *Industrial & Engineering Chemistry Research* **2013,** *52* (12), 4517-4526.
48. Wijay, E. C.; Greaves, T. L.; Drummon, C. J., Linking molecular/ion structure, solvent mesostructure, the solvophobic effect and the ability of amphiphiles to self-assemble in non-aqueous liquidst. *Faraday discussions* **2013,** *167*, 191-215.
49. Smirnova, N. A.; Vanin, A. A.; Safonova, E. A.; Pukinsky, I. B.; Anufrikov, Y. A.; Makarov, A. L., Self-assembly in aqueous solutions of imidazolium ionic liquids and their mixtures with an anionic surfactant. *Journal of Colloid and Interface Science* **2009,** *336* (2), 793-802.
50. Sohrabi, B.; Eivazzadeh, S.; Sharifi, A.; Azadbakht, R., Self-assembled catanionic surfactant mixtures in aqueous/ionic liquid systems. *Journal of Molecular Liquids* **2015,** *211*, 754-760.
51. He, Z.; Ma, Y.; Alexandridis, P., Comparison of ionic liquid and salt effects on the thermodynamics of amphiphile micellization in water. *Colloids and Surfaces A: Physicochemical and Engineering Aspects* **2018,** *559*, 159-168.
52. Wakeham, D.; Warr, G. G.; Atkin, R., Surfactant Adsorption at the Surface of Mixed Ionic Liquids and Ionic Liquid Water Mixtures. *Langmuir* **2012,** *28* (37), 13224-13231.
53. Ueno, M.; Isokawa, N.; Fueda, K.; Nakahara, S.; Teshima, H.; Yamamoto, N.; Yokoyama, H.; Noritsugu, Y.; Shibata, K.; Miyagawa, K.; Tanaka, S.; Hirano, T.; Fujito, A.; Takashima, A.; Kanno, K., Practical Chemistry of Long-Lasting Bubbles. *World Journal of Chemical Education* **2016,** *4* (2), 32-44.
54. Shah, A.-u.-H. A.; Ali, K.; Bilal, S., Surface tension, surface excess concentration, enthalpy and entropy of surface formation of aqueous salt solutions. *Colloids and Surfaces A: Physicochemical and Engineering Aspects* **2013,** *417*, 183-190.
55. Greaves, T. L.; Mudie, S. T.; Drummond, C. J., Effect of protic ionic liquids (PILs) on the formation of non-ionic dodecyl poly(ethylene oxide) surfactant self-assembly structures and the effect of these surfactants on the nanostructure of PILs. *Physical Chemistry Chemical Physics* **2011,** *13* (45), 20441-20452.
56. Pedersen, J. S., Analysis of small-angle scattering data from colloids and polymer solutions: modeling and least-squares fitting. *Advances in Colloid and Interface Science* **1997,** *70*, 171-210.
57. Greaves, T. L.; Weerawardena, A.; Fong, C.; Drummond, C. J., Many Protic Ionic Liquids Mediate Hydrocarbon-Solvent Interactions and Promote Amphiphile Self-Assembly. *Langmuir* **2007,** *23* (2), 402-404.
58. Chen, Z. F.; Greaves, T. L.; Fong, C.; Caruso, R. A.; Drummond, C. J., Lyotropic liquid crystalline phase behaviour in amphiphile-protic ionic liquid systems. *Physical Chemistry Chemical Physics* **2012,** *14* (11), 3825-3836.
59. Sprenger, K. G.; Jaeger, V. W.; Pfaendtner, J., The General AMBER Force Field (GAFF) Can Accurately Predict Thermodynamic and Transport Properties of Many Ionic Liquids. *Journal of Physical Chemistry B* **2015,** *119* (18), 5882-5895.

60. Doherty, B.; Zhong, X.; Gathiaka, S.; Li, B.; Acevedo, O., Revisiting OPLS Force Field Parameters for Ionic Liquid Simulations. *Journal of Chemical Theory and Computation* **2017,** *13* (12), 6131-6145.
61. Kolafa, J.; Perram, J. W., Cutoff Errors in the Ewald Summation Formulae for Point Charge Systems. *Molecular Simulation* **1992,** *9* (5), 351-368.
62. Goloviznina, K.; Gong, Z.; Costa Gomes, M. F.; Pádua, A. A. H., Extension of the CL&Pol Polarizable Force Field to Electrolytes, Protic Ionic Liquids, and Deep Eutectic Solvents. *Journal of Chemical Theory and Computation* **2021,** *17* (3), 1606-1617.
63. Docampo-Álvarez, B.; Gómez-González, V.; Méndez-Morales, T.; Carrete, J.; Rodríguez, J. R.; Cabeza, Ó.; Gallego, L. J.; Varela, L. M., Mixtures of protic ionic liquids and molecular cosolvents: A molecular dynamics simulation. *The Journal of Chemical Physics* **2014,** *140* (21), 214502.
64. Huang, Y.; Wan, Z.; Yang, Z.; Ji, Y.; Li, L.; Yang, D.; Zhu, M.; Chen, X., Concentration-Dependent Hydrogen Bond Behavior of Ethylammonium Nitrate Protic Ionic Liquid–Water Mixtures Explored by Molecular Dynamics Simulations. *Journal of Chemical & Engineering Data* **2017,** *62* (8), 2340-2349.
65. Duong, D. V.; Tran, H.-V.; Pathirannahalage, S. K.; Brown, S. J.; Hassett, M.; Yalcin, D.; Meftahi, N.; Christofferson, A. J.; Greaves, T. L.; Le, T. C., Machine learning investigation of viscosity and ionic conductivity of protic ionic liquids in water mixtures. *The Journal of Chemical Physics* **2022,** *156* (15), 154503.
66. Evans, D. F., Self-organization of amphiphiles. *Langmuir* **1988,** *4* (1), 3-12.
67. Chen, Z. F.; Greaves, T. L.; Caruso, R. A.; Drummond, C. J., Amphiphile Micelle Structures in the Protic Ionic Liquid Ethylammonium Nitrate and Water. *Journal of Physical Chemistry B* **2015,** *119* (1), 179-191.
68. Dolan, A.; Atkin, R.; Warr, G. G., The origin of surfactant amphiphilicity and self-assembly in protic ionic liquids. *Chemical Science* **2015,** *6* (11), 6189-6198.
69. Takekiyo, T.; Yoshida, K.; Funahashi, Y.; Nagata, S.; Abe, H.; Yamaguchi, T.; Yoshimura, Y., Helix-forming ability of proteins in alkylammonium nitrate. *Journal of Molecular Liquids* **2017,** *243*, 584-590.
70. Takekiyo, T.; Ishikawa, Y.; Yoshimura, Y., Cryopreservation of Proteins Using Ionic Liquids: A Case Study of Cytochrome c. *The Journal of Physical Chemistry B* **2017,** *121* (32), 7614-7620.
71. Ishikawa, Y.; Takekiyo, T.; Yoshimura, Y., Recovery and cryopreservation of insulin amyloid using ionic liquids. *Journal of Molecular Liquids* **2018,** *272*.
72. Satish, L.; Millan, S.; Sahoo, H., Sustained activity and stability of lysozyme in aqueous ionic liquid solutions containing carboxymethylcellulose and polyethylene glycol. *Journal of Molecular Liquids* **2019,** *278*, 329-334.
73. Garlitz, J. A.; Summers, C. A.; Flowers, R. A.; Borgstahl, G. E. O., Ethylammonium nitrate: a protein crystallization reagent. *Acta Crystallogr. Sect. D-Biol. Crystallogr.* **1999,** *55*, 2037-2038.
74. Evans, D. F.; Yamauchi, A.; Wei, G. J.; Bloomfield, V. A., Micelle size in ethylammonium nitrate as determined by classical and quasi-elastic light scattering. *The Journal of Physical Chemistry* **1983,** *87* (18), 3537-3541.
75. Hayes, R.; Warr, G. G.; Atkin, R., Structure and Nanostructure in Ionic Liquids. *Chemical Reviews* **2015,** *115* (13), 6357-6426.
76. Araos, M. U.; Warr, G. G., Self-Assembly of Nonionic Surfactants into Lyotropic Liquid Crystals in Ethylammonium Nitrate, a Room-Temperature Ionic Liquid. *The Journal of Physical Chemistry B* **2005,** *109* (30), 14275-14277.
77. Lam, Y. M.; Grigorieff, N.; Goldbeck-Wood, G., Direct visualisation of micelles of Pluronic block copolymers in aqueous solution by cryo-TEM. *Physical Chemistry Chemical Physics* **1999,** *1* (14), 3331-3334.
78. Zhou, L. L.; Tian, T. T.; Xiao, J. H.; Wang, T.; Yu, L., Aggregation behavior of pyrrolidinium-based surface active ionic liquids in H2O-EAN binary solvents. *Journal of Molecular Liquids* **2017,** *225*, 50-55.
79. Chen, Z. F.; Greaves, T. L.; Caruso, R. A.; Drummond, C. J., Long-range ordered lyotropic liquid crystals in intermediate-range ordered protic ionic liquid used as templates for hierarchically porous silica. *Journal of Materials Chemistry* **2012,** *22* (19), 10069-10076.

80. Corrin, M. L.; Harkins, W. D., The Effect of Salts on the Critical Concentration for the Formation of Micelles in Colloidal Electrolytes1. *Journal of the American Chemical Society* **1947,** *69* (3), 683-688.
81. Barry, B. W.; Gray, G. M. T., Micelle formation and coacervation in mixtures of alkyltrimethylammonium bromides with di and trihydroxy bile salts. *Journal of Colloid and Interface Science* **1975,** *52* (2), 327-339.
82. Hao, J.; Hoffmann, H., Self-assembled structures in excess and salt-free catanionic surfactant solutions. *Current Opinion in Colloid & Interface Science* **2004,** *9* (3), 279-293.
83. Johnson, S. B.; Drummond, C. J.; Scales, P. J.; Nishimura, S., Electrical double layer properties of hexadecyltrimethylammonium chloride surfaces in aqueous solution. *Colloids and Surfaces A: Physicochemical and Engineering Aspects* **1995,** *103* (3), 195-206.
84. Varga, I.; Mészáros, R.; Gilányi, T., Adsorption of Sodium Alkyl Sulfate Homologues at the Air/Solution Interface. *The Journal of Physical Chemistry B* **2007,** *111* (25), 7160-7168.
85. Doucet, M.; Cho, J. H.; Alina, G.; et al. *SasView*. Version 5.0.4, Zenodo **2021**.
86. Piana, S.; Donchev, A. G.; Robustelli, P.; Shaw, D. E., Water Dispersion Interactions Strongly Influence Simulated Structural Properties of Disordered Protein States. *The Journal of Physical Chemistry B* **2015,** *119* (16), 5113-5123.
87. Onufriev, A. V.; Izadi, S., Water models for biomolecular simulations. *WIREs Computational Molecular Science* **2018,** *8* (2), 1347.
88. Sega, M.; Dellago, C., Long-Range Dispersion Effects on the Water/Vapor Interface Simulated Using the Most Common Models. *The Journal of Physical Chemistry B* **2017,** *121* (15), 3798-3803.
89. González, M. A.; Abascal, J. L. F., A flexible model for water based on TIP4P/2005. *The Journal of Chemical Physics* **2011,** *135* (22), 224516.
90. de Jesús-González, N. E.; Pérez de la Luz, A.; López-Lemus, J.; Alejandre, J., Effect of the Dielectric Constant on the Solubility of Acetone in Water. *Journal of Chemical & Engineering Data* **2018,** *63* (5), 1170-1179.
91. Jorgensen, W. L., Quantum and statistical mechanical studies of liquids. 10. Transferable intermolecular potential functions for water, alcohols, and ethers. Application to liquid water. *Journal of the American Chemical Society* **1981,** *103* (2), 335-340.
92. Boonstra, S.; Onck, P. R.; van der Giessen, E., CHARMM TIP3P Water Model Suppresses Peptide Folding by Solvating the Unfolded State. *The Journal of Physical Chemistry B* **2016,** *120* (15), 3692-3698.
93. Paschek, D.; Day, R.; García, A. E., Influence of water–protein hydrogen bonding on the stability of Trp-cage miniprotein. A comparison between the TIP3P and TIP4P-Ew water models. *Physical Chemistry Chemical Physics* **2011,** *13* (44), 19840-19847.
94. Mark, P.; Nilsson, L., Structure and Dynamics of the TIP3P, SPC, and SPC/E Water Models at 298 K. *The Journal of Physical Chemistry A* **2001,** *105* (43), 9954-9960.
95. Case, D. A.; Cheatham, T. E., 3rd; Darden, T.; Gohlke, H.; Luo, R.; Merz, K. M., Jr.; Onufriev, A.; Simmerling, C.; Wang, B.; Woods, R. J., The Amber biomolecular simulation programs. *Journal of computational chemistry* **2005,** *26* (16), 1668-1688.
96. Abraham, M. J.; Murtola, T.; Schulz, R.; Páll, S.; Smith, J. C.; Hess, B.; Lindahl, E., GROMACS: High performance molecular simulations through multi-level parallelism from laptops to supercomputers. *SoftwareX* **2015,** *1-2*, 19-25.
97. Berendsen, H. J. C.; Postma, J. P. M.; van Gunsteren, W. F.; Hermans, J., Interaction Models for Water in Relation to Protein Hydration. *Intermolecular Forces: Proceedings of the Fourteenth Jerusalem Symposium on Quantum Chemistry and Biochemistry* **1981**, 331-342.
98. Wu, Y.; Tepper, H. L.; Voth, G. A., Flexible simple point-charge water model with improved liquid-state properties. *The Journal of Chemical Physics* **2006,** *124* (2), 024503.
99. Berendsen, H. J. C.; Grigera, J. R.; Straatsma, T. P., The missing term in effective pair potentials. *The Journal of Physical Chemistry* **1987,** *91* (24), 6269-6271.
100. Horn, H. W.; Swope, W. C.; Pitera, J. W.; Madura, J. D.; Dick, T. J.; Hura, G. L.; Head-Gordon, T., Development of an improved four-site water model for biomolecular simulations: TIP4P-Ew. *The Journal of Chemical Physics* **2004,** *120* (20), 9665-9678.
101. Fuentes-Azcatl, R.; Alejandre, J., Non-Polarizable Force Field of Water Based on the Dielectric Constant: TIP4P/ε. *The Journal of Physical Chemistry B* **2014,** *118* (5), 1263-1272.

102. Abascal, J. L. F.; Vega, C., A general purpose model for the condensed phases of water: TIP4P/2005. *The Journal of Chemical Physics* **2005,** *123* (23), 234505.
103. Izadi, S.; Anandakrishnan, R.; Onufriev, A. V., Building Water Models: A Different Approach. *Journal of Physical Chemistry Letters* **2014,** *5* (21), 3863-3871.
104. Schmitt, U. W.; Voth, G. A., The computer simulation of proton transport in water. *The Journal of Chemical Physics* **1999,** *111* (20), 9361-9381.
105. Giri, A. K.; Spohr, E., Cluster formation of NaCl in bulk solutions: Arithmetic vs. geometric combination rules. *Journal of Molecular Liquids* **2017,** *228*, 63-70.
106. Kadaoluwa Pathirannahalage, S. P.; Meftahi, N.; Elbourne, A.; Weiss, A. C. G.; McConville, C. F.; Padua, A.; Winkler, D. A.; Costa Gomes, M.; Greaves, T. L.; Le, T. C.; Besford, Q. A.; Christofferson, A. J., Systematic Comparison of the Structural and Dynamic Properties of Commonly Used Water Models for Molecular Dynamics Simulations. *Journal of Chemical Information and Modeling* **2021,** *61* (9), 4521-4536.
107. Berendsen, H. J. C.; Postma, J. P. M.; Gunsteren, W. F. v.; Hermans, J., Interaction models for water in relation to protein hydration. *Intermolecular forces* **1981**, 331-342.
108. Jorgensen, W. L.; Chandrasekhar, J.; Madura, J. D.; Impey, R. W.; Klein, M. L., Comparison of simple potential functions for simulating liquid water. *Journal of Chemical Physics* **1983,** *79* (2), 926-935.
109. W. E. R.; Theoretical studies of hydrogen bonding. *Harvard University Thesis Repository* **1985**.
110. Dauber-Osguthorpe, P.; Roberts, V. A.; Osguthorpe, D. J.; Wolff, J.; Genest, M.; Hagler, A. T., Structure and energetics of ligand binding to proteins: Escherichia coli dihydrofolate reductase-trimethoprim, a drug-receptor system. *Proteins* **1988,** *4* (1), 31-47.
111. Sun, H.; Mumby, S. J.; Maple, J. R.; Hagler, A. T., An ab Initio CFF93 All-Atom Force Field for Polycarbonates. *Journal of American Chemical Society.* **1994,** *116* (7), 2978-2987.
112. Sun, H., COMPASS: An ab Initio Force-Field Optimized for Condensed-Phase Applications_Overview with Details on Alkane and Benzene Compounds. *Journal of Physical Chemistry B* **1998,** *102*, 7338-7364.
113. Schmitt, U. W.; Voth, G. A., The computer simulation of proton transport in water. *Journal of Chemical Physics* **1999,** *111* (20), 9361-9381.
114. Mahoney, M. W.; Jorgensen, W. L., A five-site model for liquid water and the reproduction of the density anomaly by rigid, nonpolarizable potential functions. *Journal of Chemical Physics* **2000,** *112* (20), 8910-8922.
115. Price, D. J.; Brooks, C. L., A modified TIP3P water potential for simulation with Ewald summation. *Journal of Chemical Physics.* **2004,** *121* (20), 10096-10103.
116. Horn, H. W.; Swope, W. C.; Pitera, J. W.; Madura, J. D.; Dick, T. J.; Hura, G. L.; Head-Gordon, T., Development of an improved four-site water model for biomolecular simulations: TIP4P-Ew. *Journal of Chemical Physics* **2004,** *120* (20), 9665-9678.
117. Rick, S. W., A reoptimization of the five-site water potential (TIP5P) for use with Ewald sums. *Journal of Chemical Physics* **2004,** *120* (13), 6085-6093.
118. Abascal, J. L. F.; Vega, C., A general purpose model for the condensed phases of water: TIP4P/2005. *Journal of Chemical Physics* **2005,** *123* (23), 234505.
119. Abascal, J. L. F.; Sanz, E.; García Fernández, R.; Vega, C., A potential model for the study of ices and amorphous water: TIP4P/Ice. *Journal of Chemical Physics* **2005,** *122* (23), 234511.
120. Wu, Y.; Tepper, H. L.; Voth, G. A., Flexible simple point-charge water model with improved liquid-state properties. *Journal of Chemical Physics* **2006,** *124* (2), 024503.
121. Lamoureux, G.; Harder, E.; Vorobyov, I. V.; Roux, B.; MacKerell Jr, A. D., A polarizable model of water for molecular dynamics simulations of biomolecules. *Chemical Physics Letters* **2006,** *418* (1–3), 245-249.
122. González, M. A.; Abascal, J. L. F., A flexible model for water based on TIP4P/2005. *Journal of Chemical Physics* **2011,** *135* (22), 224516.
123. Izadi, S.; Anandakrishnan, R.; Onufriev, A. V., Building Water Models: A Different Approach. *Journal of Physical Chemistry Letters* **2014,** *5* (21), 3863-3871.
124. Wang, L.-P.; Martinez, T. J.; Pande, V. S., Building Force Fields: An Automatic, Systematic, and Reproducible Approach. *Journal of Physical Chemistry Letters* **2014,** *5* (11), 1885-1891.

125. Fuentes-Azcatl, R.; Mendoza, N.; Alejandre, J., Improved SPC force field of water based on the dielectric constant: SPC/ε. *Physica A: Statistical Mechanics and its Applications* **2015,** *420*, 116-123.
126. Izadi, S.; Onufriev, A. V., Accuracy limit of rigid 3-point water models. *Journal of Chemical Physics* **2016,** *145* (7), 074501.
127. Robustelli, P.; Piana, S.; Shaw, D. E., Developing a molecular dynamics force field for both folded and disordered protein states. *Proceedings of the National Academy of Sciences* **2018,** *115* (21), 4758.
128. Khalak, Y.; Baumeier, B.; Karttunen, M., Improved general-purpose five-point model for water: TIP5P/2018. *Journal of Chemical Physics* **2018,** *149* (22), 224507.
129. Qiu, Y.; Nerenberg, P. S.; Head-Gordon, T.; Wang, L.-P., Systematic Optimization of Water Models Using Liquid/Vapor Surface Tension Data. *Journal of Physical Chemistry B* **2019,** *123* (32), 7061-7073.
130. Fuentes-Azcatl, R.; Barbosa, M. C., Flexible bond and angle, FBA/ϵ model of water. *Journal of Molecular Liquids* **2020,** *303*, 112598.
131. Heinz, H.; Lin, T.-J.; Kishore Mishra, R.; Emami, F. S., Thermodynamically Consistent Force Fields for the Assembly of Inorganic, Organic, and Biological Nanostructures: The INTERFACE Force Field. *Langmuir* **2012,** *29* (6), 1754-1765.
132. Humphrey, W.; Dalke, A.; Schulten, K., VMD: Visual molecular dynamics. *Journal of Molecular Graphics* **1996,** *14* (1), 33-38.
133. Martínez, L.; Andrade, R.; Birgin, E. G.; Martínez, J. M., PACKMOL: A package for building initial configurations for molecular dynamics simulations. *Journal of Computational Chemistry* **2009,** *30* (13), 2157-2164.
134. Kohlmeyer, A.; *TopoTools: Release 1.7*, **2016**.
135. Dequidt, A.; Devémy, J.; Pádua, A. A. H., Thermalized Drude Oscillators with the LAMMPS Molecular Dynamics Simulator. *Journal of Chemical Information and Modeling* **2016,** *56* (1), 260-268.
136. Humbert, M. T.; Zhang, Y.; Maginn, E. J., PyLAT: Python LAMMPS Analysis Tools. *Journal of Chemical Information and Modeling* **2019,** *59* (4), 1301-1305.
137. Soper, A. K., The Radial Distribution Functions of Water as Derived from Radiation Total Scattering Experiments: Is There Anything We Can Say for Sure? *Improvement Science Research Network Physical Chemistry* **2013**, 279463.
138. *CRC Handbook of Chemistry and Physics*. 96th ed.; CRC Press **2015**.
139. Head-Gordon, T.; Johnson, M. E., Tetrahedral structure or chains for liquid water. *Proceedings of the National Academy of Sciences* **2006,** *103* (21), 7973.
140. Pallas, N. R.; Harrison, Y., An automated drop shape apparatus and the surface tension of pure water. *Colloids and Surfaces* **1990,** *43* (2), 169-194.
141. Malmberg, C. G.; Maryott, A. A., Dielectric Constant of Water from 0 to 100 C. *Journal of Research of the National Bureau of Standards* **1956,** *56* (1), 1.
142. Pruppacher, H. R., Self-Diffusion Coefficient of Supercooled Water. *Journal of Chemical Physics* **1972,** *56* (1), 101-107.
143. Hockney, R. W.; Eastwood, J. W., *Computer Simulation Using Particles*. 1st ed.; CRC Press **1988**.
144. Darden, T.; York, D.; Pedersen, L., Particle mesh Ewald: An N·log(N) method for Ewald sums in large systems. *Journal of Chemical Physics* **1993,** *98* (12), 10089-10092.
145. Hayes, R.; Imberti, S.; Warr, G. G.; Atkin, R., The Nature of Hydrogen Bonding in Protic Ionic Liquids. *Angewandte Chemie International Edition* **2013,** *52* (17), 4623-4627.
146. Hayes, R.; Imberti, S.; Warr, G. G.; Atkin, R., Amphiphilicity determines nanostructure in protic ionic liquids. *Physical Chemistry Chemical Physics* **2011,** *13* (8), 3237-3247.
147. Song, X.; Hamano, H.; Minofar, B.; Kanzaki, R.; Fujii, K.; Kameda, Y.; Kohara, S.; Watanabe, M.; Ishiguro, S.; Umebayashi, Y., Structural heterogeneity and unique distorted hydrogen bonding in primary ammonium nitrate ionic liquids studied by high-energy X-ray diffraction experiments and MD simulations. *Journal of Physical Chemistry B* **2012,** *116* (9), 2801-13.
148. Zentel, T.; Kühn, O., Properties of Hydrogen Bonds in the Protic Ionic Liquid Ethylammonium Nitrate. DFT versus DFTB Molecular Dynamics. *Theoretical Chemistry Accounts* **2017,** *136*.

149. Henderson, W. A.; Fylstra, P.; De Long, H. C.; Trulove, P. C.; Parsons, S., Crystal structure of the ionic liquid EtNH3NO3—Insights into the thermal phase behavior of protic ionic liquids. *Physical Chemistry Chemical Physics* **2012,** *14* (46), 16041-16046.

8 Appendix

8.1 Supplementary information for machine learning (Chapter 2)

Table 8.1. Reported data in the viscosity training set for ILs library.

ILs	KF value	Viscosity (m Pa.s)
Triethylammonium formate	0.00875	17.7
Triethylammonium di-n-butylphosphate	0.00875	94.4
Triethylammonium methanesulfonate	0.00875	100
Propylammonium formate	0.6753	96.77
Propylammonium acetate	0.5436	932.22
Propylammonium formate	0.6753	96.77
Propylammonium acetate	0.5436	932.22

Table 8.2. Reported data in the conductivity training set for ILs library.

IL	KF (wt%)	Conductivity (µS/cm)
Diisopropylethylammonium formate	0.0065	5800
N,N-diethylmethylammonium TfO	0.01	8330
Diethanolammonium formate	0.88	550
Diethanolammonium formate	0.6	770
Diethanolammonium formate	0.00875	930
Diethanolammonium acetate	0.85	130
Diethanolammonium acetate	0.00875	110
Diethanolammonium sulfamate	0.025	140
Diethanolammonium di-n-butylphosphate	0.00875	60
Diethanolammonium MsOH	0.00875	320
Diethanolammonium malonate	0.44	53
Alaninemethylester glycolate	0.18	23.6

Alanineethylester glycolate	0.62	55.4
Prolinemethylester glycolate	0.74	86.1
Ethylammonium acetate	0.018	2220
Ethylammonium heptafluorobutyrate	0.51	880
Ethylammonium pentadecafluorooctanoate	0.61	169
Glycineethylester lactate	0.17	4009
Prolinemethylester lactate	0.76	118

Figure 8.1. BRANNLP viscosity predictions for carboxylic acid based ILs.

	Formate	Acetate	Glycolate	Trifluoro acetic acid	Propionate	Lactate	Butyrate	Isobutyrate	Heptafluoro butyrate	Pentanoate	Hexanoate	Heptanoate	Octanoate	Malonate	Perfluoro octanoic acid
Methylammonium	3.34	14.21	70.61	27.05	22.25	76.84	22.25	34.33	10.65	22.25	3.76	2.89	2.89	16.64	0.11
Ethylammonium	15.54		240.19	101.16	84.87	259.23	84.87	125.34		84.87	17.25	13.66	13.66	65.36	
Ethanolammonium	95.98	294.82	1025.36	480.03	411.67	1096.56	411.67	579.20		411.67		83.91	83.91	330.04	6.72
2methoxyethylammonium	36.84	116.57	455.43	201.14	170.43	489.52	170.43	246.27	91.34	170.43	37.99	30.51	30.51	133.19	1.95
2-2-hydroxyethoxyethylammonium	106.28	310.67	1092.03	531.15	440.79	1167.40	440.79	618.91	248.24	440.79	110.93	90.73	90.73	351.24	7.39
Acetamide	0.96	5.77	26.44		7.57	28.97	7.57	12.11	3.40	7.57	1.09	0.82	0.82	5.52	0.03
Propylammonium	134.18	409.77	1324.00	631.03	543.17	1413.73	543.17	757.99	309.17	543.17	140.29	115.19	115.19	434.63	9.88
Propanolammonium	309.67	849.21	2684.92		1167.62	2854.86	1167.62	1593.83	690.36	1167.62	330.91	275.52	275.52	953.86	28.38
2-propanolammonium	610.23	1599.06	4753.21	2469.26	2163.53	5037.45	2163.53	2902.80	1317.71	2163.53	659.13	554.77	554.77	1777.86	65.81
2-methyl propyl ammonium	119.26	360.11	1246.24	591.47	508.67	1331.19	508.67	711.22	288.57	508.67	130.32	106.87	106.87	406.50	9.02
Isopropylammonium		436.15	1479.41	710.54	612.59	1578.61	612.59	851.86	350.80	612.59	160.58	132.14	132.14	491.35	11.68
Butylammonium	82.24	256.81	921.15	427.99	366.47	985.76	366.47	517.39		366.47	90.12	73.45	73.45	290.94	5.72
2-methyl butyl ammonium	79.14	247.99	892.82	413.91	354.25	955.62	354.25	500.65	197.28	354.25	86.74	70.65	70.65	281.04	5.45
Sec butyl ammonium	47.63	156.40	591.75	266.38	226.60	635.00	226.60	324.58	123.29	226.60	52.41	42.32	42.32	178.14	2.92
N-butyramide	0.77	3.80	22.14	7.72	6.22	24.29	6.22	10.03	2.76	6.22	0.87	0.65	0.65	4.52	0.03
Isobutyramide	1.84	8.31	44.03	16.24	13.25	48.06	13.25	20.80	6.15	13.25	2.07	1.58	1.58	9.79	0.06
Pentylammonium	74.68	235.27	851.80	393.58	336.62	911.98	336.62	476.45	186.97	336.62	81.89	66.64	66.64	266.78	5.08
Heptylammonium	78.76	246.92	889.39	412.21	352.78	951.98	352.78	498.62	196.42	352.78	86.33	70.31	70.31	279.85	5.42
Octylammonium	75.05	236.32	855.21	395.27	338.08	915.61	338.08	478.46	187.82	338.08	82.29	66.97	66.97	267.96	5.11
Dimethylammonium	9.35	32.14	145.16	58.83	48.97	157.19	48.97	73.61	24.51	48.97	9.23	7.23	7.23	37.26	0.33
N-methyl-2-hydroxyethylammonium	73.60	232.18	841.81	388.64		901.36		470.57	184.47		80.72	65.67	65.67	263.32	4.99
bis-2-hydroxyethylmethylammonium		405.06	1384.62	661.98	570.18	1478.06	570.18	794.54	325.34	570.18	148.15	121.75	121.75	456.68	10.57
Diethylammonium	18.16	59.29	249.75	105.49	88.57	269.48		130.61		88.57	18.10	14.35	14.35	68.26	0.77
Diethanolammonium	339.22	904.39	2807.28	1408.43	1225.24	2984.19	1225.24	1670.21	726.13	1225.24	349.24	291.03	291.03	1074.87	30.32
bis-2-methoxyethylammonium	6.40	14.03	69.80	26.71	21.97	75.96	21.97	33.91	10.51	21.97	3.70	2.85	2.85	16.42	0.11
Diallylammonium	80.07	116.12	378.93	165.11	139.51	407.77	139.51	202.84	73.97	139.51	30.29	24.23	24.23	14.89	1.47
Dinpropylammonium	17.51	63.21	264.35	112.14	94.23	285.13	94.23	138.69	48.91	94.23	19.42	15.41	15.41	72.72	0.84
Dibutylammonium	60.17	114.89	449.59	198.38	168.06	483.28	168.06	242.94		168.06	37.39	30.02	30.02	131.30	
Dimethylethylammonium	6.16	24.62	114.70	45.65	37.85	124.40	37.85	57.37	18.67	37.85	6.88	5.36	5.36	28.64	0.23
N-allyl dimethylammonium	7.59	29.74	135.55	54.65	45.44	146.84	45.44	68.46	22.65	45.44	8.48	6.63	6.63	34.51	0.30
Diethylmethylammonium	6.14	24.57	114.49	45.56	37.78	124.18	37.78	57.26	18.63	37.78	6.87	5.35	5.35	28.58	0.23
N-N-diethylmethylammonium	6.14	24.57	114.49	45.56	37.78	124.18	37.78	57.26	18.63	37.78	6.87	5.35	5.35	28.58	0.23
N-N-diallylmethylammonium	10.61	40.22	177.05	72.86	60.84	191.47	60.84	90.81	30.83	60.84	11.82	9.29	9.29	46.51	0.45
N-methyldipropylammonium	6.87	27.16	125.09	50.12	41.62	135.59	41.62	62.88	20.64	41.62	7.67	5.98	5.98	31.55	0.26
Diisopropylmethylammonium	7.20	28.34	129.89	52.19	43.37	140.76	43.37	65.44	21.56	43.37	8.04	6.28	6.28	32.91	0.28
N-N-dimethylpropylammonium	5.67	22.86	107.41	42.53	35.23	116.55	35.23	53.52	17.31	35.23	6.34	4.93	4.93	26.61	0.21
Diisopropylethylammonium	13.55	29.49	134.54	54.21	45.07	145.76	45.07	67.92	22.45	45.07	8.40	13.55	14.96	34.23	0.29
Dimethylbutylammonium	12.02	45.00	195.58	81.10	67.83	211.37	67.83	100.88	34.58	67.83	13.37	10.54	10.54	51.98	0.53
N-allyldiethylammonium	7.56	29.62	135.07	54.44	45.26	146.33	45.26	68.20	22.56	45.26	8.44	6.60	6.60	34.38	0.29
N-N-diethylpropylammonium	6.06	24.26	113.22	45.01	37.32	122.81	37.32	56.59	18.40	37.32	6.77	5.27	5.27	28.22	0.23
Triethylammonium	8.01	25.31	117.53	46.86	38.88	127.45	38.88	58.87		38.88	7.10	5.53	5.53	29.43	0.24
Triethanolammonium	267.29	744.16	2390.76	1186.57	1029.94	2543.81	1029.94	1410.92	605.23	1029.94	287.55	238.88	238.88	887.59	23.89
Tributylammonium	14.54	53.42	227.70	95.51	80.07	245.84	80.07	118.46	41.19	80.07	16.14	12.77	12.77	61.58	0.67
Trihexylammonium	13.91	51.34	219.79	91.95	77.04	237.36	77.04	114.12	39.55	77.04	15.45	12.21	12.21	59.20	0.63
Trioctylammonium	13.46	49.82	214.03	89.36	74.84	231.17	74.84	110.96	38.36	74.84	14.95	11.81	11.81	57.47	0.61
Alanine ethyl ester	21.54	3.43	11.52	7.01	5.64	22.23	5.64	9.12	2.49	5.64	0.78	0.58	0.58	4.08	0.02
Alanine methyl ester	0.35	1.87	0.70	3.94	3.14	13.12	3.14	5.18	1.34	3.14	0.40	0.29	0.29	2.24	0.01
Glycine ethyl ester		1.22	8.19	2.62	2.08	0.36	2.08	3.48	0.86	2.08	0.25	0.18	0.18	1.47	0.01
Proline methyl ester	0.24	1.99	1.99	0.53	0.41	2.21	0.41	0.73	0.16	0.41	0.05	0.04	0.04	0.28	0.00
Collidinium	8.24	17.80	86.12	33.51	27.66	93.59	27.66	42.36	13.40	27.66	4.81	3.72	3.72	20.78	0.15
Benzamide	0.55	2.83	17.10	5.83	4.68	18.79	4.68	7.62	2.04	4.68	0.63	0.47	0.47	3.37	0.02
Diphenylammonium	31.83	108.54	427.42	187.89	159.05	459.59	159.05	230.32	84.93	159.05	35.14	28.18	28.18	124.12	1.77
Lutidinium	3.89	8.58	45.31	16.75	13.68	49.46	13.68	21.45	6.36	13.68	2.15	1.64	1.64	10.11	0.06
Quinolinium	7.92	18.39	88.63	34.57	28.54	96.29	28.54	43.67	13.86	28.54	4.99	3.86	3.86	21.46	0.16
N,N,N′,N′-Tetramethylguanidine	23.34	81.96	332.95	143.69	121.17	358.58	121.17	176.95	63.76	121.17	25.82	20.60	20.60	94.02	1.20
HNC dmaH	23.34	81.96	332.95	143.69	121.17	358.58	121.17	176.95	63.76	121.17	25.82	20.60	20.60	94.02	1.20
Amilaminium		263.13	941.37	438.06	375.21	1007.26	375.21	529.35	209.57	375.21	92.54	75.46	75.46	298.02	5.91
N-(2-ethyl-hexyl)-ethylenediamine	265.60	747.27	2397.70	1190.25	1033.17	2551.15	1033.17	1415.22	607.22	1033.17	288.56	239.73	239.73	837.18	24.00
N-Butylethylenediamine	299.84	834.77	2648.40	1323.54	1150.46	2816.25	1150.46	1571.06	679.72	1150.46	325.47	270.92	270.92	934.15	27.81
N-hexylethylenediaminium	275.00	771.38	2467.04	1227.03	1065.52	2624.49	1065.52	1458.25	627.18	1065.52	298.70	248.29	248.29	863.91	25.03
N-octylethylenediaminium	258.75	729.65	2346.86	1163.32	1009.50	2497.37	1009.50	1383.71	592.63	1009.50	281.17	233.49	233.49	817.64	23.25
N-decylethylenediaminium	249.86	706.73	2280.59	1128.28	978.70	2427.26	978.70	1342.68	573.68	978.70	271.58	225.40	225.40	792.22	22.28
N-dodecylethylenediaminium	241.26	684.48	2216.01	1094.20	948.76	2358.94	948.76	1302.76	555.28	948.76	262.29	217.57	217.57	767.52	21.35
Ethyldiammonium	253.33	715.67	1521.64	732.25	631.56	1623.41	631.56	877.46	362.22	631.56	166.18	136.83	136.83	506.87	12.18

Figure 8.2. BRANNLP viscosity predictions for inorganic acid based ILs.

	Hydrogene bisfluoride	Chloride	Perchlorate	Nitrate	Thiocyanate	Dihydrogen phosphate	Dinbutyl phosphate	Mesylate	Hexafluoro isopropoxy sulfate	Hydrogen sulfate	Pulfamate	Triflate	Tf2N	BETI
Methylammonium	2.87	2.87	20.42	17.58	3.34	10.14	27.69	23.29	109.69	33.72	3.14	11.55	0.28	0.24
Ethylammonium	13.58	13.58	78.55	68.69	15.54	41.91	103.31	88.40	357.61	123.35	14.71	47.11	1.73	1.50
Ethanolammonium	83.48	83.48	384.72	342.16	93.84	222.31	488.95	426.61	1455.78	598.41	89.46	246.18	14.13	12.53
2methoxyethylammonium	30.34	30.34	158.43	139.60	34.44	87.62	205.18	177.12	663.77	242.57	32.71	97.83	4.39	3.85
2-2-hydroxyethoxyethylammonium	90.27	90.27	412.09	409.09	101.39	238.93	523.00	456.69	1547.35	647.92	96.70	264.41	15.46	13.72
Acetamide	0.81	0.81	6.89	5.86	0.96	3.22	9.59	7.95	42.56	11.88	0.90	3.71	0.08	0.07
Propylammonium	114.62	114.62	508.43	453.48	128.45	297.78	642.47	562.40	1864.69	747.66	122.62	328.92	20.34	18.10
Propanolammonium	274.26	274.26	1097.79	986.67	304.88	666.63	1365.76	1206.16	3699.79	1573.55	291.99	731.37	55.26	49.60
2-propanolammonium	552.38	552.38	2041.16	1845.56	610.23	1274.96	2508.72	2230.91	6438.78	2867.88	585.92	1391.39	122.78	110.97
2-methyl propyl ammonium	106.34	106.34	475.96	424.23	119.26	277.88	602.26	526.79	1758.51	701.48	113.81	307.12	18.66	16.59
Isopropylammonium	131.50	131.50	573.82	512.42	147.18	338.02	723.30	634.04	2076.34	840.38	140.57	372.96	23.82	21.22
Butylammonium	73.07	73.07	342.24	304.01	82.24	196.65	436.03	379.91	1312.29	510.10	78.37	217.99	12.12	10.73
2-methyl butyl ammonium	70.29	70.29	330.76	293.71	79.14	189.73	421.71	367.28	1273.20	493.57	75.40	210.40	11.59	10.26
Sec butyl ammonium	42.10	42.10	211.00	186.49	47.63	118.39	271.59	235.27	855.11	319.82	45.29	131.82	6.42	5.65
N-butyramide	0.65	0.65	5.66	4.80	0.77	2.61	7.92	6.54	35.87	9.83	0.71		0.06	0.05
Isobutyramide	1.57	1.57	12.12	10.37	1.84	5.84	16.64	13.89	69.55	20.42	1.72		0.15	0.13
Pentylammonium	66.29	66.29	314.20	278.86	74.68	179.78	401.02	349.06	1216.53	469.69	71.14	199.46	10.83	9.58
Heptylammonium	69.95	69.95	329.37	292.47	78.76	188.90	419.98	365.76	1268.47	491.58	75.04	209.48	11.53	10.20
Octylammonium	66.62	66.62	315.57	280.09	75.05	180.61	402.74	350.57	1221.24	471.68	71.49	200.36	10.90	9.64
Dimethylammonium	7.18	7.18	45.16	39.25	8.28	77.43	181.79	51.10	219.87	77.43	7.81	26.46	0.82	0.71
N-methyl-2-hydroxyethylammonium	65.33	65.33	310.18	275.25	73.60	177.37	396.00	344.63	1202.72	463.89	70.11	196.80	10.65	9.42
bis-2-hydroxyethylmethylammonium	121.15	121.15	533.87	476.40	135.70	313.40	673.93	590.27	1947.34	783.77	129.57	346.03	21.68	19.30
Diethylammonium	14.26	14.26	81.99	71.73	16.31	43.84	181.79	92.24	371.35	128.55	15.44	49.26	1.83	1.59
Diethanolammonium	289.70	289.70	1152.27	1036.13	321.89	701.28	2175.89	1265.50	3863.17	1649.04	448.52	769.06	58.83	52.83
bis-2-methoxyethylammonium	2.83	2.83	20.16	17.36	3.29	10.00	27.35	22.99	108.47	33.31	3.09	11.40	0.28	0.24
Diallylammonium	24.09	24.09	129.52	113.88	27.41	70.91	168.48	145.08	555.64	199.74	26.01	79.32	3.36	2.94
Dinpropylammonium	15.32	15.32	87.26	76.40	17.51	46.82	114.50	98.11	392.31	136.51	16.58	52.57	1.99	1.73
Dibutylammonium	29.85	29.85	156.20	137.62	33.90	86.33	202.36	174.65	655.54	239.29	32.18	96.40	4.31	3.78
Dimethylethylammonium	5.33	5.33	34.85	30.20	6.16	17.81	46.68	39.53	175.15	56.40	5.80	20.19	0.58	0.50
N-allyl dimethylammonium	6.59	6.59	41.88	36.37	7.59	21.62	55.87	47.43	205.79	67.32	7.17	43.35	0.74	0.64
Diethylmethylammonium	5.32	5.32	34.78	30.14	6.14	17.78	46.59	39.46	174.85	56.29	5.79	25.58	0.58	0.50
N-N-diethylmethylammonium	5.32	5.32	34.78	30.14	6.14	17.78	46.59	39.46	174.85	56.29	5.79	36.01	0.58	0.50
N-N-diallylmethylammonium	9.24	9.24	56.19	48.96	10.61	29.46	74.45	63.44	266.36	89.33	10.03	58.11	1.10	0.95
N-methyldipropylammonium	5.95	5.95	38.34	33.26	6.87	19.70	51.25	43.45	190.45	61.83	6.48	39.69	0.66	0.57
Diisopropylmethylammonium	6.24	6.24	39.96	34.69	7.20	20.58	53.37	45.27	197.49	64.34	6.79	23.29	0.70	0.60
N-N-dimethylpropylammonium	4.90	4.90	32.42	28.07	5.67	16.51	43.50	36.80	164.40	52.61	5.34	33.58	0.53	0.45
Diisopropylethylammonium	6.52	6.52	41.54	36.07	7.52	21.43	55.42	47.04	204.31	66.79	7.10	24.25	0.74	0.63
Dimethylbutylammonium	10.48	10.48	62.68	54.68	12.02	33.05	82.86	70.70	293.23	99.25	11.37	37.24	1.28	1.11
N-allyldiethylammonium	6.56	6.56	41.72	36.23	7.56	21.53	55.66	47.25	205.09	67.06	7.13	43.18	0.74	0.64
N-N-diethylpropylammonium	5.24	5.24	34.36	29.77	6.06	17.55	46.04	38.98	172.98	55.63	5.71	35.58	0.57	0.49
Triethylammonium	5.50	5.50	35.80	31.03	6.35	18.32	83.78	40.60	179.33	57.88	5.99	20.76	0.60	0.52
Triethanolammonium	237.77	237.77	967.65	868.63	264.67	584.18	1206.89	1064.33	3306.09	1392.76	253.34	641.61	46.94	
Tributylammonium	12.69	12.69	74.08	64.74	14.54	39.40	165.33	83.42	339.62	116.57	13.75	44.32	1.60	1.39
Trihexylammonium	12.14	12.14	71.26	62.25	13.91	37.83	93.92	80.27	328.23	112.30	13.16	42.56	1.52	1.32
Trioctylammonium	11.74	11.74	69.21	60.44	13.46	36.68	91.28	77.98	319.91	109.18	12.73	41.29	1.46	1.27
Alanine ethyl ester	0.58	0.58	5.13		0.68	2.35	7.19	5.93	32.92	8.94	0.64	2.72	0.05	0.05
Alanine methyl ester	0.29	0.29	2.84	2.39	0.35	1.26	4.04	3.31	19.74	5.08	0.32	1.47	0.03	0.03
Glycine ethyl ester	0.18	0.18	1.88	1.57	0.22	0.81	2.70	2.19	13.78	3.41	0.20	0.95	0.02	0.02
Proline methyl ester	0.04	0.04	0.37	0.05	0.04	0.15	0.55	0.44	3.38	0.71	0.04	0.18	0.01	0.00
Collidinium	3.70	3.70	25.41	21.95	4.29	12.77	34.29	28.92	132.84	41.63	4.04	14.52	0.38	0.32
Benzamide	0.46	0.46	4.25	3.59	0.55	1.93	5.99	4.93	27.97	7.47	0.51		0.04	0.04
Diphenylammonium	28.02	28.02	147.79	130.13	31.83	81.45	191.69	165.33	624.25	226.84	30.22	91.00	4.01	3.51
Lutidinium	1.63	1.63	12.51	10.71	1.90	6.04	17.16	14.34	71.51	21.05	1.79	6.92	0.15	0.13
Quinolinium	3.84	3.84	26.23	22.66	4.45	13.20	35.37	29.84	136.57	42.91	4.19	15.01	0.40	0.34
N,N,N',N'-Tetramethylguanidine	20.48	20.48	112.40	98.68	23.34	61.09	146.66	126.06	490.31	174.22	22.13	68.43	2.79	2.43
HNC dmaH	20.48	20.48	112.40	98.68	23.34	61.09	146.66	126.06	490.31	174.22	22.13	68.43	2.79	2.43
Amilaminium	75.07	75.07	350.45	311.38	84.47	201.59	446.27	388.94	1340.17	521.91	80.50	223.43	12.50	11.07
N-(2-ethyl-hexyl)-ethylenediamine	238.62	238.62	970.70	871.39	265.60	586.11	1210.62	1067.66	3315.40	1397.01	254.24	643.72		42.25
N-Butylethylenediamine	269.68	269.68	1081.56	971.94	299.84	656.33	1345.97	1188.48	3650.97	1551.04	287.14	720.15		48.65
N-hexylethylenediaminium	247.14	247.14	1001.27	899.11	275.00	605.44	1247.97	1100.99	3408.31	1439.54	263.27	664.76		43.99
N-octylethylenediaminium	232.41	232.41	948.34	851.12	258.75	571.99	1183.28	1043.27	3247.22	1365.87	247.66	628.33		40.98
N-decylethylenediaminium	224.35	224.35	919.24	824.76	249.86	553.64	1147.69	1011.54	3158.29	1325.32	239.12	608.34		39.35
N-dodecylethylenediaminium	216.56	216.56	890.96	799.14	241.26	535.82	1113.08	980.68	3071.56	1285.87	230.85	588.92		37.77
Ethyldiammonium	136.16	136.16	591.69	528.55	152.34	349.05	1161.58	653.62	2133.75	865.67	145.52	385.04	24.79	22.09

BETI: bis[(pentafluoro-ethyl)sulfonyl]ate, Tf2N: bis(trifluoromethanesulfonyl)imide.

Figure 8.3. MLREM viscosity predictions for carboxylic acid based ILs.

	Formate	Acetate	Glycolate	Trifluoro acetic acid	Propionate	Lactate	Butyrate	Isobutyrate	Heptafluor obutyrate	Pentanoate	Hexanoate	Heptanoat e	Octanoate	Malonate	Perfluoro octanoic acid
Methylammonium	22.94	80.40	514.20	152.68	80.40	514.20	80.40	80.40	152.68	80.40	80.40	80.40	80.40	121.20	80.40
Ethylammonium	30.73		688.93	204.56	107.72	688.93	107.72	107.72		107.72	107.72	107.72	107.72	162.38	
Ethanolammonium	95.98	294.82	3427.63	1017.74	535.96	3427.63	535.96	535.96		535.96		535.96	535.96	330.04	535.96
2methoxyethylammonium	36.84	102.80	657.41	195.20	102.80	657.41	102.80	102.80	195.20	102.80	102.80	102.80	102.80	154.95	102.80
2-2-hydroxyethoxyethylammonium	106.28	469.26	3001.05	531.15	469.26	3001.05	469.26	469.26	891.07	469.26	469.26	469.26	469.26	707.34	469.26
Acetamide	1.62	5.77	36.24	2.30	5.67	36.24	5.67	5.67	10.76	5.67	5.67	5.67	5.67	8.54	5.67
Propylammonium	134.18	409.77	1830.68	543.57	286.25	1830.68	286.25	286.25	543.57	286.25	286.25	286.25	286.25	431.49	286.25
Propanolammonium	309.67	849.21	7274.23		1137.43	7274.23	1137.43	1137.43	2159.87	1137.43	1137.43	1137.43	1137.43	953.86	1137.43
2-propanolammonium	109.21	382.81	2448.19	726.92	382.81	2448.19	382.81	382.81	726.92	382.81	382.81	382.81	382.81	577.04	382.81
2-methylpropylammonium	134.95	473.03	3025.21	898.25	473.03	3025.21	473.03	473.03	898.25	473.03	473.03	473.03	473.03	713.04	473.03
Isopropylammonium		107.72	688.93	204.56	107.72	688.93	107.72	107.72	204.56	107.72	107.72	107.72	107.72	162.38	107.72
Butylammonium	120.33	421.80	2697.53	800.95	421.80	2697.53	421.80	421.80		421.80	421.80	421.80	421.80	635.80	421.80
2-methylbutylammonium	189.81	665.34	4255.07	1263.42	665.34	4255.07	665.34	665.34	1263.42	665.34	665.34	665.34	665.34	1002.92	665.34
Sec-butylammonium	72.14	252.86	1617.11	480.15	252.86	1617.11	252.86	252.86	480.15	252.86	252.86	252.86	252.86	381.15	252.86
N-butyramide	6.84	23.98	153.35	45.53	23.98	153.35	23.98	23.98	45.53	23.98	23.98	23.98	23.98	36.14	23.98
Isobutyramide	7.32	25.67	164.16	48.74	25.67	164.16	25.67	25.67	48.74	25.67	25.67	25.67	25.67	38.69	25.67
Pentylammonium	124.28	435.64	2786.06	827.24	435.64	2786.06	435.64	435.64	827.24	435.64	435.64	435.64	435.64	656.67	435.64
Heptylammonium	107.53	376.94	2410.63	715.77	376.94	2410.63	376.94	376.94	715.77	376.94	376.94	376.94	376.94	568.18	376.94
Octylammonium	95.11	333.39	2132.13	633.08	333.39	2132.13	333.39	333.39	633.08	333.39	333.39	333.39	333.39	502.54	333.39
Dimethyl ammonium	9.35	26.19	167.48	49.73	26.19	167.48	26.19	26.19	49.73	26.19	26.19	26.19	26.19	39.48	26.19
N-methyl2-hydroxyethylammonium	75.70	265.33	1696.90	503.85		1696.90		265.33	503.85		265.33	265.33	265.33	399.96	265.33
bis-2-hydroxyethylmethylammonium		402.97	2577.11	765.20	402.97	2577.11	402.97	402.97	765.20	402.97	402.97	402.97	402.97	607.42	402.97
Diethylammonium	18.16	104.61	669.00	198.64	104.61	669.00	143.05	104.61		104.61	104.61	104.61	104.61	157.68	104.61
Diethanol ammonium		904.39	7746.28	2300.03	1211.24	7746.28	1211.24	1211.24	2300.03	1211.24	1211.24	1211.24	1211.24	1074.87	1211.24
bis-2-methoxyethylammonium	6.40	23.59	150.90	44.80	23.59	150.90	23.59	23.59	44.80	23.59	23.59	23.59	23.59	35.57	23.59
Diallylammonium		80.07	1008.81	299.54	157.74	1008.81	157.74	157.74	299.54	157.74	157.74	157.74	157.74	116.12	157.74
Dinpropylammonium	56.99	199.76	1277.56	379.33	199.76	1277.56	199.76	199.76	379.33	199.76	199.76	199.76	199.76	301.12	199.76
Dibutylammonium	60.17	256.01	1637.30	486.15	256.01	1637.30	256.01	256.01		256.01	256.01	256.01	256.01	385.91	
Dimethylethylammonium	7.34	25.74	164.63	48.88	25.74	164.63	25.74	25.74	48.88	25.74	25.74	25.74	25.74	38.80	25.74
N-allyldimethylammonium	7.55	26.48	169.36	50.29	26.48	169.36	26.48	26.48	50.29	26.48	26.48	26.48	26.48	39.92	26.48
Diethylmethylammonium	10.98	38.49	246.17	73.09	38.49	246.17	38.49	38.49	73.09	38.49	38.49	38.49	38.49	58.02	38.49
N-N-diethylmethylammonium	9.43	33.04	211.32	62.74	33.04	211.32	33.04	33.04	62.74	33.04	33.04	33.04	33.04	49.81	33.04
N-N-diallylmethylammonium	13.10	45.93	293.71	87.21	45.93	293.71	45.93	45.93	87.21	45.93	45.93	45.93	45.93	69.23	45.93
N-methyldipropylammonium	7.93	27.79	177.70	52.76	27.79	177.70	27.79	27.79	52.76	27.79	27.79	27.79	27.79	41.88	27.79
Diisopropylmethylammonium	9.08	31.83	203.57	60.44	31.83	203.57	31.83	31.83	60.44	31.83	31.83	31.83	31.83	47.98	31.83
N-N-dimethylpropylammonium	14.89	18.34	117.27	34.82	18.34	117.27	18.34	18.34	34.82	18.34	18.34	13.55	13.55	27.64	18.34
Diisopropylethylammonium	11.64	40.79	260.89	77.46	40.79	260.89	40.79	40.79	77.46	40.79	40.79	40.79	40.79	61.49	40.79
Dimethylbutylammonium	10.54	36.95	236.29	70.16	36.95	236.29	36.95	36.95	70.16	36.95	36.95	36.95	36.95	55.69	36.95
N-allyldiethylammonium	12.57	44.07	281.83	83.68	44.07	281.83	44.07	44.07	83.68	44.07	44.07	44.07	44.07	66.43	44.07
N-N-diethylpropylammonium	8.01	41.62	266.15	79.02	41.62	266.15	41.62	41.62		41.62	41.62	41.62	41.62	62.73	41.62
Triethylammonium	267.29	744.16	7340.65	2179.59	1147.81	7340.65	1147.81	1147.81	2179.59	1147.81	1147.81	1147.81	1147.81	887.59	1147.81
Triethanolammonium	15.96	55.94	357.77	106.23	55.94	357.77	55.94	55.94	106.23	55.94	55.94	55.94	55.94	84.33	55.94
Tributylammonium	5.11	17.90	114.45	33.98	17.90	114.45	17.90	17.90	33.98	17.90	17.90	17.90	17.90	26.98	17.90
Trihexylammonium	1.45	5.10	32.59	9.68	5.10	32.59	5.10	5.10	9.68	5.10	5.10	5.10	5.10	7.68	5.10
Alanine ethyl ester	0.70	3.19	21.54	6.05	3.19	20.37	3.19	3.19	6.05	3.19	3.19	3.19	3.19	4.80	3.19
Alanine methyl ester	0.31	1.08	14.96	2.05	1.08	6.89	1.08	1.08	2.05	1.08	1.08	1.08	1.08	1.62	1.08
Glycine ethyl ester	11.52	2.43	15.52	4.61	2.43		2.43	2.43	4.61	2.43	2.43	2.43	2.43	3.66	2.43
Proline methyl ester	0.05	0.24	1.99	0.52	0.27	2.21	0.27	0.27	0.52	0.27	0.27	0.27	0.27	0.41	0.27
Collidinium	8.24	33.06	211.43	62.78	33.06	211.43	33.06	33.06	62.78	33.06	33.06	33.06	33.06	49.83	33.06
Benzamide	8.33	29.20	186.75	55.45	29.20	186.75	29.20	29.20	55.45	29.20	29.20	29.20	29.20	44.02	29.20
Diphenylammonium	8.30	29.09	186.03	55.24	29.09	186.03	29.09	29.09	55.24	29.09	29.09	29.09	29.09	43.85	29.09
Lutidinium	3.89	14.31	91.53	27.18	14.31	91.53	14.31	14.31	27.18	14.31	14.31	14.31	14.31	21.57	14.31
Quinolinium	7.92	26.80	171.39	50.89	26.80	171.39	26.80	26.80	50.89	26.80	26.80	26.80	26.80	40.40	26.80
N,N,N',N'-Tetramethylguanidine	92.91	325.66	2082.70	618.40	325.66	2082.70	325.66	325.66	618.40	325.66	325.66	325.66	325.66	490.89	325.66
HNC dmaH	92.91	325.66	2082.70	618.40	325.66	2082.70	325.66	325.66	618.40	325.66	325.66	325.66	325.66	490.89	325.66
Amilaminium		282.21	1804.83	535.89	282.21	1804.83	282.21	282.21	535.89	282.21	282.21	282.21	282.21	425.40	282.21
N-(2-ethyl-hexyl)- ethylenediamine	215.06	753.85	4821.13	1431.49	753.85	4821.13	753.85	753.85	1431.49	753.85	753.85	753.85	753.85	1136.34	753.85
N-Butylethylenediamine	332.98	1167.18	7464.52	2216.37	1167.18	7464.52	1167.18	1167.18	2216.37	1167.18	1167.18	1167.18	1167.18	1759.38	1167.18
N-hexylethylenediaminium	252.53	885.19	5661.11	1680.90	885.19	5661.11	885.19	885.19	1680.90	885.19	885.19	885.19	885.19	1334.32	885.19
N-octylethylenediaminium	180.00	630.96	4035.20	1198.13	630.96	4035.20	630.96	630.96	1198.13	630.96	630.96	630.96	630.96	951.09	630.96
N-decylethylenediaminium	123.43	432.64	2766.90	821.55	432.64	2766.90	432.64	432.64	821.55	432.64	432.64	432.64	432.64	652.16	432.64
N-dodecylethylenediaminium	83.33	292.09	1868.04	554.66	292.09	1868.04	292.09	292.09	554.66	292.09	292.09	292.09	292.09	440.30	292.09
Ethyldiammonium	253.33	715.67	7324.93	2174.92	1145.35	7324.93	1145.35	1145.35	2174.92	1145.35	1145.35	1145.35	1145.35	1726.48	1145.35

Figure 8.4. MLREM viscosity predictions for inorganic acid based ILs.

	Hydrogene bisfluoride	Chloride	Perchlorate	Nitrate	Thiocyanate	Dihydrogen phosphate	Dinbutyl phosphate	Mesylates	Hexafluoro isopropoxy sulfate	Hydrogen sulfate	Pulfamate	Triflate	Tf2N	BETI
Methylammonium	15.22	15.22	51.25	51.25	15.22	581.30	179.64	109.95	179.64	172.60	51.25	109.95	32.65	53.34
Ethylammonium	20.39	20.39	68.66	68.66	20.39	778.83	240.68	147.31	240.68	231.25	68.66	147.31	43.74	71.46
Ethanolammonium	101.43	101.43	341.62	341.62	101.43	3874.91	1197.48	732.93	1197.48	598.41	341.62	732.93	217.62	355.56
2methoxyethylammonium	19.45	19.45	65.52	65.52	19.45	743.20	229.67	140.57	229.67	220.67	65.52	140.57	41.74	68.19
2-2-hydroxyethoxyethylammonium	88.81	88.81	299.10	409.09	88.81	3392.66	1048.45	641.72	1048.45	647.92	299.10	641.72	190.54	311.31
Acetamide	1.07	1.07	3.61	3.61	1.07	40.97	12.66	7.75	12.66	12.17	3.61	7.75	10.37	3.76
Propylammonium	54.18	54.18	182.46	182.46	54.18	2069.57	639.57	391.46	639.57	614.50	182.46	391.46	116.23	189.90
Propanolammonium	215.27	215.27	725.00	725.00	215.27	8223.47	2541.33	1555.46	2541.33	2441.72	725.00	1555.46	461.85	754.57
2-propanolammonium	72.45	72.45	244.00	244.00	72.45	2767.67	855.30	523.50	855.30	821.78	244.00	523.50	155.44	253.96
2-methylpropylammonium	89.53	89.53	301.51	301.51	89.53	3419.98	1056.89	646.88	1056.89	1015.46	301.51	646.88	192.07	313.81
Isopropylammonium	20.39	20.39	68.66	68.66	20.39	778.83	240.68	147.31	240.68	231.25	68.66	147.31	43.74	71.46
Butylammonium	79.83	79.83	268.85	268.85	79.83	3049.53	942.41	576.81	942.41	905.47	268.85	576.81	171.27	279.82
2-methylbutylammonium	125.92	125.92	424.09	424.09	125.92	4810.33	1486.55	909.87	1486.55	1428.29	424.09	909.87	270.16	441.39
Sec-butylammonium	47.86	47.86	161.17	161.17	47.86	1828.13	564.95	345.79	564.95	542.81	161.17	345.79	102.67	167.75
N-butyramide	4.54	4.54	15.28	15.28	4.54	173.36	53.57	32.79	53.57	51.47	15.28		9.74	15.91
Isobutyramide	4.86	4.86	16.36	16.36	4.86	185.58	57.35	35.10	57.35	55.10	16.36		10.42	17.03
Pentylammonium	82.45	82.45	277.68	277.68	82.45	3149.63	973.34	595.75	973.34	935.19	277.68	595.75	176.89	289.00
Heptylammonium	71.34	71.34	240.26	240.26	71.34	2725.20	842.18	515.47	842.18	809.17	240.26	515.47	153.05	250.06
Octylammonium	63.10	63.10	212.50	212.50	63.10	2410.36	744.88	455.92	744.88	715.69	212.50	455.92	135.37	221.17
Dimethyl ammonium	4.96	4.96	16.69	16.69	4.96	189.34	58.51	35.81	58.51	77.43	16.69	35.81	10.63	17.37
N-methyl2-hydroxyethylammonium	50.22	50.22	169.12	169.12	50.22	1918.34	592.83	362.85	592.83	569.59	169.12	362.85	107.74	176.02
bis-2-hydroxyethylmethylammonium	76.26	76.26	256.85	256.85	76.26	2913.40	900.34	551.07	900.34	865.05	256.85	551.07	163.62	267.33
Diethylammonium	19.80		66.68	66.68	19.80	756.30	181.79	143.05	233.72	224.56	66.68	143.05	42.48	69.40
Diethanol ammonium	229.24	229.24	772.04	772.04	229.24	8757.11	339.22	1931.84	2706.24	2600.17	448.52	1656.39	491.82	803.54
bis-2-methoxyethylammonium	4.47	4.47	15.04	15.04	4.47	170.59	52.72	32.27	52.72	50.65	15.04	32.27	9.58	15.65
Diallylammonium	29.85	29.85	100.54	100.54	29.85	1140.45	352.44	215.71	352.44	338.62	100.54	215.71	64.05	104.65
Dinpropylammonium	37.81	37.81	127.33	127.33	37.81	1444.27	446.33	273.18	446.33	428.84	127.33	273.18	81.11	132.52
Dibutylammonium	48.45	48.45	163.18	163.18	48.45	1850.96	572.01	350.11	572.01	549.59	163.18	350.11	103.95	169.84
Dimethylethylammonium	4.87	4.87	16.41	16.41	4.87	186.11	57.51	35.20	57.51	55.26	16.41	35.20	10.45	17.08
N-allyldimethylammonium	5.01	5.01	16.88	16.88	5.01	191.46	59.17	36.21	59.17	56.85	16.88	43.35	10.75	17.57
Diethylmethylammonium	7.28	7.28	24.54	24.54	7.28	278.30	86.00	47.98	86.00	82.63	24.54	36.01	15.63	25.54
N-N-diethylmethylammonium	6.25	6.25	21.06	21.06	6.25	238.89	73.83	45.19	73.83	70.93	21.06	58.11	13.42	21.92
N-N-diallylmethylammonium	8.69	8.69	29.27	29.27	8.69	332.04	102.61	62.80	102.61	98.59	29.27	39.69	18.65	30.47
N-methyldipropylammonium	5.26	5.26	17.71	17.71	5.26	200.89	62.08	38.00	62.08	59.65	17.71	38.00	11.28	18.43
Diisopropylmethylammonium	6.02	6.02	20.29	20.29	6.02	230.13	71.12	43.53	71.12	68.33	20.29	33.58	12.92	21.12
N-N-dimethylpropylammonium	3.47	3.47	11.69	11.69	3.47	132.57	40.97	25.08	40.97	39.36	11.69	25.08	7.45	12.16
Diisopropylethylammonium	7.72	7.72	26.00	26.00	7.72	294.93	91.14	55.79	91.14	87.57	26.00	55.79	16.56	27.06
Dimethylbutylammonium	6.99	6.99	23.55	23.55	6.99	267.13	82.55	50.53	82.55	79.32	23.55	43.18	15.00	24.51
N-allyldiethylammonium	8.34	8.34	28.09	28.09	8.34	318.61	98.46	60.26	98.46	94.60	28.09	35.58	17.89	29.24
N-N-diethylpropylammonium	7.88	7.88	26.53	26.53	7.88	300.88	83.78	71.50	92.98	89.34	26.53	56.91	16.90	27.61
Triethylammonium	217.23	217.23	731.62	731.62	217.23	8298.56	2564.53	1569.66	2564.53	2464.02	731.62	1569.66	466.06	
Triethanolammonium	10.59	10.59	35.66	35.66	10.59	404.46	165.33	76.50	124.99	120.09	35.66	76.50	22.72	37.11
Tributylammonium	3.39	3.39	11.41	11.41	3.39	129.39	39.98	24.47	39.98	38.42	11.41	24.47	7.27	11.87
Trihexylammonium	0.96	0.96	3.25	3.25	0.96	36.85	11.39	6.97	11.39	10.94	3.25	6.97	2.07	3.38
Alanine ethyl ester	0.60	0.60	2.03		0.60	23.03	7.12	4.36	7.12	6.84	2.03	4.36	1.29	2.11
Alanine methyl ester	0.20	0.20	0.69	0.69	0.20	7.79	2.41	1.47	2.41	2.31	0.69	1.47	0.44	0.71
Glycine ethyl ester	0.46	0.46	1.55	1.55	0.46	17.54	5.42	3.32	5.42	5.21	1.55	3.32	0.99	1.61
Proline methyl ester	0.05	0.05	0.17	0.36	0.05	1.96	0.61	0.37	0.61	0.58	0.17	0.37	0.11	0.18
Collidinium	6.26	6.26	21.07	21.07	6.26	239.02	73.87	45.21	73.87	70.97	21.07	45.21	13.42	21.93
Benzamide	5.53	5.53	18.61	18.61	5.53	211.12	65.24	39.93	65.24	62.69	18.61		11.86	19.37
Diphenylammonium	5.51	5.51	18.54	18.54	5.51	210.30	64.99	39.78	64.99	62.44	18.54	39.78	11.81	19.30
Lutidinium	2.71	2.71	9.12	9.12	2.71	103.47	31.98	19.57	31.98	30.72	9.12	19.57	5.81	9.49
Quinolinium	5.07	5.07	17.08	17.08	5.07	193.75	59.88	36.65	59.88	57.53	17.08	36.65	10.88	17.78
N,N,N',N'-Tetramethylguanidine	61.63	61.63	207.58	207.58	61.63	2354.48	727.61	445.35	727.61	699.09	207.58	445.35	132.23	216.04
HNC dmaH	61.63	61.63	207.58	207.58	61.63	2354.48	727.61	445.35	727.61	699.09	207.58	445.35	132.23	216.04
Amilaminium	53.41	53.41	179.88	179.88	53.41	2040.34	630.53	385.93	630.53	605.82	179.88	385.93	114.59	187.22
N-(2-ethyl-hexyl)- ethylenediamine	142.67	142.67	480.51	480.51	142.67	5450.26	1684.31	1030.91	1684.31	1618.30	480.51	1030.91		500.11
N-Butylethylenediamine	220.90	220.90	743.96	743.96	220.90	8438.59	2607.81	1596.15	2607.81	2505.59	743.96	1596.15		774.31
N-hexylethylenediaminium	167.53	167.53	564.22	564.22	167.53	6399.85	1977.77	1210.52	1977.77	1900.25	564.22	1210.52		587.24
N-octylethylenediaminium	119.41	119.41	402.17	402.17	119.41	4561.77	1409.74	862.85	1409.74	1354.48	402.17	862.85		418.58
N-decylethylenediaminium	81.88	81.88	275.77	275.77	81.88	3127.96	966.64	591.65	966.64	928.76	275.77	591.65		287.02
N-dodecylethylenediaminium	55.28	55.28	186.18	186.18	55.28	2111.81	652.62	399.45	652.62	627.04	186.18	399.45		193.78
Ethyldiammonium	216.77	216.77	730.05	730.05	216.77	8280.78	1161.58	1566.30	2559.04	2458.74	730.05	1566.30	465.07	759.83

BETI: bis[(pentafluoro-ethyl)sulfonyl]ate, Tf2N: bis(trifluoromethanesulfonyl)imide.

Figure 8.5. MLREM/BRANNLP conductivity predictions for carboxylic acid based ILs.

	Formate	Acetate	Glycolate	Trifluoro acetic acid	Propionate	Lactate	Butyrate	Isobutyrate	Heptafluor obutyrate	Pentanoate	Hexanoate	Heptanoate	Octanoate	Malonate	Perfluoro octanoic acid
Methylammonium	18.61	1.02	0.16	7.70	0.54	0.21	0.41	0.67	0.71	0.34	0.30	0.29	0.27	0.10	0.10
Ethylammonium	27.58	0.74	0.23	10.54	0.89	0.31	0.68	1.11	1.67	0.58	0.51	0.49	0.45	0.16	0.21
Ethanolammonium	4.27	0.31	0.06	1.98	0.18	0.08	0.14	0.22	0.30	0.12		0.10	0.09	0.04	0.04
2methoxyethylammonium	2.26	0.37	0.07	1.16	0.24	0.09	0.20	0.29	0.22	0.18	0.16	0.16	0.15	0.06	0.05
2-2-hydroxyethoxyethylammonium	1.37	0.20	0.04	0.66	0.13	0.05	0.10	0.15	0.13	0.09	0.08	0.08	0.08	0.03	0.03
Acetamide	6.29	0.24	0.06		0.17	0.08	0.13	0.21	0.27	0.11	0.09	0.09	0.08	0.04	0.04
Propylammonium		0.29	0.10	2.16	0.36	0.13	0.29	0.43	0.35	0.26	0.23	0.22	0.21	0.08	0.07
Propanolammonium	1.34	0.17	0.04		0.11	0.05	0.09	0.13	0.12	0.08	0.07	0.07	0.06	0.03	0.03
2-propanolammonium	1.66	0.20	0.04	0.78	0.13	0.05	0.10	0.15	0.14	0.09	0.08	0.08	0.07	0.03	0.03
2-methylpropylammonium	6.38	0.72	0.12	2.63	0.44	0.16	0.36	0.53	0.42	0.32	0.28	0.27	0.26	0.09	0.09
Isopropylammonium		0.79	0.13	3.07	0.48	0.17	0.39	0.58	0.46	0.34	0.31	0.29	0.28	0.10	0.10
Butylammonium	3.06	0.41	0.08	1.35	0.26	0.10	0.22	0.32	0.32	0.20	0.18	0.17	0.16	0.06	0.06
2-methylbutylammonium	3.69	0.50	0.09	1.59	0.32	0.11	0.26	0.38	0.29	0.23	0.21	0.21	0.19	0.07	0.07
Sec-butylammonium	6.57	0.69	0.12	2.71	0.42	0.15	0.34	0.51	0.41	0.30	0.27	0.26	0.24	0.09	0.09
N-butyramide	1.10	0.12	0.03	0.54	0.08	0.04	0.06	0.09	0.09	0.05	0.05	0.05	0.04	0.02	0.02
Isobutyramide	2.25	0.21	0.04	1.04	0.12	0.06	0.10	0.15	0.15	0.08	0.08	0.07	0.07	0.03	0.03
Pentylammonium	6.71	0.65	0.11	2.78	0.39	0.14	0.31	0.47	0.40	0.28	0.25	0.24	0.22	0.08	0.08
Heptylammonium	3.31	0.42	0.08	1.45	0.26	0.10	0.22	0.32	0.25	0.19	0.17	0.17	0.16	0.06	0.06
Octylammonium	3.30	0.42	0.08	1.45	0.26	0.10	0.22	0.32	0.25	0.19	0.17	0.17	0.16	0.06	0.06
Dimethyl ammonium	30.28	3.45	0.65	17.56	1.98	0.85	1.56	2.37	2.42	1.34	1.20	1.14	1.07	0.48	0.47
N-methyl2-hydroxyethylammonium	5.18	0.63	0.11	2.18		0.14		0.47	0.36		0.26	0.25	0.23	0.08	0.08
bis-2-hydroxyethylmethylammonium		0.38	0.07	1.23	0.24	0.09	0.20	0.29	0.23	0.18	0.16	0.16	0.15	0.06	0.05
Diethylammonium	13.14	1.72	0.30	7.16	1.03	0.40	10.16	1.22	0.98	0.71	0.64	0.61	0.58	0.24	0.23
Diethanol ammonium	1.30	0.22	0.05	0.70	0.14	0.06	0.12	0.17	0.14	0.11	0.10	0.10	0.09	0.03	0.04
bis-2-methoxyethylammonium	2.17	0.96	0.21	2.77	0.64	0.27	0.53	0.74	0.62	0.48	0.44	0.42	0.40	0.18	0.17
Diallylammonium		1.30	0.19	3.37	0.64	0.24	0.52	0.75	0.61	0.46	0.42	0.40	0.38	0.14	0.14
Dinpropylammonium	7.78	1.03	0.19	3.44	0.65	0.25	0.53	0.77	0.62	0.47	0.43	0.41	0.39	0.16	0.15
Dibutylammonium	1.68	0.74	0.14	2.16	0.48	0.18	0.40	0.57		0.36	0.33	0.32	0.30	0.12	
Dimethylethylammonium	39.97	3.24	0.58	16.94	1.84	0.76	1.44	2.21	2.22	1.24	1.10	1.05	0.98	0.43	0.42
N-allyldimethylammonium	35.11	2.86	0.50	14.67	1.63	0.66	1.28	1.96	1.92	1.10	0.98	0.93	0.87	0.37	0.36
Diethylmethylammonium	26.12	2.32	0.40	10.97	1.35	0.53	1.06	1.62	1.52	0.92	0.82	0.78	0.74	0.31	0.29
N-N-diethylmethylammonium	12.39	1.45	0.27	5.46	0.89	0.35	0.72	1.05	0.91	0.63	0.57	0.55	0.52	0.21	0.20
N-N-diallylmethylammonium	11.30	1.33	0.24	4.93	0.81	0.31	0.66	0.97	0.82	0.58	0.52	0.50	0.47	0.19	0.18
N-methyldipropylammonium	34.91	2.64	0.42	13.99	1.49	0.57	1.16	1.80	1.71	0.99	0.88	0.84	0.79	0.32	0.31
Diisopropylmethylammonium	35.77	2.91	0.51	14.98	1.66	0.67	1.30	2.00	1.96	1.12	1.00	0.95	0.89	0.38	0.37
N-N-dimethylpropylammonium	5.25	1.89	0.30	9.02	1.09	0.39	0.85	1.31	1.16	0.74	0.66			0.23	0.22
Diisopropylethylammonium	10.19	1.33	0.26	4.64	0.83	0.34	0.68	0.98	0.85	0.60	0.54	0.52	0.49	0.21	0.20
Dimethylbutylammonium	8.89	1.12	0.20	3.89	0.70	0.26	0.57	0.83	0.68	0.50	0.45	0.44	0.41	0.17	0.16
N-allyldiethylammonium	8.41	1.06	0.19	3.66	0.66	0.25	0.54	0.79	0.64	0.48	0.43	0.41	0.39	0.16	0.15
N-N-diethylpropylammonium	10.52	1.67	0.28	7.17	0.99	0.37	0.79	1.19	0.83	0.69	0.62	0.59	0.55	0.22	0.21
Triethylammonium	1.50	0.21	0.04	0.53	0.12	0.05	0.10	0.15	0.12	0.09	0.09	0.08	0.08	0.03	0.03
Triethanolammonium	4.50	0.68	0.12	1.98	0.44	0.16	0.36	0.52	0.39	0.32	0.30	0.29	0.27	0.10	0.10
Tributylammonium	8.68	0.97	0.16	3.56	0.59	0.21	0.48	0.71	0.56	0.42	0.38	0.37	0.35	0.13	0.12
Trihexylammonium	8.27	0.93	0.15	3.38	0.57	0.20	0.46	0.68	0.54	0.40	0.36	0.35	0.33	0.12	0.12
Alanine ethyl ester	1.25	0.17	0.03	0.62	0.11	0.05	0.09	0.12	0.12	0.08	0.07	0.07	0.06	0.03	0.03
Alanine methyl ester	1.51	0.17	0.03	0.72	0.10	0.05	0.08	0.12	0.12	0.07	0.07	0.06	0.06	0.03	0.03
Glycine ethyl ester	1.79	0.18	0.04	0.92	0.11	0.04	0.08	0.13	0.14	0.07	0.07	0.06	0.06	0.03	0.03
Proline methyl ester		0.70	0.13	2.26	0.47	0.16	0.39	0.56	0.43	0.35	0.32	0.30	0.29	0.11	0.10
Collidinium	4.63	1.59	0.26	6.83	0.94	0.35	0.75	1.13	0.97	0.65	0.58	0.56	0.52	0.20	0.19
Benzamide	9.26	0.77	0.13	3.73	0.45	0.17	0.36	0.55	0.48	0.31	0.28	0.26	0.25	0.09	0.09
Diphenylammonium	11.75	1.59	0.34	5.57	1.00	0.43	0.82	1.17	1.06	0.72	0.65	0.63	0.60	0.27	0.26
Lutidinium	7.28	2.35	0.37	12.19	1.32	0.49	1.03	1.60	1.48	0.89	0.79	0.75	0.70	0.28	0.26
Quinolinium	4.89	1.65	0.33	6.18	1.02	0.42	0.82	1.20	1.08	0.72	0.65	0.63	0.59	0.26	0.25
N,N,N′,N′-Tetramethylguanidine	27.81	2.43	0.42	11.67	1.40	0.56	1.11	1.69	1.59	0.96	0.85	0.81	0.76	0.32	0.31
HNC dmaH	27.81	2.43	0.42	11.67	1.40	0.56	1.11	1.69	1.59	0.96	0.85	0.81	0.76	0.32	0.31
Amilaminium	0.91	0.48	0.09	1.62	0.30	0.11	0.25	0.36	0.28	0.22	0.20	0.19	0.18	0.07	0.06
N-(2-ethyl-hexyl)- ethylenediamine	31.93	2.36	0.36	12.48	1.32	0.49	1.03	1.61	1.48	0.88	0.79	0.75	0.70	0.27	0.26
N-Butylethylenediamine	28.00	2.08	0.31	10.77	1.17	0.42	0.91	1.42	1.28	0.78	0.70	0.66	0.62	0.23	0.22
N-hexylethylenediaminium	28.43	2.11	0.32	10.95	1.19	0.42	0.93	1.44	1.30	0.80	0.71	0.67	0.63	0.24	0.23
N-octylethylenediaminium	28.91	2.14	0.32	11.16	1.21	0.43	0.94	1.47	1.32	0.81	0.72	0.68	0.64	0.24	0.23
N-decylethylenediaminium	28.88	2.14	0.32	11.14	1.20	0.43	0.94	1.46	1.32	0.81	0.72	0.68	0.64	0.24	0.23
N-dodecylethylenediaminium	29.14	2.16	0.33	11.26	1.21	0.44	0.95	1.48	1.33	0.81	0.72	0.69	0.64	0.24	0.23
Ethyldiammonium	10.29	0.70	0.27	19.57	0.99	0.38	0.72	1.27	1.52	0.59	0.51	0.48	0.44	0.17	0.17

Figure 8.6. MLREM/BRANNLP conductivity predictions for inorganic acid based ILs.

	Hydrogene bisfluoride	Chloride	Perchlorate	Nitrate	Thiocyanate	Dihydrogen phosphate	Dinbutyl phosphate	Mesylates	Hexafluoro isopropoxy sulfate	Hydrogen sulfate	Pulfamate	Triflate	Tf2N	BETI
Methylammonium	12.87	16.03	9.82	10.54	15.55	5.46	0.15	13.91	1.72	7.28	5.45	23.10	32.79	2.28
Ethylammonium	16.43	21.11	12.07	13.09	20.38	6.24	0.23	17.95	2.27	8.62	6.23	26.39	37.62	2.41
Ethanolammonium	4.21	5.07	3.34	3.55	4.94	2.01	0.06	4.49	0.54	2.22	2.00	11.41	17.02	0.86
2methoxyethylammonium	1.53	1.96	1.14	1.23	1.89	0.60	0.08	1.67	0.35	0.82	0.60	5.42	9.11	0.23
2-2-hydroxyethoxyethylammonium	1.12	1.38	0.87	0.67	1.34	0.50	0.04	1.21	0.23	0.54	0.50	4.68	7.81	0.21
Acetamide	5.85	6.90	4.76	5.03	6.74	3.02	0.05	6.20	0.72	3.79	3.02	14.20	20.41	1.42
Propylammonium	3.28	4.19	2.42	2.62	4.05	1.27	0.11	3.57	0.60	1.74	1.26	9.51	15.04	0.47
Propanolammonium	1.12	1.37	0.88	0.94	1.33	0.52	0.04	1.20	0.22	0.67	0.52	4.81	7.92	0.22
2-propanolammonium	1.28	1.57	1.00	1.07	1.53	0.58	0.04	1.38	0.25	0.76	0.58	5.23	8.59	0.24
2-methylpropylammonium	3.81	4.93	2.78	3.02	4.76	1.41	0.14	4.18	0.71	1.97	1.41	10.38	16.38	0.51
Isopropylammonium	4.66	6.03	3.40	3.69	5.82	1.73	0.15	5.11	0.81	2.41	1.73	11.83	18.39	0.62
Butylammonium	1.84	2.35	1.37	1.48	2.27	0.72	0.09	2.01	0.40	0.99	0.72	6.30	10.42	0.28
2-methylbutylammonium	2.10	2.71	1.54	1.67	2.61	0.79	0.10	2.30	0.46	1.10	0.79	6.80	11.21	0.30
Sec-butylammonium	4.23	5.43	3.12	3.38	5.25	1.62	0.13	4.63	0.73	2.23	1.61	11.18	17.42	0.59
N-butyramide	1.02	1.21	0.82	0.87	1.18	0.51	0.03	1.08	0.18	0.64	0.51		7.53	0.22
Isobutyramide	2.11	2.54	1.68	1.78	2.48	1.01	0.04	2.26	0.31	1.30	1.01		11.54	0.42
Pentylammonium	4.66	5.93	3.46	3.74	5.73	1.83	0.12	5.07	0.74	2.50	1.83	11.91	18.33	0.68
Heptylammonium	2.10	2.67	1.57	1.70	2.58	0.84	0.08	2.29	0.43	1.14	0.83	7.05	11.47	0.32
Octylammonium	2.10	2.67	1.57	1.69	2.58	0.83	0.08	2.29	0.42	1.14	0.83	7.04	11.46	0.32
Dimethyl ammonium	25.42	35.95	16.18	18.19	34.36	6.33	0.66	28.93	4.43	8.18	6.31	30.90	45.83	1.82
N-methyl2-hydroxyethylammonium	3.04	3.93	2.22	2.41	3.79	1.13	0.12	3.33	0.60	1.58	1.13	8.92	14.29	0.42
bis-2-hydroxyethylmethylammonium	1.69	2.14	1.26	1.36	2.07	0.67	0.08	1.84	0.37	0.91	0.66	5.92	9.83	0.26
Diethylammonium	9.08		6.18	6.83	11.94	2.74	0.19	10.16	1.76	4.07	2.73	17.16	26.45	0.88
Diethanol ammonium	0.96	1.20	0.73	0.78	1.16	0.40	0.03	0.31	0.23	0.54	0.15	3.89	6.71	0.17
bis-2-methoxyethylammonium	2.60	3.67	1.71	1.91	3.50	0.71	0.25	2.93	0.85	1.09	0.71	5.58	9.93	0.24
Diallylammonium	3.73	5.06	2.58	2.84	4.85	1.18	0.22	4.16	0.90	1.73	1.18	9.35	15.31	0.41
Dinpropylammonium	3.80	5.16	2.62	2.89	4.94	1.19	0.22	4.23	0.92	1.75	1.19	9.44	15.45	0.41
Dibutylammonium	2.19	2.96	1.52	1.67	2.84	0.70	0.17	2.44	0.61	1.02	0.70	5.95	10.25	0.25
Dimethylethylammonium	23.86	33.90	15.56	17.39	32.32	6.38	0.60	27.04	4.07	9.83	6.36	30.36	44.73	1.93
N-allyldimethylammonium	20.32	28.51	13.48	15.00	27.19	5.71	0.52	22.90	3.44	8.66	5.69	10.50	41.15	1.77
Diethylmethylammonium	14.85	20.62	9.97	11.06	19.69	4.32	0.44		2.60	6.49	4.31	8.46	34.64	1.35
N-N-diethylmethylammonium	6.37	8.78	4.32	4.78	8.40	1.90	0.30	7.14	1.41	2.83	1.90	4.37	21.35	0.62
N-N-diallylmethylammonium	5.79	7.91	3.96	4.37	7.57	1.78	0.28	6.46	1.26	2.62	1.77	4.15	20.29	0.59
N-methyldipropylammonium	19.46	26.73	13.24	14.64	25.57	5.88	0.46	21.77	3.09	8.72	5.86	27.68	40.54	1.93
Diisopropylmethylammonium	20.78	29.22	13.75	15.31	27.85	5.80	0.53	23.43	3.53	8.82	5.78		41.63	1.80
N-N-dimethylpropylammonium	12.84	17.30	8.94	9.82	16.59	4.15	0.33	14.27	2.05	6.03	4.14	21.66	32.25	1.39
Diisopropylethylammonium	5.06	7.04	3.39	3.76	6.72	1.46	0.30	5.69	1.26	2.20	1.46	11.07	18.03	0.48
Dimethylbutylammonium	4.43	6.02	3.05	3.37	5.77	1.39	0.24	4.94	1.02	2.04	1.39	3.33	17.18	0.47
N-allyldiethylammonium	4.20	5.68	2.91	3.20	5.44	1.34	0.23	4.67	0.96	1.96	1.34	3.23	16.70	0.46
N-N-diethylpropylammonium	9.53	12.95	6.56	7.23	12.41	2.98	0.18	2.36	1.71	4.38	2.97	17.83	27.22	0.97
Triethylammonium	0.69	0.86	0.52	0.56	0.83	0.29	0.04	0.74	0.18	0.39	0.29	2.81	5.04	
Triethanolammonium	2.14	2.86	1.51	1.66	2.74	0.72	0.09	2.37	0.56	1.03	0.72	6.18	10.52	0.26
Tributylammonium	4.75	6.28	3.38	3.70	6.04	1.64	0.19	5.24	0.92	2.33	1.64	11.75	18.49	0.57
Trihexylammonium	4.57	6.01	3.26	3.56	5.79	1.60	0.18	5.03	0.88	2.26	1.59	11.49	18.10	0.56
Alanine ethyl ester	1.01	1.23	0.79	0.66	1.20	0.46	0.04	1.09	0.20	0.60	0.46	4.41	7.35	0.20
Alanine methyl ester	1.28	1.55	1.01	1.08	1.51	0.60	0.04	1.37	0.23	0.78	0.60	5.33	8.65	0.26
Glycine ethyl ester	1.92	2.30	1.54	1.63	2.24	0.94	0.04	2.05	0.28	1.20	0.94	6.97	10.89	0.40
Proline methyl ester	2.55	3.40	1.80	1.45	3.26	0.86	0.16	2.83	0.63	1.23	0.86	7.24	12.08	0.31
Collidinium	9.29	12.53	6.45	7.09	12.02	2.98	0.30	10.33	1.63	4.34	2.97	17.65	26.88	0.98
Benzamide	6.56	8.33	4.89	5.28	8.05	2.60	0.13	7.14	0.95	3.54	2.59		22.21	0.98
Diphenylammonium	6.10	8.67	3.94	4.41	8.27	1.59	0.37	6.92	1.61	2.47	1.58	11.74	19.27	0.50
Lutidinium	17.18	23.34	11.84	13.04	22.36	5.39	0.40	19.14	2.68	7.90	5.38	25.84	37.92	1.80
Quinolinium	7.06	9.95	4.66	5.19	9.48	1.95	0.36	7.97	1.68	2.98	1.95	13.85	22.13	0.62
N,N,N′,N′-Tetramethylguanidine	15.88	22.10	10.64	11.81	21.10	4.59	0.45	17.85	2.76	6.90	4.57	24.04	35.94	1.43
HNC dmaH	15.88	22.10	10.64	11.81	21.10	4.59	0.45	17.85	2.76	6.90	4.57	24.04	35.94	1.43
Amilaminium	2.29	2.93	1.70	1.84	2.83	0.89	0.10	2.50	0.47	1.22	0.89	7.41	12.04	0.34
N-(2-ethyl-hexyl)- ethylenediamine	17.66	23.91	12.21	13.44	22.91	5.60	0.40	19.65	2.71	8.19	5.59	26.37	16.96	1.89
N-Butylethylenediamine	15.63	20.94	10.94	12.01	20.10	5.14	0.35	17.33	2.36	7.43	5.13	24.64	17.05	1.77
N-hexylethylenediaminium	15.85	21.25	11.08	12.16	20.40	5.19	0.35	17.58	2.40	7.51	5.18	24.83	16.00	1.78
N-octylethylenediaminium	16.09	21.60	11.23	12.34	20.73	5.25	0.36	17.85	2.44	7.60	5.24	25.04	16.13	1.80
N-decylethylenediaminium	16.07	21.58	11.22	12.32	20.71	5.25	0.36	17.83	2.44	7.60	5.23	25.03	16.13	1.80
N-dodecylethylenediaminium	16.21	21.78	11.31	12.42	20.89	5.28	0.36	17.99	2.46	7.65	5.26	25.15	16.20	1.81
Ethyldiammonium	27.07	33.73	20.63	22.16	32.71	11.47	0.11	29.26	4.60	15.30	11.44	37.79	51.21	4.97

BETI: bis[(pentafluoro-ethyl)sulfonyl]imide, Tf2N: bis(trifluoromethanesulfonyl)imide.

8.2 Supplementary information for surfactant self-assembly (Chapter 3)

Figure 8.7. CMC graphs for SOS, CTAB and $C_{12}E_4$ in EAN-water concentrations 5, 14, 25, 33, 50 and 75 mol% EAN.

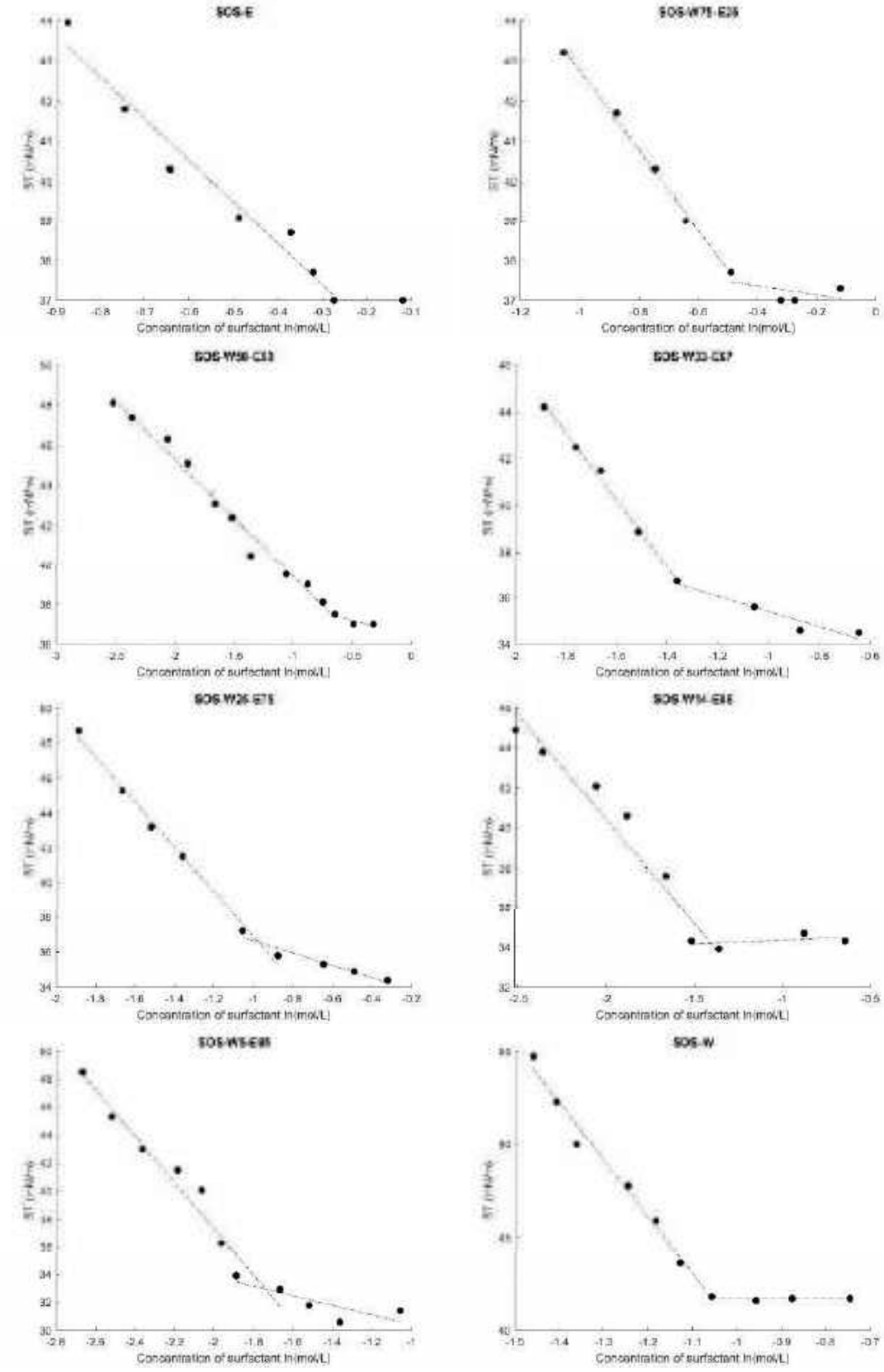

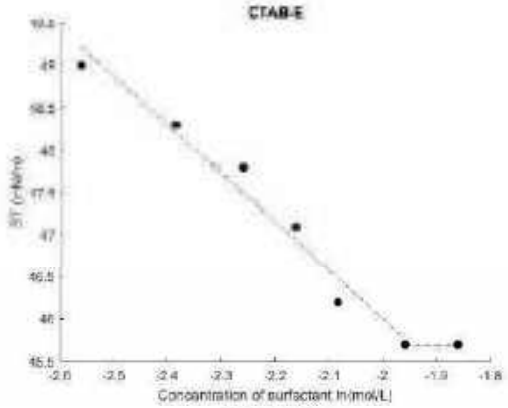
CTAB-E
Concentration of surfactant ln(mol/L)

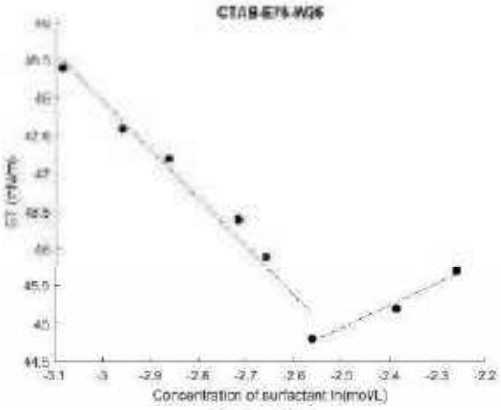
Concentration of surfactant ln(mol/L)

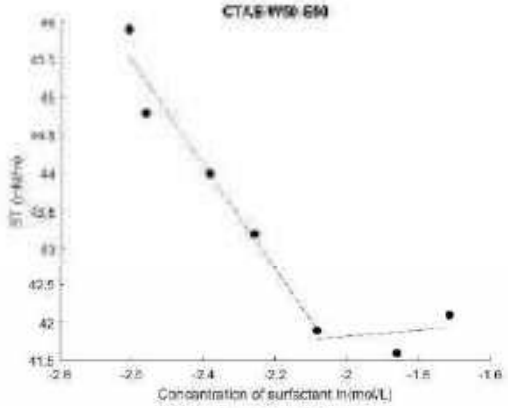
Concentration of surfactant ln(mol/L)

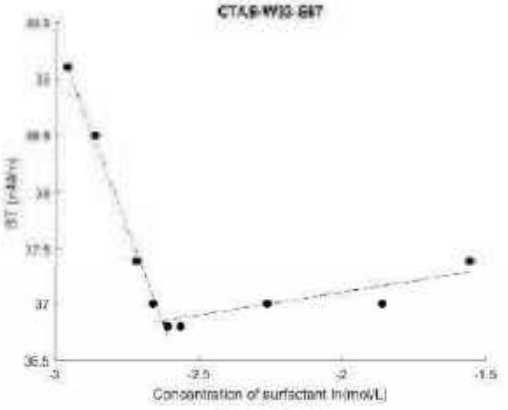
Concentration of surfactant ln(mol/L)

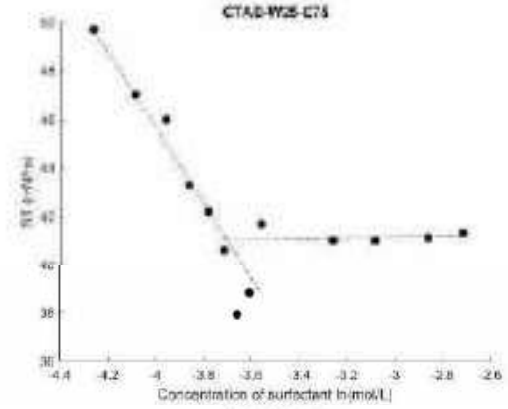
Concentration of surfactant ln(mol/L)

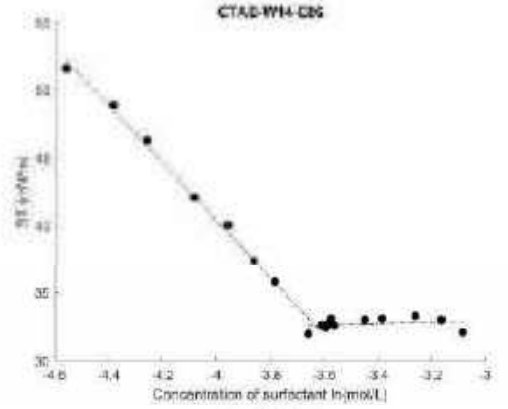
Concentration of surfactant ln(mol/L)

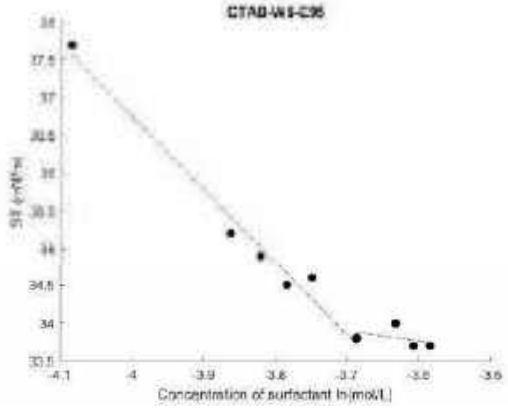
Concentration of surfactant ln(mol/L)

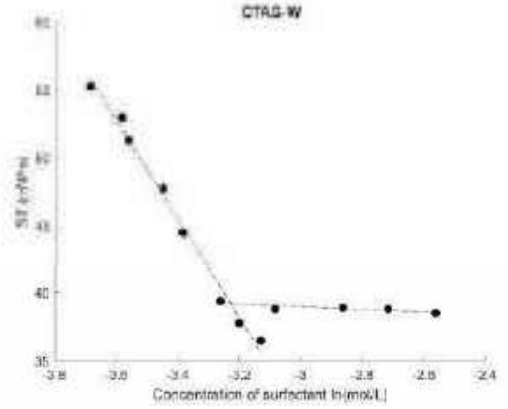
CTAG-W
Concentration of surfactant ln(mol/L)

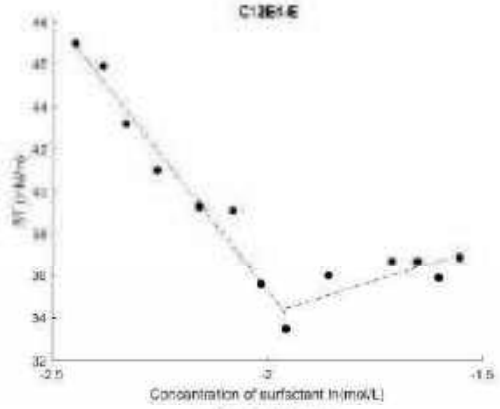
Concentration of surfactant ln(mol/L)

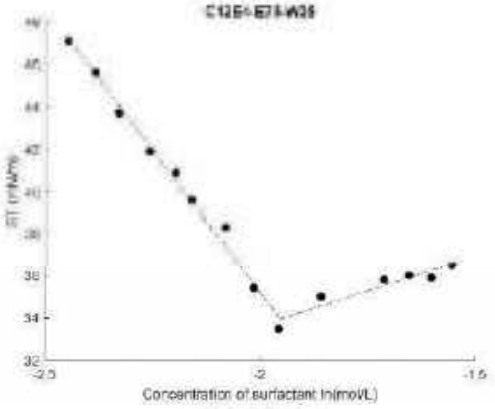
Concentration of surfactant ln(mol/L)

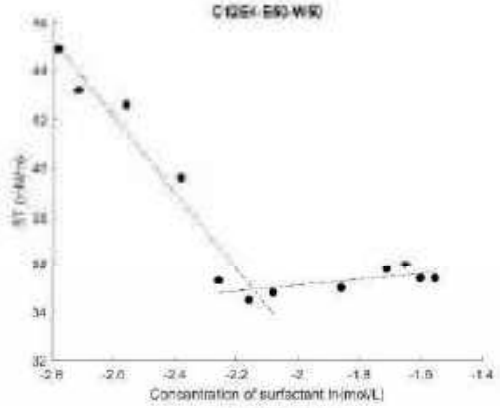
Concentration of surfactant ln(mol/L)

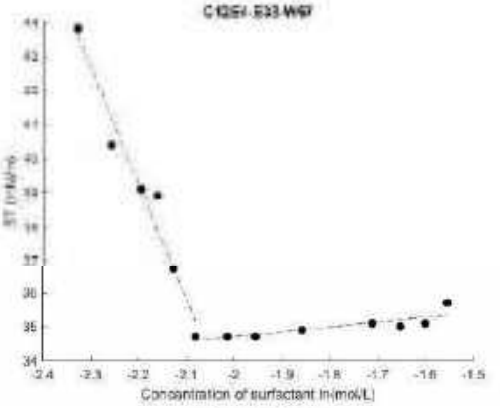
Concentration of surfactant ln(mol/L)

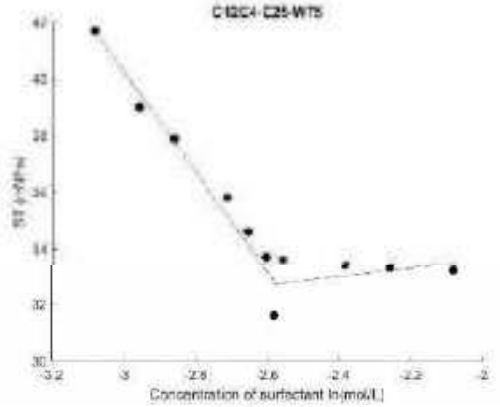
Concentration of surfactant ln(mol/L)

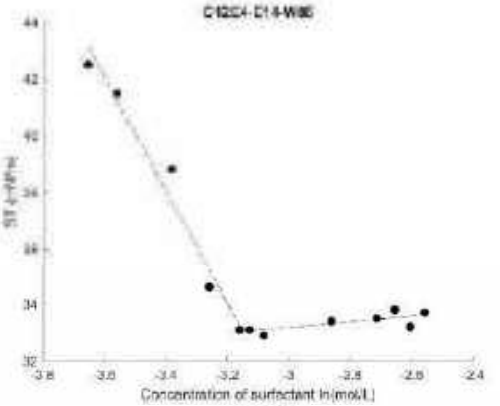
Concentration of surfactant ln(mol/L)

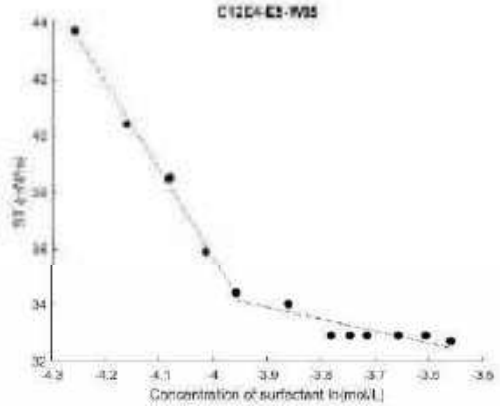
Concentration of surfactant ln(mol/L)

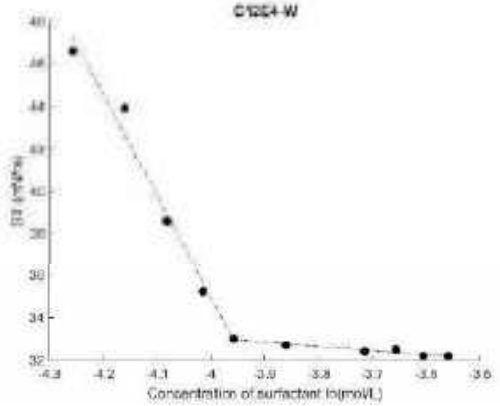
Concentration of surfactant ln(mol/L)

8.3 Supplementary material for Molecular Dynamics (Chapter 4)

Figure 8.8. Radial distribution functions (RDFs) for the water models examined in this work. The experimental RDFs are taken from A. K. Soper.

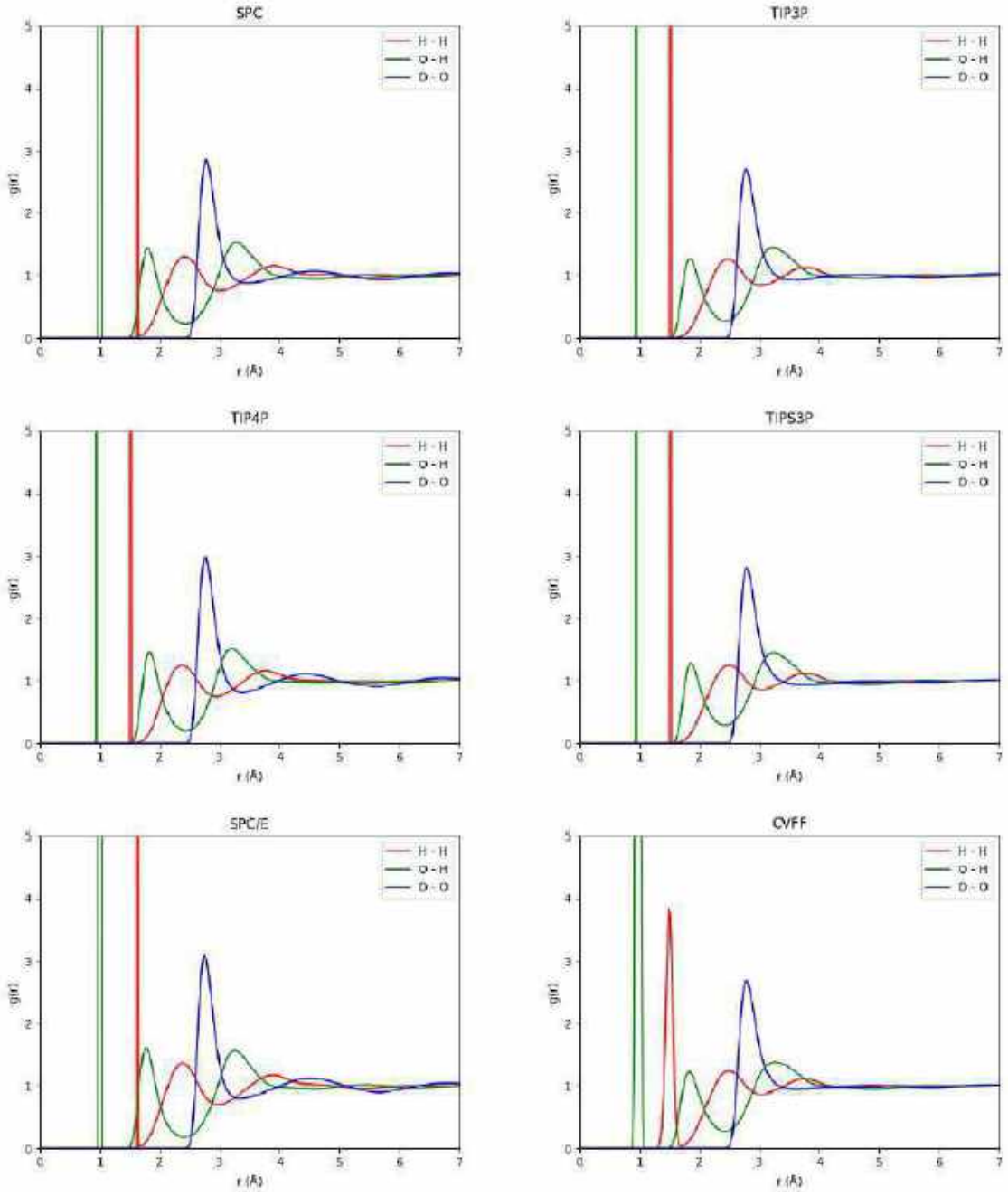

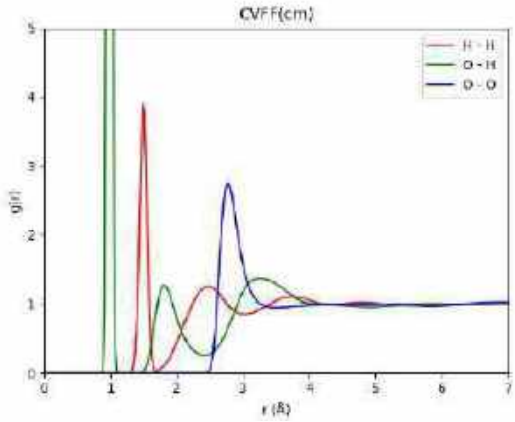
CVFF(cm)
H - H
O - H
O - O
g(r)
r (Å)

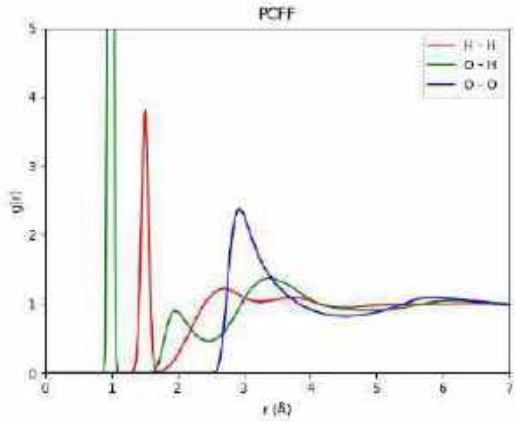
PCFF
H - H
O - H
O - O
g(r)
r (Å)

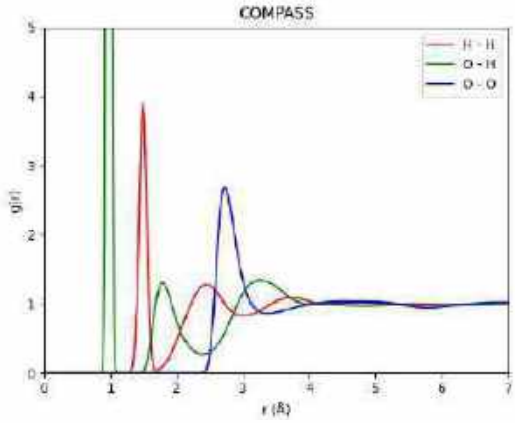
COMPASS
H - H
O - H
O - O
g(r)
r (Å)

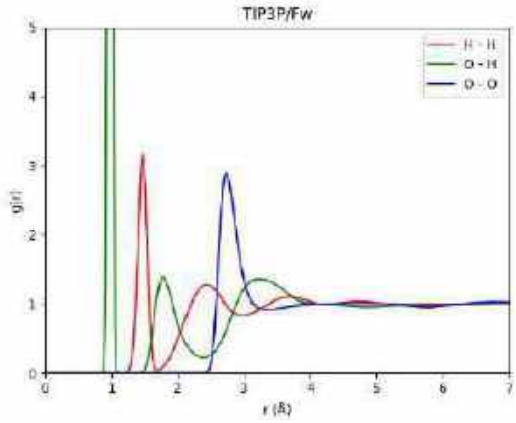
TIP3P/Fw
H - H
O - H
O - O
g(r)
r (Å)

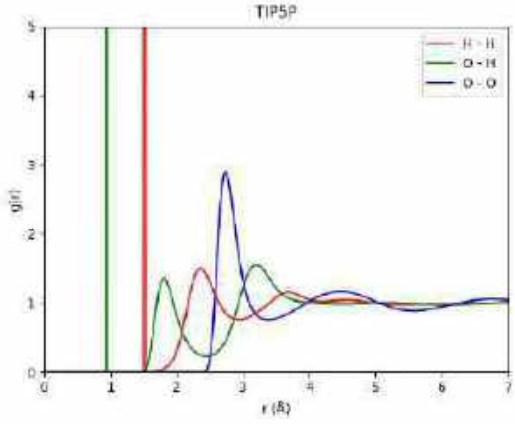
TIP5P
H - H
O - H
O - O
g(r)
r (Å)

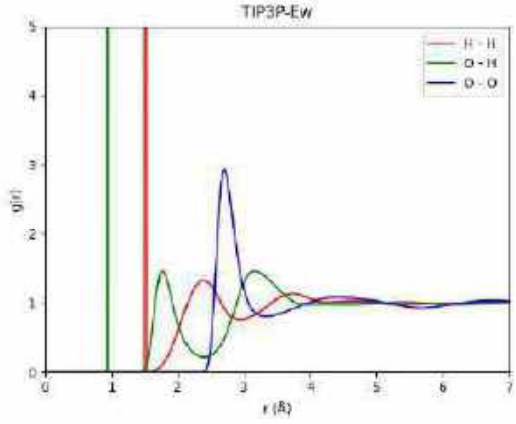
TIP3P-Ew
H - H
O - H
O - O
g(r)
r (Å)

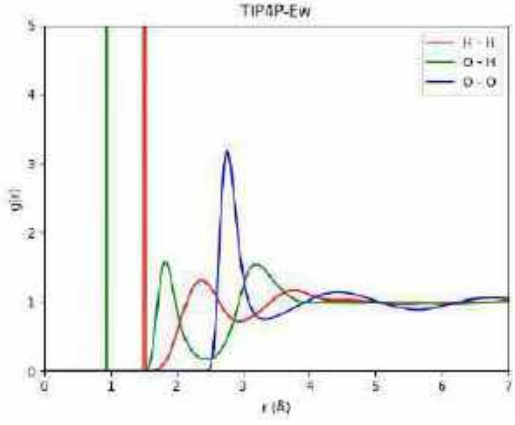
TIP4P-Ew
H - H
O - H
O - O
g(r)
r (Å)

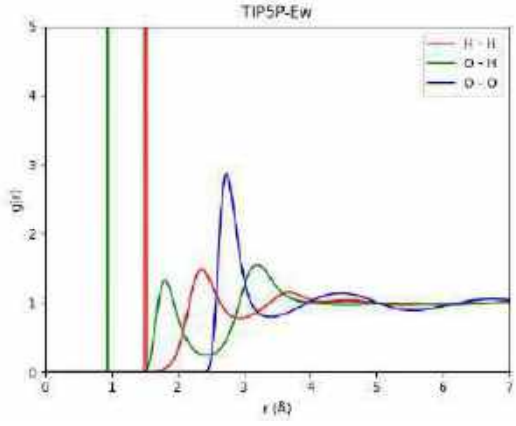
TIP5P-Ew
H - H
O - H
O - O
g(r)
r (Å)

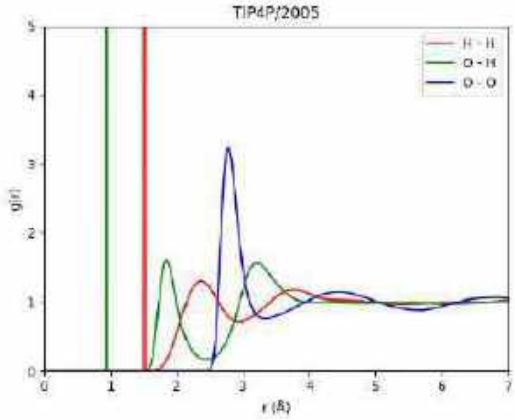
TIP4P/2005
H - H
O - H
O - O
g(r)
r (Å)

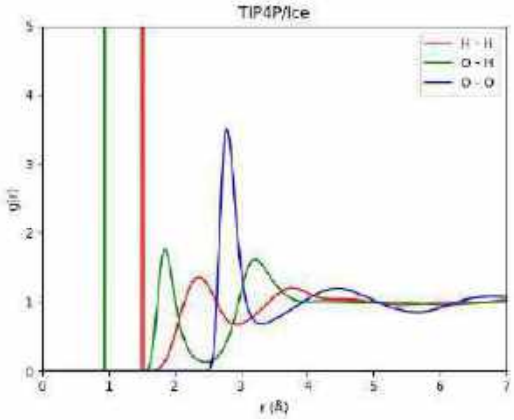
TIP4P/Ice
H - H
O - H
O - O
g(r)
r (Å)

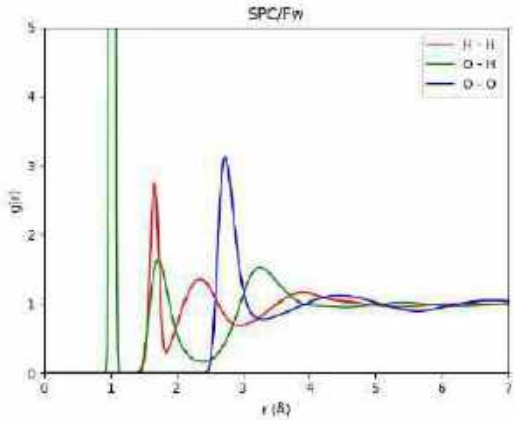
SPC/Fw
H - H
O - H
O - O
g(r)
r (Å)

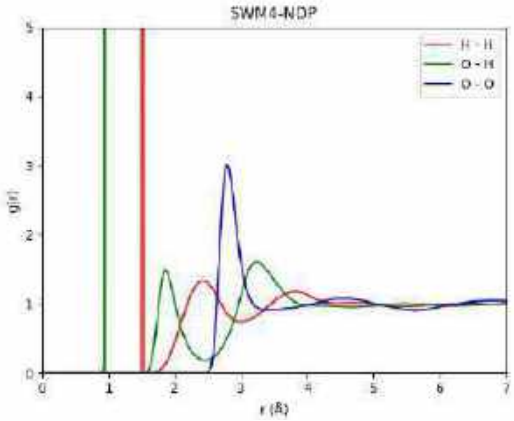
SWM4-NDP
H - H
O - H
O - O
g(r)
r (Å)

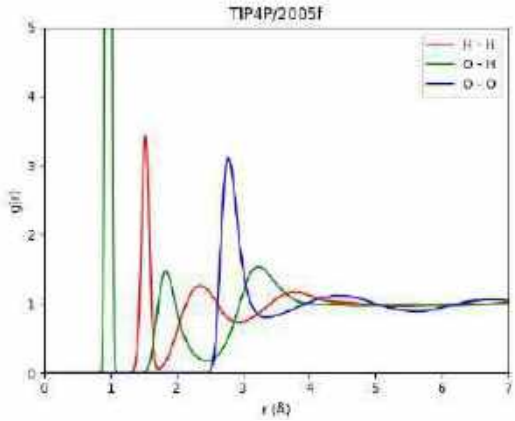
TIP4P/2005f
H - H
O - H
O - O
g(r)
r (Å)

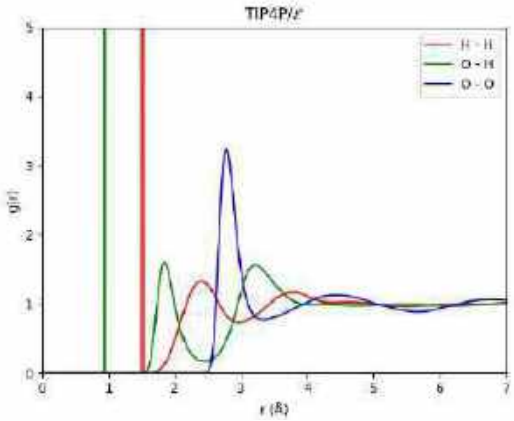
TIP4P/ε
H - H
O - H
O - O
g(r)
r (Å)

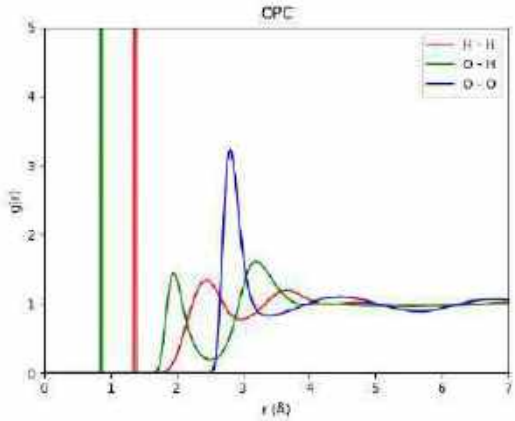
OPC
H - H
O - H
O - O
g(r)
r (Å)

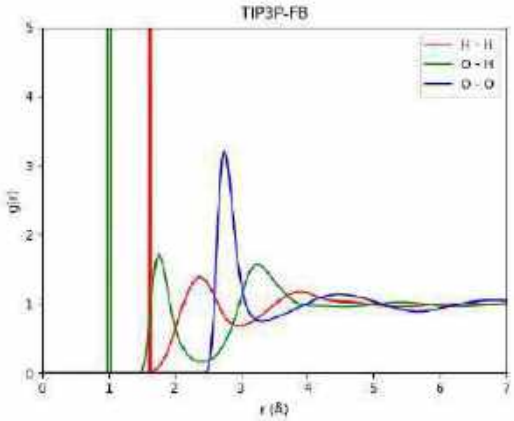
TIP3P-FB
H - H
O - H
O - O
g(r)
r (Å)

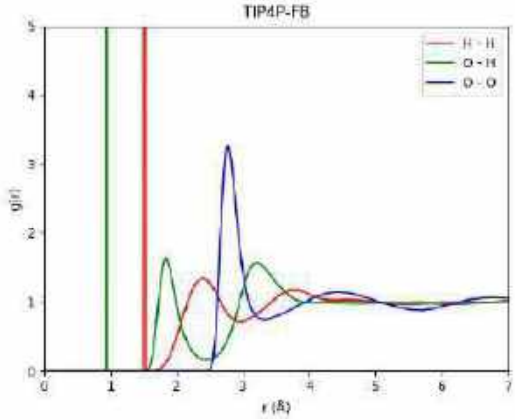
TIP4P-FB
H - H
O - H
O - O
g(r)
r (Å)

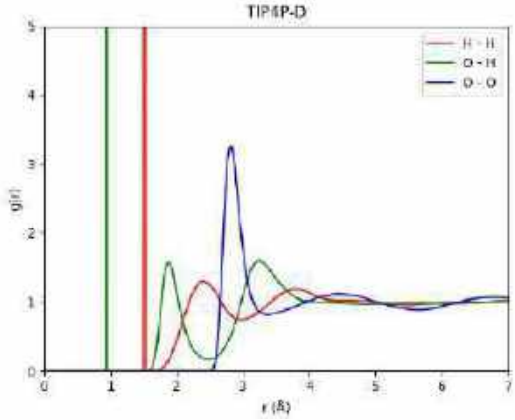
TIP4P-D
H - H
O - H
O - O
g(r)
r (Å)

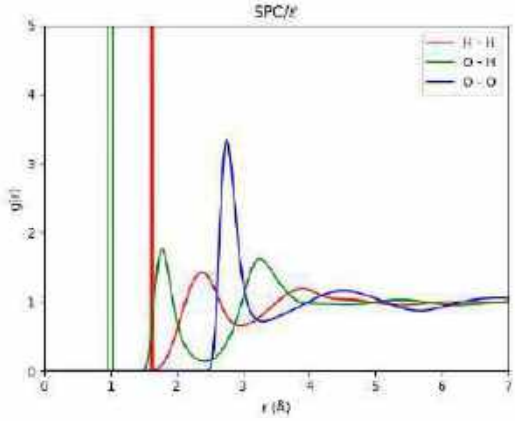
SPC/E
H - H
O - H
O - O
g(r)
r (Å)

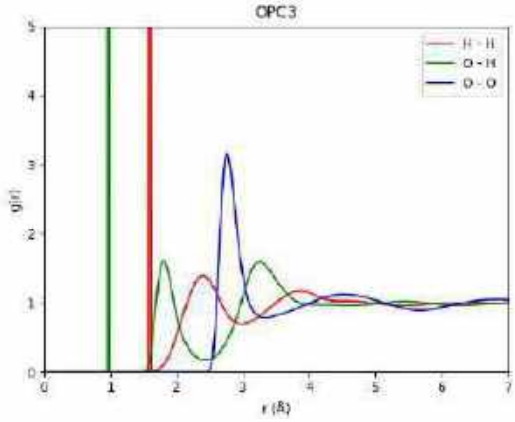
OPC3
H - H
O - H
O - O
g(r)
r (Å)

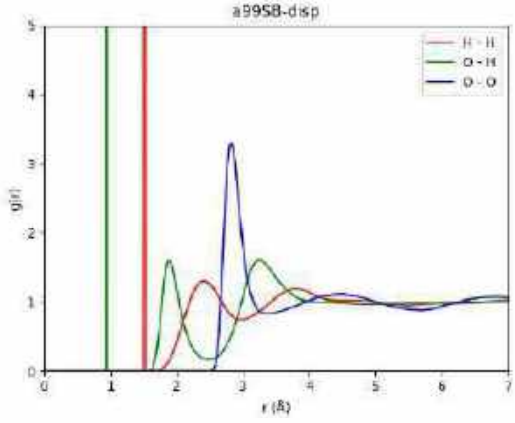
a99SB-disp
H - H
O - H
O - O
g(r)
r (Å)

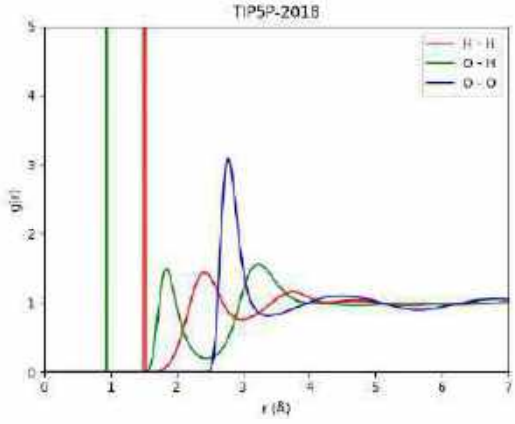
TIP5P-2018
H - H
O - H
O - O
g(r)
r (Å)

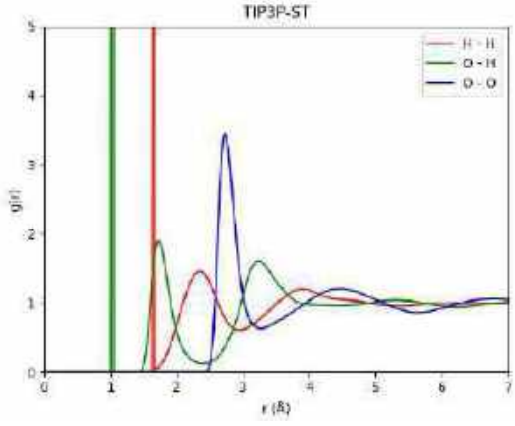
TIP3P-ST
H - H
O - H
O - O
g(r)
r (Å)

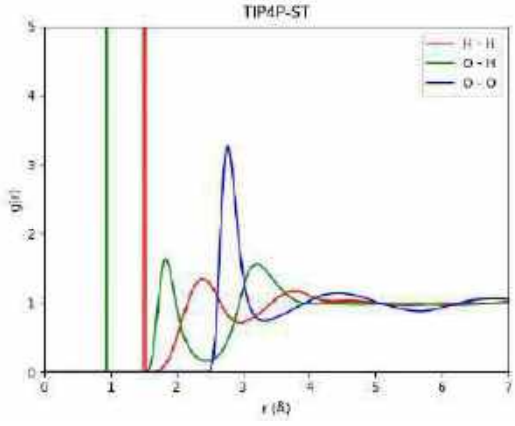
TIP4P-ST
H - H
O - H
O - O
g(r)
r (Å)

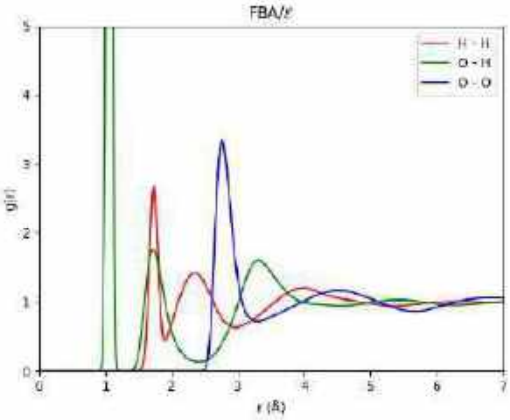
FBA/F
H - H
O - H
O - O
g(r)
r (Å)

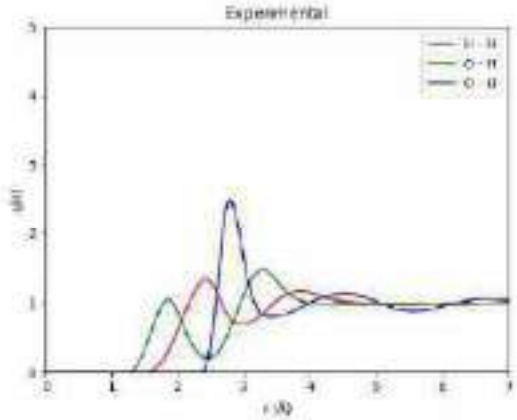
Experimental
H - H
O - H
O - O
g(r)
r (Å)

COVID-19 Thesis Impact Statement

Majority of the work included in this thesis was completed during the COVID-19 pandemic in Victoria, Australia. Victoria experienced six lockdowns between March 2020 and October 2021 that collectively totalled 262 days. The initial plan for the thesis was an experimental one, where experiments would be performed in both Australia and France. The co-tutelle agreement under which project was undertaken also required me to spend 6 months in each country every year from 2019 to 2021. Despite obtaining external funding to fund this collaboration in the form of a SAAFE travel grant from AINSE, only one visit could be arranged in March 2020 which had to be cut short due to the beginning of global pandemic travel restrictions. During the lockdowns, I was unable to complete experimental work to full capacity, had no access to facilities such as the Australian Synchrotron or Neutron scattering facilities and was unable to travel back to France. Therefore, the direction of the thesis changed quite drastically to focus more on the computational aspects of the project, which were initially supposed to complement the experiments. Molecular dynamics simulations and machine learning algorithms were devised during the height of the pandemic to understand how these computational methods could be used to bridge the gaps in the experimental data collected during the first year of the PhD and existing data from literature. While this might seem like a setback, and it was to a degree, the overall quality and impact of the thesis was improved by considering computational methods which have not previously been used for the systems we have experimentally investigated.

Publications and conferences

Publications

- **Sachini P K Pathirannahalage**, Nastaran Meftahi, Aaron Elbourne, Alessia C G Weiss, Chris F McConville, Agilio Padua, David A Winkler, Margarida Costa Gomes, Tamar L Greaves, Tu C Le, Quinn A Besford, Andrew J Christofferson, Systematic Comparison of the Structural and Dynamic Properties of Commonly Used Water Models for Molecular Dynamics Simulations. Journal of Chemical Information and Modelling 2021, 61 (9) 4521–4536.
- Haitao Yu, Brendan P Dyett, **Sachini P K Pathirannahalage**, Miaosi Li, Calum J Drummond, Tamar L Greaves. Formation of surface protic ionic liquid nanodroplets for nanofabrication. Advance Materials Interfaces 2019, 7, 1901647.
- Dung Viet Duong, Hung-Vu Tran, **Sachini P K Pathirannahalage**, Stuart Brown, Michael Hassett, Dilek Yalcin, Nastaran Meftahi, Andrew J Christofferson, Tamar L Greaves, Tu C. Le Machine Learning Investigation of Viscosity and Ionic Conductivity of Protic Ionic Liquids in Water Mixtures. Journal of Chemical Physics 2022, 156, 154503.
- Jack Binns, Connie Darmanin, Cameron M. Kewish, **Sachini P K Pathirannahalge**, Peter Berntsen, Patrick Adams, Stefan Paporakis, Daniel Wells, Francisco Gian Roque, Brian Abbey, Gary Bryant, Charlotte Conn, Stephan Mudie, Adrian M Hawley, Timothy M Ryan, Tamar L Greaves, Andrew V Martin. Preferred orientation and its effects on intensity correlation measurements. International Union of Crystallography Journal. 2022, 9(2).
- Daniel Wells, Peter Berntsen, Eugeniu Balaur, Cameron Kewish, Patrick Adams, Eva Bajnoczi, Jack Binns, Olle Bjornholm, Hayden Broomhall, Carl Caleman, Andrew Christofferson, Charlotte Conn, Caroline Dahlqvist, Ibrahim Dawod, Leonie Flueckiger, Francisco Gian Roque, Tamar Greaves, Majid Hejazian, Marjan Hadian Jazi, Olof Jonsson, **Sachini P K Pathirannahalage**, Rick Kirian, Alex Kozlov, Ruslan Kurta, Hugh Marman, Derek Mendez, Andrew Morgan, Keith Nugent, Dominik Oberthuer, Ingmar Persson, Harry Quiney, Clara Saak, Saumitra Saha, Jonas Sellberg, Nicosur Timneanu, Max Wiedorn, Brian Abbey, Andrew V. Martin, Connie Darmanin. Observations of phase changes in lipidic cubic phase systems during high viscous injection. Journal of Synchrotron Radiation, 2022, 29(3).

Conferences

- ChemComm Symposium 2019, RMIT University European (poster)
- Colloids and Interface Society Conference 2019, KU Leuven (poster)
- European Materials Research Society Fall Meeting 2019, Warsaw University of Technology (poster)
- RMIT ECR Symposium 2019, RMIT University (poster)
- Emerging Polymer Technologies Summit 2019, University of Melbourne (poster)
- Sydney surfaces and soft stuff (SASSY) Virtual Conference 2020 (oral)
- Synchrotron User meeting 2020 (oral)
- Australian Colloids and Interface Society Conference 2021, Monash University (poster)
- Synchrotron User meeting 2021 (oral)